

INVESTIGATING LIMIT CYCLE PERFORMANCE AND ASYMPTOTIC BODE BEHAVIOR OF FRACTIONAL-ORDER CONTROLLERS

*A thesis submitted
in partial fulfillment for the degree of*

Doctor of Philosophy

by

AMEYA ANIL KESARKAR



Department of Avionics

INDIAN INSTITUTE OF SPACE SCIENCE AND TECHNOLOGY

Thiruvananthapuram - 695547

May 2015

CERTIFICATE

This is to certify that the thesis titled **Investigating Limit Cycle Performance and Asymptotic Bode Behavior of Fractional-Order Controllers**, submitted by **Ameya Anil Kesarkar**, to the Indian Institute of Space Science and Technology, Thiruvananthapuram, for the award of the degree of **Doctor of Philosophy**, is a bona fide record of the research work done by him under my supervision. The contents of this thesis, in full or in parts, have not been submitted to any other Institute or University for the award of any degree or diploma.

Name of the Supervisor

Dr. N. Selvagesan

Associate Professor and Head,

Department of Avionics,

Indian Institute of Space Science and Technology (IIST)

Place: Thiruvananthapuram

May, 2015

DECLARATION

I declare that this thesis titled **Investigating Limit Cycle Performance and Asymptotic Bode Behavior of Fractional-Order Controllers** submitted in fulfillment of the Degree of Doctor of Philosophy is a record of original work carried out by me under the supervision of **Dr. N. Selvagesan**, and has not formed the basis for the award of any degree, diploma, associateship, fellowship or other titles in this or any other Institution or University of higher learning. In keeping with the ethical practice in reporting scientific information, due acknowledgments have been made wherever the findings of others have been cited.

Ameya Anil Kesarkar

SC10D006

Place: Thiruvananthapuram

May, 2015

ACKNOWLEDGEMENTS

It would have never been possible for me to write this doctoral thesis without the support and encouragement of numerous people around me. At this moment of accomplishment, I would first like to express my deepest gratitude to my research supervisor **Dr. N. Selvagesan** for his guidance, support, and patience. His technical and editorial advice was very important for the completion of this thesis.

I am also extremely indebted to **Dr. H. Priyadarshan**, who lent his technical expertise in my work in the form of invaluable brainstorming sessions which gave me a deep insight and perspective for attacking my problem at its core. Working with him made me realize my true potential and the ideal way of tapping it.

I gratefully acknowledge chair of my doctoral committee, **Dr. Thomas Kurien** for his technical inputs which played a big role in my research progress. I would also like to offer my sincere thanks to the other members of my doctoral committee **Dr. P. S. V. Nataraj, Dr. Santanu Dasgupta, Dr. Rajesh Joseph Abraham**, and **Dr. Nicholas Sabu** for their periodic assessments of my research work.

I further take this opportunity to thank **Shri. M. V. Dhekane** and **Shri. Sam Zachariah** for their kind support and assistance.

I am also thankful to my institute, especially **Department of Avionics**, for picking me up as a doctoral student and providing me an excellent research environment. I would like to express my sincere gratitude to our current Director **Dr. K. S. Dasgupta** and our former director **Dr. B. N. Suresh** as well for their encouragement and support.

I wish to thank my father (**Anil Kesarkar**), my mother (**Anita Kesarkar**), and my brother (**Tushar Kesarkar**) for their unconditional love.

Last but by no means least, a heartfelt thanks goes out to my dear **Richa**, who stood by me through all the thicks and thins.

-Ameya Anil Kesarkar

ABSTRACT

Fractional Calculus (FC) is a branch of mathematics which generalizes classical integer-order calculus to handle integrals and derivatives of *arbitrary* orders. Recently, the FC has received attentions in various science and engineering fields including control theory. In control theory, one deals with the design and analysis of Fractional-Order Controllers (FOCs), whose dynamics are governed by fractional-order differential equations. In this thesis, our main objective is to investigate the limit cycle performance and asymptotic Bode characteristics of such FOCs. We also derive unified tuning expressions for three-parameter FOCs which meet Wang-et-al specifications.

The thesis begins by considering the unification of tuning expressions for three-parameter FOCs such as PI^α , $[PI]^\alpha$, PD^β , and $[PD]^\beta$ to meet desired gain crossover frequency, phase margin and isodamping property (Wang-et-al specifications) with the help of a proposed universal plant structure.

Then, we focus on the plants containing separable nonlinearity and observe the limit cycle suppression capabilities of FOCs when they are tuned for the Transfer Function (TF) of such plants to meet the Wang-et-al specifications. A typical motion-servo plant containing separable backlash nonlinearity is considered for this purpose and three-parameter FOCs such as PI^α , $[PI]^\alpha$ and integer PID are tuned by using our earlier derived unified expressions. When the limit cycle performances of such controllers are examined in the presence of plant nonlinearity, it is found that the FOCs remarkably suppress amplitude of limit cycles than the integer PID which subsequently results into lesser amplitude sustained oscillations in the steady state of closed loop response. This is further justified using Describing Function (DF) analysis method. It is noticed that the reason for such distinct performance lies in the location of intersection point corresponding to Nyquist condition for limit cycles. The confirmation of such fractional superiority is further made for the Precision Modular Servo (PMS) laboratory set-up under the similar tuning conditions.

Motivated by the above simulation and experimental studies, a more detailed in-

vestigation is pursued towards suppressing the sustained oscillation amplitudes for two kinds of plants, one containing backlash and the other with relay nonlinearity. For each plant, the controller design is formulated as a constrained optimization problem to obtain the desirable limit cycle performance. Additionally, the controller is forced to meet certain loop performance specifications. The DF of the nonlinearity is efficiently utilized during the construction of these frameworks. Under such novel formulation, the superiority of FOCs over their integer-order counterparts is investigated in detail.

In the thesis, we further contribute towards characterizing the asymptotic Bode behavior of FOCs such as PI^α , $[PI]^\alpha$, PD^β , $[PD]^\beta$, and $PI^\alpha D^\beta$. The work introduces a few basic fractional-order terms for this purpose and develops their asymptotic magnitude and phase Bode plots. Later, such plots are utilized in constructing the asymptotic magnitude and phase Bode plots for the said FOCs. We also develop such plots for the fractional commensurate order TFs in general. Identification of fractional-order TF from the given asymptotic magnitude Bode plot is illustrated in detail. Additionally, the application of asymptotic magnitude and phase Bode plots for analyzing a given fractional control loop is also explained using a numerical example.

TABLE OF CONTENTS

CERTIFICATE	i
DECLARATION	iii
ACKNOWLEDGEMENTS	v
ABSTRACT	vii
LIST OF FIGURES	xv
LIST OF TABLES	xix
ABBREVIATIONS	xxi
NOTATIONS	xxiii
1 Introduction	1
1.1 Literature Survey and Motivation	1
1.2 Research Contributions	8
1.3 Organization of Thesis	8
2 Preliminaries of Fractional Calculus and Fractional-Order Control	11
2.1 Introduction	11
2.2 Definitions in Fractional Calculus	12
2.3 Laplace Transform of Fractional Derivatives	17
2.4 Fractional-Order Transfer Functions	18

2.5	Continuous Domain Approximation Methods	19
2.6	Fractional-Order Controllers	25
2.7	Summary	26
3	Unified Tuning Expressions for Fractional-Order Controllers to Meet Wang-et-al specifications	27
3.1	Introduction	27
3.2	Closed Loop Control System	27
3.3	Universal Plant Structure	28
3.4	Fractional-Order Controllers and their Unified Tuning Expressions .	30
3.4.1	Tuning Expressions for PI^α and PD^β Controllers	30
3.4.2	Tuning Expressions for $[PI]^\alpha$ Controller	34
3.4.3	Tuning Expressions for $[PD]^\beta$ Controller	35
3.5	Illustration with examples	35
3.5.1	PI^α and PD^β Controllers	36
3.5.2	$[PI]^\alpha$ Controller	39
3.5.3	$[PD]^\beta$ Controller	42
3.6	Summary	44
4	Limit Cycle Performance of Fractional-Order Controllers Meeting Wang-et-al Specifications	45
4.1	Introduction	45
4.2	Control of Servo System with Gears	45
4.2.1	Controller Design for Wang-et-al Specifications	46
4.2.2	Performance of Loop Transfer Function	47
4.3	Limit Cycle Performance of Controllers	48

4.3.1	Closed Loop Nonlinear Simulation	48
4.3.2	Describing Function Analysis	50
4.4	Control of Precision Modular Servo Set-up	52
4.4.1	Plant Description	53
4.4.2	Designed Controllers	54
4.4.3	Performance of Loop Transfer Function	54
4.5	Limit Cycle Performance with Laboratory Experimental Set-up	55
4.6	Summary	57
5	Limit Cycle Performance of Fractional-Order Controllers for Plants with Backlash and Relay Nonlinearities	59
5.1	Introduction	59
5.2	FOCs for Plants with Backlash Nonlinearity	59
5.2.1	Optimization Problem for Limit Cycle Minimization	60
5.2.2	Graphical Interpretation of the Optimization Problem	61
5.2.3	Demonstration with a Servo System Containing Static Backlash	64
5.2.4	Solution to Constrained Optimization Problem	65
5.2.5	Performance Analysis Using Graphical Interpretation	66
5.2.6	Performance Analysis Using Closed Loop Simulation in the Presence of Plant Nonlinearity	71
5.2.7	Comparison between FOCs and their Integer-Order Counterparts	73
5.3	FOCs for Plants with Relay Nonlinearity	75
5.3.1	Relay Nonlinearity and Stable Limit Cycles	75
5.3.2	Controlling Transient Behaviour using Describing Function	77
5.3.3	Proposed Closed Loop Stability Conditions	78

5.3.4	Maximization of Limit Cycle Frequency	80
5.3.5	Loop Performance Specifications	81
5.3.6	Optimization Problem for Controller Design	82
5.3.7	Application: PI^α Controller Design	84
5.3.8	Graphical Performance Analysis of Designed Controller	85
5.3.9	Verification of Limit Cycles with Closed Loop Simulation	87
5.4	Summary	89
6	Development of Asymptotic Bode Plots for Fractional-Order Controllers	91
6.1	Introduction	91
6.2	Asymptotic Magnitude Bode Plots for Fractional-Order Controllers	92
6.2.1	Constant Gain	92
6.2.2	Fractional Zero	93
6.2.3	Fractional Double-Term Pole	94
6.2.4	Asymptotic Magnitude Bode Plots for Fractional-Order Controllers	98
6.3	Asymptotic Phase Bode Plots for Fractional-Order Controllers	101
6.3.1	Phase Characteristics of Basic Fractional-Order Terms	101
6.3.2	Asymptotic Phase Bode Plots for Basic Fractional-Order Terms	104
6.3.3	Asymptotic Phase Bode Plots for Fractional-Order Controllers	108
6.4	Asymptotic Magnitude and Phase Bode Plots for Fractional Commensurate Order TFs	112
6.5	Applications	113
6.5.1	Identification of Fractional-Order Transfer Function	113
6.5.2	Analysis of Fractional Control Loop	118
6.6	Summary	119

7	Conclusions and Future Scope	121
	REFERENCES	123
A	Some Important Properties in Fractional Calculus	135
A.1	Stability of Fractional-Order Linear Time-Invariant Systems	135
A.2	Analytical Solution of Fractional-Order Differential Equations	136
B	Derivations of Unified Tuning Expressions for $[PI]^\alpha$ and $[PD]^\beta$ Controllers	139
B.1	$[PI]^\alpha$ Controller	139
B.2	$[PD]^\beta$ Controller	142
C	Unified Tuning Expressions for PID Controller	147
D	Limit Cycle Stability Condition for PI^α and $G(s) = \frac{K}{s(s+b)}$	149
E	Monotonicity Property of Phase Angles	151
E.1	Fractional Zero	151
E.2	Fractional [Zero]	152
E.3	Fractional Double-Term Zero	153
F	Selection of Critical Frequency	155
F.1	Fractional-Zero	155
F.2	Fractional-[Zero]	156
F.3	Fractional Double-Term Zero	157
	LIST OF PUBLICATIONS BASED ON THESIS	159

LIST OF FIGURES

2.1	Magnitude Bode Plots	24
2.2	Phase Bode Plots	24
3.1	Typical Unity Feedback Control System	28
3.2	Bode Plot (FOPDT) (PI^α Controller)	37
3.3	Unit Step Response (FOPDT) (PI^α Controller)	37
3.4	Bode Plot (Fractional-Order Thermal Process) (PD^β Controller)	38
3.5	Unit Step Response (Fractional-Order Thermal Process) (PD^β Controller)	38
3.6	Bode Plot (Fractional Horsepower Dynamometer) ($[PI]^\alpha$ Controller)	40
3.7	Unit Step Response (Fractional Horsepower Dynamometer) ($[PI]^\alpha$ Controller)	40
3.8	Bode Plot (Velocity Servo System) ($[PI]^\alpha$ Controller)	41
3.9	Unit Step Response (Velocity Servo System) ($[PI]^\alpha$ Controller)	41
3.10	Bode Plot (Fractional-Order Thermal Process) ($[PD]^\beta$ Controller)	43
3.11	Unit Step Response (Fractional-Order Thermal Process) ($[PD]^\beta$ Controller)	43
3.12	Bode Plot (Position Servo System) ($[PD]^\beta$ Controller)	44
3.13	Unit Step Response (Position Servo System) ($[PD]^\beta$ Controller)	44
4.1	A Servo System with Gears	46
4.2	Closed Loop Control Scheme	46
4.3	Superimposed Nyquist Plots of Loop TFs with PID , PI^α , $[PI]^\alpha$	47

4.4	Limit Cycles with PID , PI^α , and $[PI]^\alpha$ Controllers	49
4.5	Sustained Oscillations in the Plant Output with PID , PI^α , and $[PI]^\alpha$ Controllers	49
4.6	Computation of Limit Cycle Details: PID Case	51
4.7	Computation of Limit Cycle Details: PI^α Case	51
4.8	Computation of Limit Cycle Details: $[PI]^\alpha$ Case	52
4.9	Pictorial View of the Precision Modular Servo Set-up	53
4.10	Superimposed Nyquist Plots for Loop TFs with PID , PI^α , and $[PI]^\alpha$ Controllers	55
4.11	Sustained Oscillations with PID , PI^α , and $[PI]^\alpha$ Controllers	56
4.12	Zoomed View From Figure 4.11	56
5.1	Closed Loop Control System Schematics	60
5.2	Graphical Interpretation of Optimization Problem	63
5.3	A Servo System with Gears	64
5.4	Closed Loop Control Scheme	65
5.5	Points ② and ③ occur before point ① for $-\frac{1}{N(X)}$ plot seen in the arrow direction indicating superiority of PI^α and $[PI]^\alpha$ over PI	69
5.6	Zoomed view of Figure 5.5: fractional and integer PI meeting required phase margin and gain crossover frequency	69
5.7	Point ⑤ occurs before point ④ for $-\frac{1}{N(X)}$ plot seen in the arrow direction indicating superiority of $PI^\alpha D^\beta$ over PID	70
5.8	Zoomed view of Figure 5.7: fractional and integer PID meeting required phase margin and gain crossover frequency	70
5.9	Limit Cycles with PI , PI^α , and $[PI]^\alpha$ Controllers	71
5.10	Sustained Oscillations with PI , PI^α , and $[PI]^\alpha$ Controllers	72
5.11	Limit Cycles with PID and $PI^\alpha D^\beta$ Controllers	72

5.12	Sustained Oscillations with PID and $PI^\alpha D^\beta$ Controllers	73
5.13	Closed Loop Control Schematics	75
5.14	Stability of Limit Cycles for Relay Nonlinearity	76
5.15	Condition for Closed Loop Stability	79
5.16	Nyquist plot of $C(s)N(P)G(s)$ with Performance Specifications and Closed Loop Stability	82
5.17	Limit Cycle and Loop Performance Together when $N(P) = 1$	84
5.18	Performance Analysis using Graph	86
5.19	Zoomed View of Figure 5.18	86
5.20	Limit Cycles	88
5.21	Closed Loop Response	88
6.1	Asymptotic Magnitude Bode Plot for Fractional Zero	94
6.2	Asymptotic Magnitude Bode Plot for Fractional double-term Pole	96
6.3	Asymptotic Phase Bode Plot for Fractional Zero	106
6.4	Asymptotic Phase Bode Plot for Fractional Double-Term Pole	107
6.5	Identification of Fractional-Order TF from Asymptotic Magnitude Bode Plot	114
6.6	Asymptotic Magnitude Bode Plot for ks^α when $\alpha > 0$	115
6.7	Asymptotic Magnitude Bode Plot for ks^α when $\alpha < 0$	115
6.8	Asymptotic Magnitude Bode Plot for $\frac{(s+a)^\alpha}{a^\alpha}$ when $\alpha > 0$	116
6.9	Asymptotic Magnitude Bode Plot for $\frac{(s+a)^\alpha}{a^\alpha}$ when $\alpha < 0$	116
6.10	Loop Analysis using Asymptotic Magnitude and Phase Bode Plots	119
A.1	Pictorial Representation of Matignon's Stability	135

LIST OF TABLES

2.1	Numerical Details for Different Rational Approximation Methods	23
3.1	Results for PI^α and PD^β Controller	36
3.2	Results for $[PI]^\alpha$ Controller	39
3.3	Results for $[PD]^\beta$ Controller	42
4.1	Resultant Designed Controllers	47
4.2	Controller Performance in the Presence of Nonlinearity	52
4.3	List of Parameters	54
4.4	Designed Controllers	54
4.5	Sustained Oscillation Amplitudes with Various Controllers	57
5.1	Design of Integer PI Controller	67
5.2	Design of PI^α Controller	67
5.3	Design of $[PI]^\alpha$ Controller	67
5.4	Design of Integer PID Controller	68
5.5	Design of $PI^\alpha D^\beta$ Controller	68
5.6	Details of Limit Cycle and Sustained Oscillation Amplitudes	74
5.7	Superiority of PI^α and $[PI]^\alpha$ over Integer PI	74
5.8	Superiority of $PI^\alpha D^\beta$ over Integer PID	74
5.9	Limit Cycle Details	89
6.1	Basic Fractional-Order Terms	92

6.2	Asymptotic Magnitude Bode Plots for Remaining Basic Fractional-Order Terms	97
6.3	Asymptotic Magnitude Bode Plot for PI^α Controller	99
6.4	Asymptotic Magnitude Bode Plots for Other FOCs	100
6.5	Asymptotic Phase Bode Plots for Remaining Basic Fractional-Order Terms	109
6.6	Asymptotic Phase Bode Plot for PI^α Controller	110
6.7	Asymptotic Phase Bode Plots for Other FOCs	111

ABBREVIATIONS

FC	Fractional Calculus
FOC	Fractional-Order Controller
PI	Proportional-Integral
PD	Proportional-Derivative
PID	Proportional-Integral-Derivative
TF	Transfer Function
CFE	Continued Fraction Expansion
PSE	Power Series Expansion
IAE	Integral Absolute Error
ITAE	Integral Time Absolute Error
ISE	Integral Square Error
FOPDT	First Order Plus Dead Time
DF	Describing Function
LTI	Linear Time-Invariant
CRONE	Commande Robuste d'Ordre Non-Entier
SOPDT	Second Order Plus Dead Time
PMS	Precision Modular Servo

NOTATIONS

J^n	n -fold Integration
$\mathbb{R}^+, \mathbb{R}_{>0}$	Set of Positive Real Numbers
J_{RL}^α	Riemann-Liouville Fractional Integral
$\Gamma(\alpha)$	Gamma Function
D^n	n^{th} Order Derivative
D_{RL}^α	Riemann-Liouville Fractional Derivative
\mathbb{N}	Set of Natural Numbers
D_C^α	Caputo Fractional Derivative
D_{GL}^α	Grunwald-Letnikov derivative
J_{GL}^α	Grunwald-Letnikov Integral
\mathbb{R}	Set of Real Numbers
$\mathcal{L}\{\cdot\}$	Laplace Transform
$f^{(k)}(t)$	k^{th} Derivative of $f(t)$
\mathbb{Z}	Set of Integer Numbers
$F_{CRONE}(s)$	CRONE Approximation of $F(s)$
dB	decibels
$F_{Matsuda}(s)$	Matsuda Approximation of $F(s)$
$F_{HighCFE}(s)$	High-CFE Approximation of $F(s)$
$F_{LowCFE}(s)$	Low-CFE Approximation of $F(s)$
$F_{Oustaloup}(s)$	Oustaloup Approximation of $F(s)$
$F_{GenOustaloup}(s)$	Generalized Oustaloup Approximation of $F(s)$
$F_{ModOustaloup}(s)$	Modified Oustaloup Approximation of $F(s)$
$F_{GenModOustaloup}(s)$	Generalized Modified Oustaloup Approximation of $F(s)$
$F_{Chareff}(s)$	Chareff Approximation of $F(s)$
$C(s)$	Controller Transfer Function
$G(s)$	Plant Transfer Function
ω_{gc}	Gain Crossover Frequency

ϕ_m	Phase Margin
$N(\cdot)$	Describing Function
GM	Gain Margin
ω_{pc}	Phase Crossover Frequency
$\mathbb{R}_{\geq 0}$	Set of Non-negative Real Numbers
ω_{cr}	Corner/Break Frequency
$\mathbb{R}_{\neq 0}$	Set of Real Numbers Except 0
ω_c	Critical Frequency

CHAPTER 1

Introduction

Classical calculus deals with integer-order differentiation and n -fold integration. Its generalization to handle integrals and derivatives of arbitrary orders (say for instance, the derivative of 1.2635th order) leads to a branch in mathematics widely known as *Fractional Calculus (FC)*. In FC, the word *fractional* is a misnomer, since the order can be real or complex.

In control theory, FC finds applications in systems modeling as well as controller design. The dynamics of the *Fractional-Order Controllers (FOCs)* are governed by fractional-order differential equations. The FOCs such as $(PI^\alpha, [PI]^\alpha)$, $(PD^\beta, [PD]^\beta)$ and $(PI^\alpha D^\beta)$ are superclass of their integer-order counterparts, (PI) , (PD) , and (PID) respectively. Therefore, FOCs are expected to perform better. The work in this thesis primarily investigates the limit cycle performance and asymptotic Bode characteristics of such FOCs. In addition, the thesis also develops unified tuning expressions for three-parameter FOCs to meet Wang-et-al specifications.

1.1 Literature Survey and Motivation

The idea of FC came into existence immediately after the classical calculus was invented. Its first mention is found in a letter written by Leibnitz to L'Hospital in 1695 [Miller and Ross (1993)]. In more than 300 years since then, the concept developed mainly as a pure theoretical field of mathematics that generalized the conventional integer-order calculus to arbitrary orders [Oldham and Spanier (1974)], [Samko et al. (1993)], [Gorenflo and Mainardi (1997)], [Butzer and Westphal (2000)]. Significant contributions were made during this time by some famous mathematicians across the world. A few notable names include L. Euler, J. L. Lagrange, P. S. Laplace, J. B. J. Fourier, N. H. Abel, J. Liouville, B. Riemann, A. K. Grunwald, A. V. Letnikov, J. Hadamard, G. H. Hardy, etc [Torvik and Bagley (1984)], [Kilbas et al. (2006)], [Machado et al. (2011)]. These contributions led to an increased understanding about

the potential of FC in describing the memory and hereditary properties of various materials and processes. The classical calculus, on the other hand, revealed limited abilities in these regards [*Caputo and Mainardi (1971)*], [*Podlubny (1999a)*], [*Mainardi (2010)*], [*Tarasov (2011)*], [*Baleanu (2012)*].

Last few decades witnessed advancements in the computer technology and also the development of numerical methods for finding solutions of fractional-order differential equations. This encouraged the researchers to find applications of FC in various science and engineering fields [*Gorenflo and Mainardi (1997)*], [*Cafagna (2007)*], [*Herrmann (2011)*], [*Ortigueira (2011)*]. The fields include viscoelasticity [*Bagley and Torvik (1983)*], [*Koeller (1984)*], capacitor theory [*Jesus and Machado (2009)*], control theory [*Axtell and Bise (1990)*], [*Vinagre and Chen (2002)*], [*Vinagre et al. (2002)*], fractals [*TATOM (1995)*], [*Mainardi (1997)*], oscillators [*Ahmad et al. (2001)*], [*Petráš (2008)*], polymer physics and rheology [*Schiessel et al. (2000)*], [*Hilfer et al. (2000)*], bioengineering [*Magin (2006)*], [*Magin (2010)*], multipoles and electromagnetic theory [*Engheta (1996)*], [*Engheia (1997)*], electrochemistry [*Oldham (2010)*], signals and systems [*Ortigueira and Machado (2006)*], and many more [*Ross (1975)*], [*Kiryakova (1993)*], [*Sabatier et al. (2007)*], [*Baleanu et al. (2010)*], [*Das (2011)*].

In control theory, the FC is applied in two ways: 1) System modeling, 2) Controller design [*DiStefano et al. (1967)*], [*Chen (2006)*], [*Monje et al. (2008)*], [*Monje et al. (2010)*], [*Valerio and Da Costa (2013)*]. In the latter application, one designs FOCs whose dynamics are governed by fractional-order differential equations [*de Oliveira Valério (2005)*], [*Caponetto (2010)*], [*Chen and Vinagre (2010)*], [*Petras (2011)*], [*Baleanu (2012)*].

The continuous domain Transfer Function (TF) of a FOC has irrational form structure, which is a ratio of polynomials having arbitrary powers (also known as *pseudopolynomials* [*Petráš et al. (2002a)*]). For the rational approximation of such TFs, several methods have been proposed in the literature. A survey of these methods is found in [*Vinagre et al. (2000)*], [*Podlubny et al. (2002)*]. Some of the popular methods include Carlson [*Carlson and Halijak (1964)*], Charef [*Charef (2006)*], Matsuda [*Matsuda and Fujii (1993)*], Crone [*de Oliveira Valério (2005)*], Continued Fraction Expansion (CFE) [*Roy (1967)*], [*Podlubny et al. (2002)*], Oustaloup [*Oustaloup et al. (2000)*], etc.

The selection of a particular method for rational approximation depends on factors

such as allowable order of the resultant TF, degree of accuracy in the desired frequency range, time-domain behaviour, etc. Considering such factors together, it is difficult to claim one of these methods as the best one [*de Oliveira Valério (2005)*]. However, amongst them, the Oustaloup method [*Oustaloup et al. (2000)*] is used popularly to obtain a reasonably good rational fit for the given fractional-order TF within the specified frequency range [*Xue et al. (2006b)*]. A modified version of Oustaloup method provides better approximation at lower and upper frequency ends, though at the cost of increased order [*Xue et al. (2006b)*], [*Xue et al. (2007)*].

Several methods are proposed in the literature for the discretization of fractional-order TF as well. The methods include direct discretization using Al-Alaoui operator via CFE [*Chen and Moore (2002)*], direct recursive discretization with Tustin operator, discretization using backward-difference operator via Power Series Expansion (PSE) [*Chen et al. (2009)*], discretization algorithm based on the quadrature formula [*Diethelm (1997)*], an approach based on B-splines function [*Heleschewitz and Matignon (1998)*], etc.

The irrational form TF of FOCs enables them to possess better abilities over their integer-order counterparts in meeting stringent loop shaping requirements. The FOCs such as PI^α , $[PI]^\alpha$, PD^β , $[PD]^\beta$, $PI^\alpha D^\beta$ [*Barbosa et al. (2004)*], [*Xue et al. (2007)*], [*Tavazoei (2012)*] are superclass of their integer counterparts (i.e. PI , PD , PID). Therefore, one expects them to perform better owing to the design flexibility offered by their additional parameters [*Vinagre and Chen (2002)*], [*Chen et al. (2009)*], [*Yeroglu and Tan (2011)*]. For instance, the $PI^\alpha D^\beta$ controller has additional tuning parameters α , β than the PID , which makes it better [*Podlubny (1999b)*].

Design of FOCs has received a considerable attention in the literature from both academic and industrial point of view [*de Oliveira Valério (2005)*], [*Micharet (2006)*], [*Vinagre et al. (2007)*]. In [*Monje et al. (2004a)*], [*Monje et al. (2005)*], the design of $PI^\alpha D^\beta$ has been presented to meet five design specifications (We refer them as *Monje et-al specifications*) by numerically solving a constrained optimization problem. The solution in this case is possible with $PI^\alpha D^\beta$ controller due to its five parameters unlike the conventional PID which has only three parameters. The above work is further extended in [*Valério and Da Costa (2006)*] to develop analytical rules for $PI^\alpha D^\beta$ controllers meeting Monje et-al specifications. For this purpose, the change in the nu-

merically obtained controller parameters due to variations in the plant parameters is translated into tuning rules by means of least square fitting.

Another interesting work in [Zhao et al. (2005)] discusses the superiority of $PI^\alpha D^\beta$ over PID for controlling fractional-order systems in order to meet desired stability margins. The work in [Padula and Visioli (2011)] constructs tuning rules for $PI^\alpha D^\beta$ to minimize the Integral Absolute Error (IAE) with a constraint on the maximum sensitivity. In [Xue et al. (2006a)], it has been shown that under the given optimization condition of minimizing performance indices such as Integral Time Absolute Error (ITAE) and Integral Square Error (ISE), the best $PI^\alpha D^\beta$ controller outperforms the best PID controller. The work in [Kesarkar and Narayanasamy (2014)] presents the superiority of $PI^\alpha D^\beta$ over conventional PID in minimizing IAE and ISE for the cart-servo laboratory set-up.

In the existing fractional control literature, a large number of works are devoted to the tuning of three-parameter FOCs such as PI^α , $[PI]^\alpha$, PD^β , $[PD]^\beta$. The design of PI^α and $[PI]^\alpha$ controllers for robust velocity servo plant has been presented in [Wang et al. (2009a)]. The work in [Wang et al. (2009b)] considers First Order Plus Dead Time (FOPDT) systems and designs PI^α and $[PI]^\alpha$ controllers. The design of PI^α and $[PI]^\alpha$ controllers for a class of fractional-order systems which can accurately model many real systems in bioengineering (e.g. Cole-Cole model [Magin (2006)]) is discussed in [Luo et al. (2010)]. The paper also discusses the design for fractional horsepower dynamometer. Design of PI^α controllers for the class of plants studied in [Wallén et al. (2002)] has been discussed in [Chen et al. (2006)].

Design of PD^β for a class of typical second-order plants is discussed in [Li and Chen (2008)]. Design of PD^β controller for the position control of dynamometer is presented in [Li et al. (2010)]. In [Luo et al. (2011a)], PD^β controller is designed systematically for the generalized fractional capacitor membrane model. $[PD]^\beta$ controller design is proposed for robust motion control systems in [Luo and Chen (2009b)]. The $[PD]^\beta$ controller design for the FC model of membrane charging has been presented in [Luo and Chen (2009a)].

In the above works, the preferred specifications are gain crossover frequency, phase margin, and isodamping [Chen et al. (2003)], [Wang et al. (2009a)], [Wang et al. (2009b)] (For convenience, we collectively refer these specifications as Wang-et-al

specifications)¹. It is interesting to observe in these works that the tuning expressions of the controllers meeting Wang-et-al specifications have been derived by considering a particular plant TF. If one desires to tune them for some other plant TF, the exercise of deriving the corresponding expressions needs to be carried out again, which is complex and time-consuming. Instead, one can aim at unifying the above works and develop the controller expressions which are ready-to-use for any plant TF of integer or fractional-order. The exploration in this direction can considerably save the controller designer's time and efforts. In this thesis, we develop such unified tuning expressions for PI^α , $[PI]^\alpha$, PD^β , $[PD]^\beta$ controllers by introducing a universal plant structure.

For the systems containing separable nonlinearity in cascade, the designed controllers usually produce undesirable sustained oscillations in the plant output response. This phenomenon is due to the existence of stable limit cycles [Gopal (2012)] in the loop. Generally, the *Describing Function (DF)* method is adopted for the analysis of these limit cycles so as to obtain the approximate values of their amplitude and frequency [Atherton (1975)], [Slotine et al. (1991)], [Chang and Chang (1994)], [Azenha and Machado (1998)], [Khalil and Grizzle (2002)]. DF is a linearization of a nonlinear element subjected to a sinusoidal input [Vander Velde (1968)], [Olsson (1995)]. In DF method, the limit cycle details are obtained based on the intersection point between the Nyquist plot of the loop TF and the plot of the negative inverse of the DF [Gopal (2012)]. The work in [Azenha and Machado (1998)], for instance, computes such limit cycle details using DF method for the loop containing a *PID* controller and a system with nonlinear friction or dynamic backlash.

The fractional-order behavior can appear for the control loop containing systems with separable nonlinearities at two places, 1) DF model of the nonlinearity, 2) loop TF. Application of FC in modeling the DF of a few nonlinearities has been investigated in recent works. In [Duarte and Machado (2009b)] and [Duarte and Machado (2009c)], the dynamics of a system consisting of a mass subjected to nonlinear friction is analyzed from the DF perspective which reveals a fractional-order behavior. Fractional-order DF for two masses with backlash has been discussed in [Duarte and Machado (2009a)]. In [Tenreiro Machado (2014)], the concept of DF was generalized to fractional orders for the static backlash nonlinearity. The fractional-order dynamics of systems containing

¹One may also refer them as *Chen-et-al specifications* considering the works by Chen-et-al in [Chen et al. (2003)], [Chen et al. (2006)], [Luo and Chen (2009b)], [Luo and Chen (2009a)].

backlash and impact phenomena have been investigated through DF method in [Barbosa and Machado (2002)]. Fractional order modeling for the DF of dynamic backlash is explored in [Tenreiro Machado (2013)].

On the other hand, control loops which consist of fractional-order TFs and a separable nonlinearity have been considered in the literature [Yeroglu and Tan (2010)], [Atherton et al. (2014)]. The work in [Yeroglu and Tan (2010)] deals with limit cycle prediction for systems which have fractional-order TF and a separable nonlinearity. In [Atherton et al. (2014)], the approximate details of the limit cycles are computed for a feedback system containing fractional-order plant and relay nonlinearity using DF method and the accurate details of limit cycles are obtained using Tsytkin method of A loci [TSytkin (1984)], [Atherton (2011)]. The work in [Valério and da Costa (2004)] introduces a MATLAB toolbox for analyzing fractional-order systems with fixed parameter values and hard nonlinearities. The construction of limit cycle locus for uncertain fractional-order systems with separable nonlinearities has been investigated in [Nataraj and Kalla (2009)]. The stability analysis of autonomous fractional-order systems with such nonlinearities by means of investigating the existence of limit cycles has been discussed in [Petras (2011)].

Only a few works are reported in the fractional-control-literature that address the study of FOC-performance in the presence of separable nonlinearities. The effects of saturation nonlinearity on the fractional-order loop TF are studied in [Manabe (1963)], [Manabe (2003)], [Manabe (2004)]. The works suggest that when the saturation and time delay are present in the loop, the open-loop TF must take a form of fractional-order integral for the better control performance. The advantage of designed fractional-order PD controller to obtain a better position tracking performance for the ultra low-speed position servo system containing nonlinear friction is illustrated in [Luo et al. (2011b)]. A notable work in this regard is also found in [Barbosa et al. (2007)], where a fractional derivative controller D^α is designed and examined for the double integrator plant in the presence of separable nonlinearities such as saturation and backlash. The work examines the effects of variation in the fractional-order α on the limit cycle performance of the control loop and illustrates the use of DF method for the limit cycle analysis of such fractional-control loops.

The works in [Ma and Hori (2003)], [Ma and Hori (2004a)] observe a significant

improvement in the vibration suppression in the closed loop system output with PI^1D^β (i.e. $\alpha = 1$) over integer PID for a torsional system containing gear-backlash. In [Ma and Hori (2004b)], the authors introduce a fractional-order version of Q-filter to substitute the integer-order Q-filter used in conventional disturbance observer for vibration suppression control of torsional system. It is shown that the fractional-order Q-filter can achieve a clear-cut and effective adjustment of trade-off between stability margin loss and the strength of vibration suppression. It is also important to notice the studies in [Oliveira et al. (2003)], [Oliveira et al. (2006)] and [Oliveira et al. (2012)], which illustrate the use of DF for the synthesis of integer-order controllers in order to produce the given limit cycle effects.

Motivated from the above works, one can systematically examine the possible superiority of FOCs over their integer-order counterparts in suppressing the sustained oscillation amplitudes by minimizing the limit cycle effects for plants containing separable nonlinearities. In this regard, we begin with observing the limit cycle performance of FOCs when they are tuned to meet Wang-et-al specifications. Later, we develop a DF based controller design framework and specifically target the limit cycle performance for the plants which contain separable nonlinearity such as backlash and relay. Under such framework, the advantage of FOCs over their integer-order counterparts for the suppression of sustained oscillation amplitudes is examined in detail.

In classical control, one performs design and analysis of the loop TF by using techniques such as root locus, Bode plot, Nyquist plot, Nichol chart, etc [Ogata and Yang (1970)], [Kuo (1981)], [Nagrath and Gopal (1982)], [Dorf and Bishop (2011)]. Bode plots are popular in control engineering for analyzing the frequency response of a given TF [Bode (1940)], [Bode (1945)]. Obtaining exact Bode plot for the given TF requires certain amount of computation for which one generally prefers software tools such as MATLAB [MATLAB (2010)], SCILAB etc. However, it is also possible to draw their approximate versions known as *Asymptotic Bode Plots* by doing relatively simpler calculations [Cheever and Li (1998)], [Dorf and Bishop (2011)]. These are straight-line approximations that are sketched to perform a quick manual analysis of the designed control system without much compromise on the accuracy [DiStefano et al. (1967)]. They are also useful for understanding the role of each parameter of the given TF in deciding the shape of its Bode response [Gajdošík and Žáková (2011)].

In the context of asymptotic Bode plots of fractional-order TFs, only a brief mention is found in the literature [Monje et al. (2004b)], [Chen and Vinagre (2010)] for fractional-order lead compensator. We explore further in this direction and develop asymptotic magnitude and phase Bode plots for FOCs such as PI^α , PD^β , $[PI]^\alpha$, $[PD]^\beta$, and $PI^\alpha D^\beta$. The asymptotic plots are also constructed for the general fractional commensurate order TFs. The identification of fractional-order TF from the given asymptotic magnitude Bode plot is demonstrated. Furthermore, the application of asymptotic magnitude and phase Bode plots for manual analysis of designed fractional-control loop is presented in detail.

1.2 Research Contributions

The research contributions of our thesis are summarized as follows:

1. Development of unified tuning expressions for FOCs such as PI^α , PD^β , $[PI]^\alpha$, $[PD]^\beta$ to meet Wang-et-al specifications.
2. Investigations on the superiority of FOCs for suppressing the limit cycle effects while meeting Wang-et-al Specifications.
3. Construction of a framework to design and compare limit cycle minimizing controllers for plants with backlash nonlinearity: Demonstration with integer and fractional-order controllers to claim the fractional superiority.
4. Design of controllers to reduce amplitude of sustained oscillations for plants with relay nonlinearity: Illustration with PI^α controller.
5. Development of asymptotic magnitude and phase Bode plots for FOCs such as PI^α , PD^β , $[PI]^\alpha$, $[PD]^\beta$, and $PI^\alpha D^\beta$.

The chapter-wise organization of this thesis is explained in the next section in detail.

1.3 Organization of Thesis

- Chapter 2 discusses the preliminaries of FC and FOCs.

- In chapter 3, a universal plant structure is proposed which accommodates any integer or fractional-order plant TF. For such a plant, the tuning expressions are derived for PI^α , $[PI]^\alpha$, PD^β , $[PD]^\beta$ to satisfy the Wang-et-al specifications. With the help of numerical examples for different class of plants, the usefulness of the deduced expressions is demonstrated.
- Chapter 4 presents an observation that the FOCs such as PI^α , $[PI]^\alpha$ are better than integer-order PID controller in limit cycle suppression, when a typical motion-servo plant with separable backlash nonlinearity is considered. The controllers are tuned for the plant TF to meet Wang-et-al specifications. Furthermore, such a fractional superiority is observed for the precision modular servo laboratory set-up.
- Chapter 5 considers the controller design in order to suppress the limit cycle effects for two cases: 1) plant with backlash and 2) plant containing relay.
 - In the first case, a constrained optimization problem is formulated using which the integer-order controllers (PI and PID) and their respective fractional-order counterparts (PI^α , $[PI]^\alpha$ and $PI^\alpha D^\beta$) are designed for the plant with backlash. Furthermore, its graphical interpretation is presented which is useful to compare the designed controllers in terms of limit cycle suppression. The illustration is made with a numerical example and the superiority of FOCs over integer-order controllers is claimed.
 - In the second case, a plant having relay nonlinearity in its model is considered for which an optimization problem is formulated for the controller design so as to meet the desired loop performance and to shape the limit cycles in a certain way. A FOC design is demonstrated under this framework.
- Chapter 6 presents the development of asymptotic magnitude and phase bode plots for FOCs such as PI^α , PD^β , $[PI]^\alpha$, $[PD]^\beta$, and $PI^\alpha D^\beta$. For this purpose, first a few basic terms are defined and their asymptotic plots are formulated. Later, such plots are utilized to obtain the asymptotic magnitude and phase bode plots for FOCs. The development of such plots for general fractional commensurate order TFs is also shown. Two applications of this work are presented, 1) Identification of fractional-order TF from the given asymptotic magnitude Bode plot, 2)

Analysis of a given fractional control loop using asymptotic magnitude and phase Bode plots.

- Chapter 7 draws the concluding remarks and presents the scope of future work in this area.

CHAPTER 2

Preliminaries of Fractional Calculus and Fractional-Order Control

2.1 Introduction

Similar to the generalization of integer exponents into fractional exponents, the idea of Fractional Calculus (FC) can be perceived as a natural outgrowth of conventional integer-order calculus. In case of an integer exponent (say) $x^4 = 1 \cdot x \cdot x \cdot x \cdot x$, its physical meaning can be interpreted as the multiplication of 1 four times by x . In case of fractional exponent $x^{3.45}$, this interpretation is not possible since one cannot conceive the meaning of multiplying one 3.45 number of times by x . But still, the term $x^{3.45}$ exists and has definite value for the given x which is verifiable by infinite series expansion.

In the same way, the meaning of derivatives and integrals of arbitrary orders is arguably impossible to grasp [Loverro (2004)] unlike their integer-order counterparts. Nevertheless, they still exist as long as one sticks to the mathematical world alone. Their formulations emerge quite naturally by extending the notions of integer-order calculus to arbitrary orders. It is important to note that such extension can lead to orders which are real or even complex. We restrict the work in this thesis only to arbitrary real orders.

Let us consider an infinite sequence of n -fold integrals and n^{th} order derivatives, which is presented as follows:

$$\dots, \int_a^t d\tau_2 \int_a^{\tau_2} f(\tau_1) d\tau_1, \int_a^t f(\tau_1) d\tau_1, f(t), \frac{df(t)}{dt}, \frac{d^2f(t)}{dt^2}, \dots \quad (2.1)$$

The sequence (2.1) can be made continuous by considering the derivatives and integrals of arbitrary real orders.

In this chapter, we discuss the basics of such FC operations and their applications to the control theory in terms of development of Fractional-Order Controllers (FOCs).

2.2 Definitions in Fractional Calculus

The following definitions are used to describe the fractional derivative and integration operation:

1. Riemann-Liouville Fractional Integral [*Loverro (2004)*]

This definition is derived directly from the traditional expression of repeated integration. For this purpose, it starts with the following Cauchy's formula for evaluating n^{th} integration (J^n) of the function $f(t)$:

$$J^n f(t) = \frac{1}{(n-1)!} \int_a^t (t-\tau)^{n-1} f(\tau) d\tau \quad (2.2)$$

The subscripts a and t denote the two limits (or terminals [*Ross (1977)*]) related to the operation. Since (2.2) contains factorial, it cannot be used for non-integer n . By replacing the factorial by its analytical expansion i.e. gamma function in order to generalize (2.2) for all $\alpha \in \mathbb{R}^+$, we obtain Riemann-Liouville fractional integral J_{RL}^α as follows:

$$J_{RL}^\alpha f(t) = \frac{1}{\Gamma(\alpha)} \int_a^t (t-\tau)^{\alpha-1} f(\tau) d\tau \quad (2.3)$$

where, the gamma function $\Gamma(\alpha)$ is defined by the integral

$$\Gamma(\alpha) = \int_0^\infty e^{-t} t^{\alpha-1} dt \quad (2.4)$$

Properties

(a) Integration of order, $\alpha = 0$

$$J_{RL}^0 f(t) = f(t) \quad (2.5)$$

(b) Repeated Integration

$$J_{RL}^\alpha J_{RL}^\beta f(t) = J_{RL}^{\alpha+\beta} f(t) \quad (2.6)$$

where, $\alpha, \beta \in \mathbb{R}^+$.

(c) Convolution

Let the $\phi_\alpha(t)$ be defined as:

$$\phi_\alpha(t) = \frac{t^{\alpha-1}}{\Gamma(\alpha)} \quad (2.7)$$

Then, (2.3) can be expressed as the following convolution:

$$J_{RL}^\alpha f(t) = \phi_\alpha(t) * f(t) \quad (2.8)$$

2. Riemann-Liouville Fractional Derivative [*Podlubny (1999a)*]

The fractional derivative D_{RL}^α is expressed as:

$$D_{RL}^\alpha := D^n D^{\alpha-n} = D^n J_{RL}^{n-\alpha} \quad (2.9)$$

Where, D denotes derivative operation and $(n-1) < \alpha \leq n$; ($n \in \mathbb{N}$).

Therefore, from (2.3) and (2.9), the Riemann-Liouville fractional derivative is obtained as follows:

$$D_{RL}^\alpha f(t) = \frac{d^n}{dt^n} \left[\frac{1}{\Gamma(n-\alpha)} \int_a^t \frac{f(\tau)}{(t-\tau)^{\alpha-n+1}} d\tau \right] \quad (2.10)$$

3. Caputo Fractional Derivative [*Vinagre et al. (2002)*]

The fractional derivative D_C^α is expressed as:

$$D_C^\alpha := D^{\alpha-n} D^n = J_{RL}^{n-\alpha} D^n \quad (2.11)$$

Therefore, from (2.3) and (2.11), the Caputo fractional derivative is obtained as follows:

$$D_C^\alpha f(t) = J_{RL}^{n-\alpha} f^n(t) = \frac{1}{\Gamma(n-\alpha)} \int_a^t \frac{f^n(\tau)}{(t-\tau)^{\alpha-n+1}} d\tau \quad (2.12)$$

4. Grunwald-Letnikov Derivative [*Xue et al. (2007)*]

We have the following fundamental definition of n^{th} order derivative ($n \in \mathbb{N}$):

$$D^n f(t) = \lim_{h \rightarrow 0} \frac{1}{h^n} \sum_{k=0}^n (-1)^k \binom{n}{k} f(t - kh) \quad (2.13)$$

where,

$$\binom{n}{k} = \frac{n!}{(n-k)!k!} = \frac{\Gamma(n+1)}{\Gamma(n-k+1)\Gamma(k+1)}$$

The generalization of (2.13) to α^{th} order ($\alpha \in \mathbb{R}^+$) leads to the following Grunwald-Letnikov derivative (D_{GL}^α):

$$D_{GL}^\alpha f(t) = \lim_{h \rightarrow 0} \frac{1}{h^\alpha} \sum_{k=0}^{\lceil \frac{t-a}{h} \rceil} (-1)^k \binom{\alpha}{k} f(t - kh) \quad (2.14)$$

where,

$$\binom{\alpha}{k} = \frac{\Gamma(\alpha+1)}{\Gamma(\alpha-k+1)\Gamma(k+1)}$$

In (2.14), $f(t)$ is defined over $[a, t]$. Also, $\lceil \frac{t-a}{h} \rceil$ truncates $(\frac{t-a}{h})$ to integer.

5. Grunwald-Letnikov Integral [Loverro (2004)]

Generalization of (2.13) to $(-\alpha)^{th}$ order ($\alpha \in \mathbb{R}^+$) leads to the following Grunwald-Letnikov integral (J_{GL}^α):

$$J_{GL}^\alpha f(t) = D^{-\alpha} f(t) = \lim_{h \rightarrow 0} \frac{1}{h^{-\alpha}} \sum_{k=0}^{\lceil \frac{t-a}{h} \rceil} (-1)^k \binom{-\alpha}{k} f(t - kh) \quad (2.15)$$

Using the identity $\binom{-\alpha}{k} = (-1)^k \frac{\Gamma(\alpha+k)}{\Gamma(\alpha)k!}$, we rewrite (2.15) as follows:

$$J_{GL}^\alpha f(t) = \lim_{h \rightarrow 0} h^\alpha \sum_{k=0}^{\lceil \frac{t-a}{h} \rceil} \frac{\Gamma(\alpha+k)}{\Gamma(\alpha)k!} f(t - kh) \quad (2.16)$$

6. Miller-Ross Sequential Fractional Derivative [Podlubny (1999a)]

It is defined as follows:

$$D^\alpha f(t) = D^{\alpha_1} D^{\alpha_2} \dots D^{\alpha_n} f(t) \quad (2.17)$$

where,

$$\alpha = \sum_{k=1}^n \alpha_k, 0 < \alpha_k \leq 1 \quad (2.18)$$

This definition is useful for obtaining fractional derivative of any arbitrary order. The derivative operator D^α can be Riemann-Liouville or Caputo.

7. Oldham and Spanier [Das (2011)]

$$\frac{d^q f(\beta x)}{dx^q} = \beta^q \frac{d^q f(\beta x)}{d(\beta x)^q} \quad (2.19)$$

This makes it suitable for the study of scaling and scale invariance. There is connection between local-scaling, box-dimension of an irregular function and order of Local Fractional Derivative.

8. Kolwankar and Gangal [Das (2011)]

Local fractional derivative is defined by Kolwankar and Gangal to explain the behavior of *continuous but nowhere differentiable* function. For $0 < q < 1$, the local fractional derivative at point $x = y$, for $f : [0, 1] \rightarrow \mathbb{R}$ is:

$$D^q f(y) = \lim_{x \rightarrow y} \frac{d^q(f(x) - f(y))}{d(x - y)^q} \quad (2.20)$$

Some Important Observations

1. By virtue of its form, the definition (2.14) is utilized for the numerical evaluation of fractional derivatives. On the other hand, Riemann-Liouville (2.10) and Caputo (2.12) definitions are useful in finding the fractional derivatives analytically [Loverro (2004)].
2. Grunwald-Letnikov derivative given in (2.14) can also be expressed as follows [Podlubny (1999a)]:

$$D_{GL}^\alpha f(t) = \sum_{k=0}^m \frac{f^{(k)}(a)(t - a)^{-\alpha+k}}{\Gamma(-\alpha + k + 1)} + \frac{1}{\Gamma(-\alpha + m + 1)} \int_a^t (t - \tau)^{m-\alpha} f^{(m+1)}(\tau) d\tau \quad (2.21)$$

This is true under the assumption that the derivatives $f^{(k)}(t)$, ($k = 1, 2, \dots, m + 1$) are continuous in the closed interval $[a, t]$ and that m is an integer number

satisfying the condition $m > \alpha - 1$. The smallest possible value for m is obtained by the inequality $m \leq \alpha < m + 1$.

For the above assumptions, Riemann-Liouville fractional derivative given in (2.10) can also be expressed as follows:

$$D_{RL}^{\alpha} f(t) = \sum_{k=0}^m \frac{f^{(k)}(a)(t-a)^{-\alpha+k}}{\Gamma(-\alpha+k+1)} + \frac{1}{\Gamma(-\alpha+m+1)} \int_a^t (t-\tau)^{m-\alpha} f^{(m+1)}(\tau) d\tau \quad (2.22)$$

Therefore, from (2.21) and (2.22), the Grunwald-Letnikov derivative definition (2.14) is equivalent to the Riemann-Liouville derivative definition (2.10) under the above discussed assumptions.

3. On substituting $n = m + 1$, Riemann-Liouville derivative definition (2.22) can be rewritten as:

$$\begin{aligned} D_{RL}^{\alpha} f(t) &= \sum_{k=0}^{n-1} \frac{f^{(k)}(a)(t-a)^{-\alpha+k}}{\Gamma(-\alpha+k+1)} + \frac{1}{\Gamma(-\alpha+n)} \int_a^t (t-\tau)^{n-1-\alpha} f^{(n)}(\tau) d\tau \\ &= \frac{1}{\Gamma(n-\alpha)} \int_a^t \frac{f^{(n)}(\tau)}{(t-\tau)^{\alpha-n+1}} d\tau + \sum_{k=0}^{n-1} \frac{f^{(k)}(a)(t-a)^{-\alpha+k}}{\Gamma(-\alpha+k+1)} \end{aligned} \quad (2.23)$$

Therefore, using (2.7), (2.12), and (2.23), we get:

$$D_{RL}^{\alpha} f(t) = D_C^{\alpha} f(t) + \sum_{k=0}^{n-1} \phi_{k-\alpha+1}(t-a) f^{(k)}(a) \quad (2.24)$$

The equation (2.24) represents the relationship between Riemann-Liouville and Caputo derivatives.

4. With $a = 0$, Caputo's derivative (2.12) of a constant is 0 whereas the Riemann-Liouville derivative of a constant is unbounded at $t = 0$. However, if one considers the lower terminal a as $-\infty$ in the Riemann-Liouville derivative definition (2.10), the derivative of a constant is 0.
5. Short Memory Principle [Podlubny (1999a)]: It follows from the coefficients in the Grunwald-Letnikov definition (2.14) that for $t \gg a$, the role of the *history*

of the behavior of the function $f(t)$ near the lower terminal a can be neglected. This leads to the following *short memory principle* which takes into account the behavior of $f(t)$ only in the recent past, i.e. in the interval $[t - L, t]$ instead of $[a, t]$, where L is the memory length:

$$D_{GL}^\alpha f(t) := {}_a D_t^\alpha \approx {}_{t-L} D_t^\alpha, \quad (t < a + L) \quad (2.25)$$

Thus, according to (2.25), the Grunwald-Letnikov fractional derivative with the fixed lower terminal a is approximated by the one with moving lower terminal $t - L$. Due to this, the number of addends in the approximated derivative definition never exceeds $[L/h]$. This simplification, however, leads to some inaccuracy due to loss in information.

2.3 Laplace Transform of Fractional Derivatives

Laplace transform of the function $f(t)$ is a function $F(s)$ of the complex variable s . The $F(s)$ is obtained as:

$$F(s) := \mathcal{L}\{f(t)\} = \int_0^\infty e^{-st} f(t) dt \quad (2.26)$$

The Laplace transform of fractional derivatives (with the lower terminal $a = 0$) are as follows [Podlubny (1999a)]:

1. Laplace Transform of Riemann-Liouville Derivative

$$\mathcal{L}\{D_{RL}^\alpha f(t)\} = s^\alpha F(s) - \sum_{k=0}^{n-1} s^k D_{RL}^{(\alpha-k-1)} f(0) \quad (2.27)$$

where, $F(s) = \mathcal{L}\{f(t)\}$ and $(n - 1) \leq \alpha < n$.

2. Laplace Transform of Caputo Derivative

$$\mathcal{L}\{D_C^\alpha f(t)\} = s^\alpha F(s) - \sum_{k=0}^{n-1} s^{\alpha-k-1} f^{(k)}(0) \quad (2.28)$$

where, $(n - 1) \leq \alpha < n$.

3. Laplace Transform of Grunwald-Letnikov Derivative (2.21) with $a = 0$

$$\mathcal{L}\{D_{GL}^\alpha f(t)\} = s^\alpha F(s) \quad (2.29)$$

As seen from (2.27), for calculating Laplace transform of Riemann-Liouville derivative one requires initial conditions $D_{RL}^{(\alpha-k-1)} f(0)$, which are fractional derivatives. On the other hand, the Laplace transform of Caputo derivative (2.28) requires initial conditions $f^{(k)}(0)$, which are integer-order derivatives. Since such initial conditions can be easily interpreted from physical data and observations, Caputo derivative is a more practical definition than Riemann-Liouville derivative.

2.4 Fractional-Order Transfer Functions

Fractional-order differential/integral equation are composed of fractional-order derivatives/integrals. A system of such equations describes the dynamics of fractional-order processes.

Let us consider a Linear Time-Invariant (LTI) fractional-order system which is governed by the following fractional-order ordinary differential equation:

$$\begin{aligned} a_n D^{\alpha_n} y(t) + a_{n-1} D^{\alpha_{n-1}} y(t) + \dots + a_0 D^{\alpha_0} y(t) = \\ b_m D^{\beta_m} u(t) + b_{m-1} D^{\beta_{m-1}} u(t) + \dots + b_0 D^{\beta_0} u(t) \end{aligned} \quad (2.30)$$

where $y(t)$ and $u(t)$ denote output and input signals, respectively.

Also, $a_i, \alpha_i (i = 0, 1, \dots, n), b_k, \beta_k (k = 0, 1, \dots, m) \in \mathbb{R}; n, m \in \mathbb{N}$.

In (2.30), Caputo's derivative definition (2.12) is preferred (with $a = 0$) as it allows consideration of conventional initial conditions.

The Laplace transform of (2.30) assuming zero initial conditions results into the

following Transfer Function (TF):

$$\frac{Y(s)}{U(s)} = \frac{b_m s^{\beta_m} + b_{m-1} s^{\beta_{m-1}} + \dots + b_0 s^{\beta_0}}{a_n s^{\alpha_n} + a_{n-1} s^{\alpha_{n-1}} + \dots + a_0 s^{\alpha_0}} \quad (2.31)$$

where, $Y(s) = \mathcal{L}\{y(t)\}$, $U(s) = \mathcal{L}\{u(t)\}$

The TF of the form (2.31) represents either a *commensurate* or a *non-commensurate* order system. It is a *commensurate* order system, if there exists a greatest common divisor $q \in \mathbb{R}$ such that $\alpha_i = qe_i$, $\beta_k = qf_k$; $e_i, f_k \in \mathbb{Z}$. In such case, q is the commensurate order, which can be rational or irrational.

The discussions on the stability of fractional-order LTI systems and the analytical solutions of fractional-order ordinary differential equations have been provided in APPENDIX A.

2.5 Continuous Domain Approximation Methods

The fractional-order TFs have irrational form, which is the ratio of pseudo-polynomials, i.e. polynomials of arbitrary orders. From their approximation using rational functions, several methods have been proposed in the literature, which are as follows:

1. Carlson [*Carlson and Halijak (1964)*]

The Carlson rational approximation of the fractional-order term $H(s) = [G(s)]^\alpha$ is obtained recursively as follows:

$$H_i(s) = H_{i-1}(s) \frac{(v-1)(H_{i-1}(s))^v + (v+1)G(s)}{(v+1)(H_{i-1}(s))^v + (v-1)G(s)} \quad (2.32)$$

Where, $i \in \mathbb{N}$; $H_0(s) = 1$; $\alpha = \frac{1}{v}$. $G(s)$ is a rational function of complex variable s . The approximation (2.32) is applicable only if $v \in \mathbb{N}$. In other words, α can only assume values $1, \frac{1}{2}, \frac{1}{3}, \frac{1}{4}$, etc.

2. CRONE [*de Oliveira Valério (2005)*]

(CRONE is the (French) acronym of *Commande Robuste d'Ordre Non-Entier*)

For $F(s) = s^\alpha$ ($0 < \alpha \leq 1$), its CRONE approximation is given as follows:

$$F_{CRONE}(s) = C_0 \prod_{n=1}^N \frac{1 + \frac{s}{\omega_{zn}}}{1 + \frac{s}{\omega_{pn}}} \quad (2.33)$$

where,

$$\begin{aligned} k &= \left(\frac{\omega_h}{\omega_l} \right)^{\frac{|\alpha|}{N}}, \eta = \left(\frac{\omega_h}{\omega_l} \right)^{\frac{1-|\alpha|}{N}}, \omega_{z1} = \omega_l \sqrt{\eta} \\ \omega_{pn} &= \omega_{zn} k \quad n = 1, 2, \dots, N \\ \omega_{z(n+1)} &= \omega_{pn} \eta \quad n = 1, 2, \dots, (N-1) \end{aligned}$$

N is order of approximation. $[\omega_l, \omega_h]$ is the frequency range of interest. C_0 is such that $F_{CRONE}(s)$ magnitude of 0 decibels (dB) at $\omega = 1$ rad/s.

3. Matsuda [Matsuda and Fujii (1993)]

For the Matsuda approximation of $F(s) = s^\alpha$, its gain ($|F(j\omega)|$) is found at several frequencies. The number of frequencies determines the order of approximation. Let the frequencies chosen be $\omega_0, \omega_1, \omega_2, \dots, \omega_N$. Then, the Matsuda approximation $F_{Matsuda}(s)$ is obtained as follows:

$$F_{Matsuda}(s) = \beta_0 + \frac{s - \omega_0}{\beta_1 + \frac{s - \omega_1}{\beta_2 + \frac{s - \omega_2}{\beta_3 + \dots}}} \quad (2.34)$$

where,

$$\begin{aligned} \beta_0 &= d_0(\omega_0), \beta_k = \frac{\omega_k - \omega_{k-1}}{d_{k-1}(\omega_k) - d_{k-1}(\omega_{k-1})} \\ d_0(\omega) &= |\omega^\alpha|, d_k(\omega) = \frac{\omega - \omega_{k-1}}{d_{k-1}(\omega) - d_{k-1}(\omega_{k-1})} \\ k &= 1, 2, \dots, N \end{aligned}$$

4. Continued Fraction Expansion (CFE) [Roy (1967)]

Let us consider the approximation of $F(s) = s^\alpha$. There are following two categories of this method:

(a) High CFE ($F_{HighCFE}(s)$)

This is a good approximation for higher frequencies ($\omega > \lambda; \lambda > 0$), which is obtained as follows:

$$F_{HighCFE}(s) = \lambda^\alpha \left[0; \frac{1}{1}; \frac{-\alpha s}{1}; \left\{ \frac{\frac{i(i+\alpha)s}{(2i-1)2i\lambda}}{1}, \frac{\frac{i(i-\alpha)s}{(2i+1)2i\lambda}}{1} \right\}_{i=1}^n \right] \quad (2.35)$$

where n decides the order of approximation.

$$\left[\frac{p_0}{q_0}; \frac{p_1}{q_1}; \frac{p_2}{q_2}; \frac{p_3}{q_3} \dots \right] \text{ implies the term } \frac{p_0}{q_0} + \frac{p_1}{q_1 + \frac{p_2}{q_2 + \frac{p_3}{\dots}}}$$

(b) Low CFE ($F_{LowCFE}(s)$)

This is a good approximation for lower frequencies ($\omega < \lambda; \lambda > 0$), which is obtained as follows:

$$F_{LowCFE}(s) = \lambda^\alpha \left[0; \frac{1}{1}; \frac{\alpha \lambda}{s}; \left\{ \frac{\frac{i(i-\alpha)\lambda}{(2i-1)2i s}}{1}, \frac{\frac{i(i+\alpha)\lambda}{(2i+1)2i s}}{1} \right\}_{i=1}^n \right] \quad (2.36)$$

5. Oustaloup [*Oustaloup et al. (2000)*]

The Oustaloup approximation $F_{Oustaloup}(s)$ of $F(s) = s^\alpha$ assuming that the expected fitting range $[\omega_b, \omega_h]$ is obtained as follows:

$$F_{Oustaloup}(s) = K \prod_{k=-N}^N \frac{s + z_k}{s + p_k} \quad (2.37)$$

where,

$$\begin{aligned} z_k &= \omega_b \left(\frac{\omega_h}{\omega_b} \right)^{\frac{k+N+\frac{1}{2}(1-\alpha)}{2N+1}} \\ p_k &= \omega_b \left(\frac{\omega_h}{\omega_b} \right)^{\frac{k+N+\frac{1}{2}(1+\alpha)}{2N+1}} \\ K &= \omega_h^\alpha \end{aligned}$$

In this method, order of approximation is $(2N + 1)$, which is an odd number ($N = 1, 2, \dots$) The following generalized Oustaloup method can be used to obtain the approximation $F_{GenOustaloup}(s)$ having order, $N = 1, 2, \dots$

$$F_{GenOustaloup}(s) = K \prod_{k=1}^N \frac{s + z_k}{s + p_k} \quad (2.38)$$

where,

$$\begin{aligned} z_k &= \omega_b \left(\frac{\omega_h}{\omega_b} \right)^{\frac{2k-1-\alpha}{2N}} \\ p_k &= \omega_b \left(\frac{\omega_h}{\omega_b} \right)^{\frac{2k-1+\alpha}{2N}} \\ K &= \omega_h^\alpha \end{aligned}$$

6. Modified Oustaloup [Xue et al. (2007)]

This method provides a better approximation than Oustaloup method with respect to both low frequency and high frequency at the cost of increase in the order of approximation. The modified Oustaloup approximation $F_{ModOustaloup}(s)$ of $F(s) = s^\alpha$ is obtained as follows:

$$F_{ModOustaloup}(s) = \left(\frac{d\omega_h}{b} \right)^\alpha \frac{ds^2 + b\omega_h s}{d(1-\alpha)s^2 + b\omega_h s + d\alpha} \prod_{k=-N}^N \frac{s + z_k}{s + p_k} \quad (2.39)$$

where,

$$z_k = \left(\frac{d\omega_h}{b} \right)^{\frac{\alpha-2k}{2N+1}}, p_k = \left(\frac{b\omega_h}{d} \right)^{\frac{\alpha+2k}{2N+1}}$$

In above method, order of approximation is $(2N + 1)$, which is an odd number ($N = 1, 2, \dots$). The following generalized modified Oustaloup method can be used to obtain the approximation $F_{GenModOustaloup}(s)$ having order, $N = 1, 2, \dots$

$$F_{GenModOustaloup}(s) = \left(\frac{d\omega_h}{b} \right)^\alpha \frac{ds^2 + b\omega_h s}{d(1-\alpha)s^2 + b\omega_h s + d\alpha} \prod_{k=1}^N \frac{s + z_k}{s + p_k} \quad (2.40)$$

$$\begin{aligned} z_k &= \omega_b \left(\frac{\omega_h}{\omega_b} \right)^{\frac{2k-1-\alpha}{2N}} \\ p_k &= \omega_b \left(\frac{\omega_h}{\omega_b} \right)^{\frac{2k-1+\alpha}{2N}} \end{aligned}$$

7. Chareff [Charef (2006)]

The Chareff approximation $F_{Chareff}(s)$ of the irrational TF of the form $F(s) = \frac{1}{(1+\frac{s}{pT})^\alpha}$ is obtained as follows:

$$F_{Chareff}(s) = \frac{\prod_{i=0}^{N-1} \left(1 + \frac{s}{z_i}\right)}{\prod_{i=0}^N \left(1 + \frac{s}{p_i}\right)} \quad (2.41)$$

where, the coefficients are computed for obtaining a maximum deviation of y in dB from the original magnitude response in the frequency domain as follows:

$$p_i = p_0(ab)^i, z_i = ap_0(ab)^i, p_0 = pT\sqrt{b}, a = 10^{\frac{y}{10(1-\alpha)}}, b = 10^{\frac{y}{10\alpha}}$$

The above approximation methods are illustrated with the help of a numerical example as follows:

Example 1 Let us consider the rational approximation of $F(s) = s^{0.5}$. The numerical details considered for each method are presented in Table 2.1. The magnitude and phase bode plots of $s^{0.5}$ (i.e. Original) and its rational approximations obtained using different methods are shown in Figures 2.1 and 2.2 respectively. The Chareff method is not considered as the TF under consideration is not in the suitable form, i.e. $\frac{1}{(1+\frac{s}{pT})^\alpha}$.

Table 2.1: Numerical Details for Different Rational Approximation Methods

Method	Parameters
Carlson	$i = 2$
CRONE	$N = 3, \omega_l = 0.01, \omega_h = 100$
Matsuda	$[\omega_0, \omega_1, \dots, \omega_n] = 15$ logarithmically spaced points between $[0.1, 10]$
High CFE	$\lambda = 1, n = 4$
Low CFE	$\lambda = 1, n = 4$
Oustaloup	$N = 2, \omega_b = 0.01, \omega_h = 100$
Modified Oustaloup	$N = 2, b = 10, d = 9, \omega_b = 0.01, \omega_h = 100$

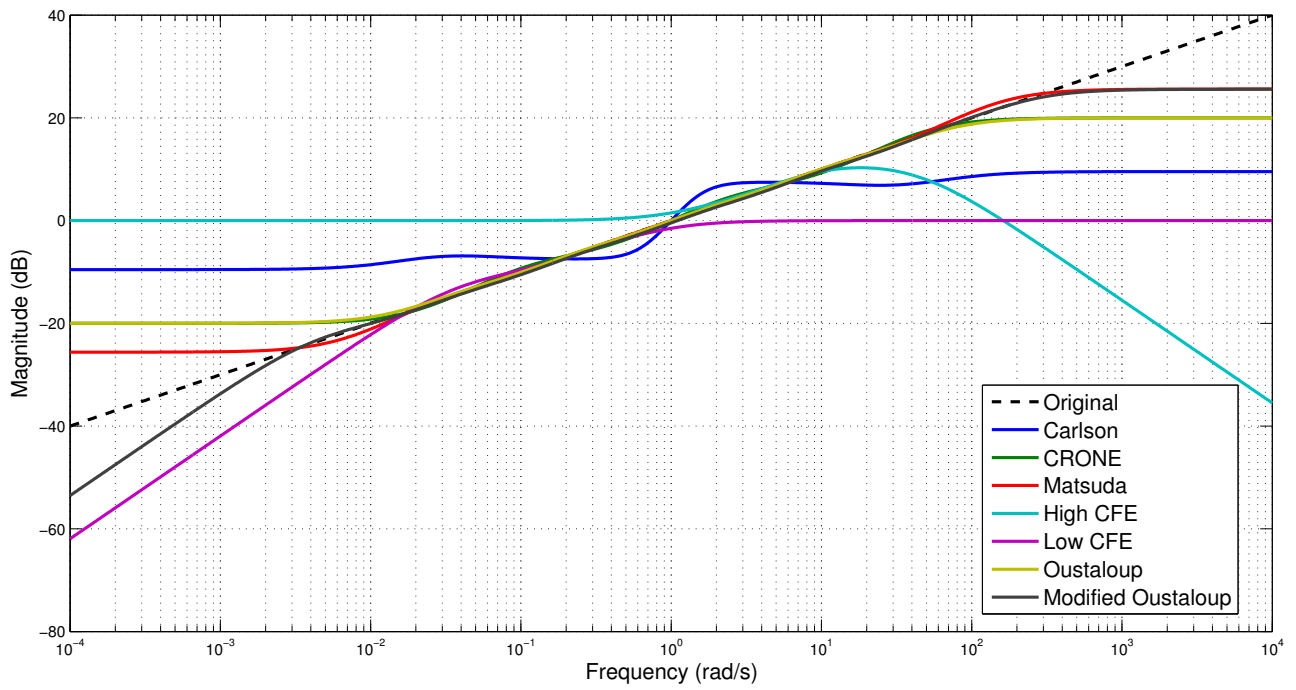


Figure 2.1: Magnitude Bode Plots

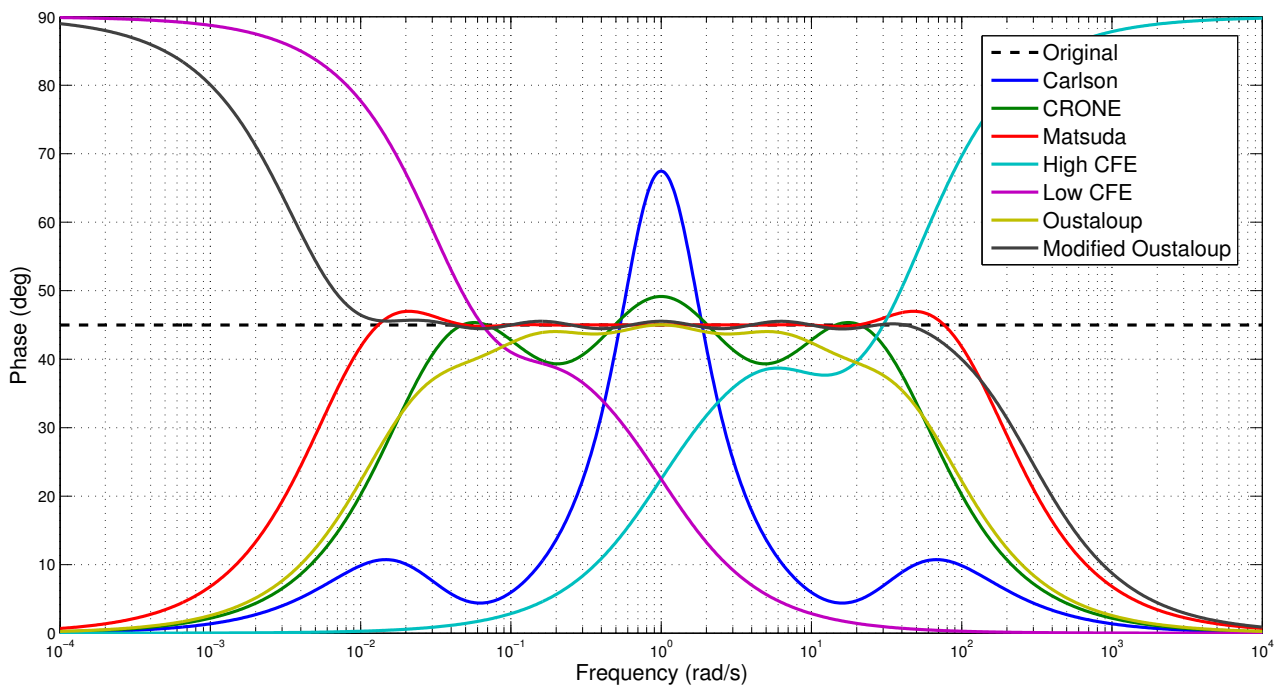


Figure 2.2: Phase Bode Plots

The Oustaloup approximation obtained using (2.37) with $N = 2$ is same as the one obtained using (2.38) for $N = 5$. This is because the order of approximation in the formal case is $2N + 1$ and is N in the latter one. The above is true for the modified Oustaloup approximation as well when obtained using (2.39) and (2.40) .

Although we have different methods for the rational approximation, it is difficult to claim one of them as the best method [*de Oliveira Valério (2005)*]. The relative merits of each method depend on the differentiation order, on whether one is more interested in an accurate frequency behavior or in accurate time responses, on how large admissible TFs may be, etc. However, the Oustaloup method is used in many occasions to obtain reasonably good rational fit for the given fractional-order TF within the specified frequency range [*Xue et al. (2006b)*].

2.6 Fractional-Order Controllers

Fractional-order controllers (FOCs) are the ones which possess dynamics that are governed by FC. Some of the popular LTI fractional-order controllers ($C(s)$) are as follows:

1. Fractional-order proportional-integral controller

It is of two types,

(a) PI^α

$$C(s) = K_p \left(1 + \frac{K_i}{s^\alpha} \right) \quad (2.42)$$

(b) $[PI]^\alpha$

$$C(s) = K_p \left(1 + \frac{K_i}{s} \right)^\alpha \quad (2.43)$$

Where, $\alpha > 0$; $K_p, K_i \in \mathbb{R}$.

For $\alpha = 1$, (2.42) and (2.43) represent integer PI controller, $C(s) = K_p \left(1 + \frac{K_i}{s} \right)$.

2. Fractional-order proportional-derivative controller

It is of two types,

(a) PD^β

$$C(s) = K_p (1 + K_d s^\beta) \quad (2.44)$$

(b) $[PD]^\beta$

$$C(s) = K_p (1 + K_d s)^\beta \quad (2.45)$$

Where, $\beta > 0$; $K_p, K_d \in \mathbb{R}$.

For $\beta = 1$, (2.44) and (2.45) represent integer PD controller, $C(s) = K_p (1 + K_d s)$.

3. Fractional-order proportional-integral-derivative controller

(a) $PI^\alpha D^\beta$

$$C(s) = K_p \left(1 + \frac{K_i}{s^\alpha} + K_d s^\beta \right) \quad (2.46)$$

Where, $\alpha > 0, \beta > 0$; $K_p, K_i, K_d \in \mathbb{R}$.

For $\alpha = 1$ and $\beta = 1$, (2.46) represents integer PID controller, $C(s) = K_p \left(1 + \frac{K_i}{s} + K_d s \right)$.

4. Fractional-order lead-lag compensator

Fractional-order version of classical lead-lag compensator is given as:

$$C(s) = K_c \left(\frac{s + \frac{1}{\lambda}}{s + \frac{1}{x\lambda}} \right)^\alpha \quad (2.47)$$

where, $0 < x < 1, K_c > 0, \lambda > 0$. α is the fractional-order. When $\alpha > 0$, (2.47) is fractional lead compensator. For $\alpha < 0$, (2.47) is fractional lag compensator.

In this thesis, we have considered FOCs such as PI^α , $[PI]^\alpha$, PD^β , $[PD]^\beta$, $PI^\alpha D^\beta$ for investigating their limit cycle performance and asymptotic Bode characteristics.

2.7 Summary

This chapter covered the preliminaries related to FC and FOCs. The various definitions in FC and their properties were discussed. The chapter further presented continuous domain approximation methods which are useful for rationalizing the fractional-order TFs. The chapter concluded by providing the TF details of FOCs such as PI^α , $[PI]^\alpha$, PD^β , $[PD]^\beta$, $PI^\alpha D^\beta$, and fractional-order lead-lag compensator.

CHAPTER 3

Unified Tuning Expressions for Fractional-Order Controllers to Meet Wang-et-al specifications

3.1 Introduction

Existing literature on fractional-order control widely explores tuning of three-parameter Fractional-Order Controllers (FOCs) such as PI^α , $[PI]^\alpha$, PD^β , and $[PD]^\beta$ to meet *Wang-et-al specifications* [Wang et al. (2009a)]. However, it is observed that the controller tuning expressions in this literature have been derived individually for the given class of plant Transfer Function (TF). For instance, the works [Li et al. (2010)], [Li and Chen (2008)], [Luo and Chen (2009b)], [Wang et al. (2009a)] derive such expressions for position and velocity servo TF. On the other hand, the controller expressions corresponding to First Order Plus Dead Time (FOPDT) process have been obtained in [Wang et al. (2009b)]. Similar work in the context of a fractional-order plant is found in [Luo et al. (2010)]. Instead of such individual derivations, if one obtains the controller tuning expressions applicable to all class of plant TFs, it will considerably save the control engineer's efforts and time. In this chapter, such unified tuning expressions are derived for meeting Wang-et-al specifications by proposing a universal plant structure.

3.2 Closed Loop Control System

Let us consider a typical unity feedback control loop as shown in Figure 3.1. In Figure 3.1, $C(s)$ and $G(s)$ represent the TFs of controller and plant respectively.

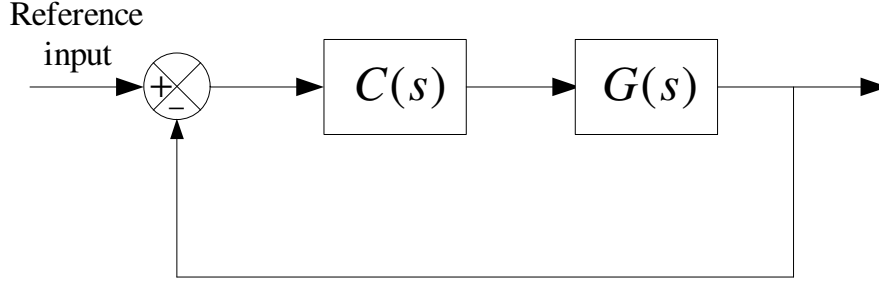


Figure 3.1: Typical Unity Feedback Control System

To derive the controller expressions, the following Wang-et-al specifications are considered:

1. Gain Crossover Frequency (ω_{gc})

$$|C(j\omega_{gc})G(j\omega_{gc})| = 1 \quad (3.1)$$

2. Phase Margin (ϕ_m)

$$\angle[C(j\omega_{gc})G(j\omega_{gc})] = -\pi + \phi_m \quad (3.2)$$

3. Robustness to Gain Variations (i.e. isodamping condition [*Chen et al. (2003)*])

$$\left(\frac{d(\angle[C(j\omega)G(j\omega)])}{d\omega} \right)_{\omega=\omega_{gc}} = 0 \quad (3.3)$$

The condition (3.3) ensures constant phase margin irrespective of plant gain variations. The effect of such robustness is seen in the closed loop step response in the form of constant maximum peak overshoot despite the gain variations.

3.3 Universal Plant Structure

For deriving the unified tuning expressions for the controller $C(s)$ in Figure 3.1, we introduce the following universal plant structure $G(s)$, which can accommodate any known class of integer or fractional-order plant TF:

$$G(s) = K \frac{(a_0 s^{\alpha_0} + a_1 s^{\alpha_1} + \dots + a_m s^{\alpha_m})}{(b_0 s^{\beta_0} + b_1 s^{\beta_1} + \dots + b_n s^{\beta_n})} e^{-Ls} = K \frac{\sum_{i=0}^m (a_i s^{\alpha_i})}{\sum_{k=0}^n (b_k s^{\beta_k})} e^{-Ls} \quad (3.4)$$

Where, K , a_i , α_i ($i = 0, 1, 2, \dots, m$), b_k , β_k ($k = 0, 1, 2, \dots, n$), L are real constants. m and n are integers. L denotes time delay or dead time of the plant. K is positive without loss of generality. When α_i, β_k assume integer values, (3.4) represents integer-order plant.

The structure (3.4) can represent any given integer or fractional-order plant TF with appropriate choice of its parameters. Let us consider a few cases for illustration:

1. Choosing $m = 0$, $a_0 = 1$, $\alpha_0 = 0$, $n = 1$, $b_0 = T$, $\beta_0 = 1$, $b_1 = 1$, $\beta_1 = 0$, (3.4) becomes FOPDT plant,

$$G(s) = \frac{K}{Ts + 1} e^{-Ls}$$

2. When one selects $m = 0$, $a_0 = 1$, $\alpha_0 = 0$, $n = 2$, $b_0 = T_1 \cdot T_2$, $\beta_0 = 2$, $b_1 = (T_1 + T_2)$, $\beta_1 = 1$, $b_2 = 1$, $\beta_2 = 0$, (3.4) represents Second Order Plus Dead Time (SOPDT) plant,

$$G(s) = \frac{K}{(T_1 s + 1)(T_2 s + 1)} e^{-Ls}$$

3. For Position Servo plant, the parameters of (3.4) are: $m = 0$, $a_0 = 1$, $\alpha_0 = 0$, $n = 1$, $b_0 = a$, $\beta_0 = 2$, $b_1 = 1$, $\beta_1 = 1$, $L = 0$.

$$G(s) = \frac{K}{s(as + 1)}$$

4. When $m = 0$, $a_0 = 1$, $\alpha_0 = 0$, $n = 1$, $b_0 = a$, $\beta_0 = 0.5$, $b_1 = 1$, $\beta_1 = 0$, $L = 0$, (3.4) represents Half-order Fractional Velocity Servo structure [Luo et al. (2010)],

$$G(s) = \frac{K}{as^{0.5} + 1}$$

Thus, the choice of parameters is important for representing the given class of TF using (3.4). If we derive the controller expressions for (3.4), they can be suitable for any given plant TF by appropriately substituting these parameters.

Remark 3.1. *In (3.4), it is further possible to replace the exponential term e^{-Ls} by its generalized form e^{-Ls^γ} , where $\gamma \in \mathbb{R}$. However, no physical interpretation for such term exists in the present literature. Therefore, we currently consider only the conventional exponential term e^{-Ls} in (3.4).*

3.4 Fractional-Order Controllers and their Unified Tuning Expressions

In this section, the unified tuning expressions for three-parameter FOCs such as PI^α , PD^β , $[PI]^\alpha$, $[PD]^\beta$ are derived so as to meet Wang-et-al specifications. The controller structures have been described in (2.42), (2.44), (2.43), and (2.45) of Section 2.6. Although the work in this section focuses only on Wang-et-al specifications for developing the unified tuning expressions, one may also select any other set of three specifications and adopt the similar approach to obtain corresponding unified expressions.

3.4.1 Tuning Expressions for PI^α and PD^β Controllers

PI^α and PD^β controllers given in (2.42) and (2.44) respectively are combined using the following general expression:

$$C(s) = K_1 (1 + K_2 s^\gamma) \quad (3.5)$$

In (3.5), When $\gamma > 0$, it represents PD^β controller (2.44) with $K_p = K_1$, $K_d = K_2$, and $\beta = \gamma$. Whereas, when $\gamma < 0$, (3.5) becomes the PI^α controller (2.42) with $K_p = K_1$, $K_i = K_2$, and $\alpha = -\gamma$.

From (3.4) and (3.5),

$$\begin{aligned}
[G(s)C(s)]_{s=j\omega} &= K \frac{\sum_{i=0}^m (a_i (j\omega)^{\alpha_i})}{\sum_{k=0}^n (b_k (j\omega)^{\beta_k})} e^{-L(j\omega)} K_1 (1 + K_2 (j\omega)^\gamma) \\
&= K \frac{\sum_{i=0}^m (a_i \omega^{\alpha_i} e^{j\frac{\pi}{2}\alpha_i})}{\sum_{k=0}^n (b_k \omega^{\beta_k} e^{j\frac{\pi}{2}\beta_k})} e^{-L(j\omega)} K_1 \left(1 + K_2 \omega^\gamma \left(\cos\left(\frac{\pi}{2}\gamma\right) + j \sin\left(\frac{\pi}{2}\gamma\right) \right) \right)
\end{aligned}$$

Therefore,

$$[G(s)C(s)]_{s=j\omega} = K \frac{\sum_{i=0}^m (a_i \omega^{\alpha_i} e^{j\frac{\pi}{2}\alpha_i})}{\sum_{k=0}^n (b_k \omega^{\beta_k} e^{j\frac{\pi}{2}\beta_k})} e^{-L(j\omega)} K_1 \left(1 + K_2 \omega^\gamma \cos\left(\frac{\pi}{2}\gamma\right) + j K_2 \omega^\gamma \sin\left(\frac{\pi}{2}\gamma\right) \right)$$

Substituting $\omega = \omega_{gc}$:

$$[G(s)C(s)]_{s=j\omega_{gc}} = K \frac{p_1 + jq_1}{p_2 + jq_2} e^{-L(j\omega_{gc})} K_1 \left(1 + K_2 \omega_{gc}^\gamma \cos\left(\frac{\pi}{2}\gamma\right) + j K_2 \omega_{gc}^\gamma \sin\left(\frac{\pi}{2}\gamma\right) \right)$$

where,

$$p_1 = \sum_{i=0}^m \left(a_i \omega_{gc}^{\alpha_i} \cos\left(\frac{\pi}{2}\alpha_i\right) \right) \quad (3.6a)$$

$$q_1 = \sum_{i=0}^m \left(a_i \omega_{gc}^{\alpha_i} \sin\left(\frac{\pi}{2}\alpha_i\right) \right) \quad (3.6b)$$

$$p_2 = \sum_{k=0}^n \left(b_k \omega_{gc}^{\beta_k} \cos\left(\frac{\pi}{2}\beta_k\right) \right) \quad (3.6c)$$

$$q_2 = \sum_{k=0}^n \left(b_k \omega_{gc}^{\beta_k} \sin\left(\frac{\pi}{2}\beta_k\right) \right) \quad (3.6d)$$

Recalling the gain crossover frequency specification (3.1),

$$|C(j\omega_{gc})G(j\omega_{gc})| = 1$$

Therefore,

$$K \frac{\sqrt{p_1^2 + q_1^2}}{\sqrt{p_2^2 + q_2^2}} K_1 \sqrt{\left(1 + K_2 \omega_{gc}^\gamma \cos\left(\frac{\pi}{2}\gamma\right)\right)^2 + \left(K_2 \omega_{gc}^\gamma \sin\left(\frac{\pi}{2}\gamma\right)\right)^2} = 1$$

This gives,

$$K_1 = \frac{1}{K} \sqrt{\frac{(p_2^2 + q_2^2)}{(p_1^2 + q_1^2) \left(\left(1 + K_2 \omega_{gc}^\gamma \cos\left(\frac{\pi}{2}\gamma\right)\right)^2 + \left(K_2 \omega_{gc}^\gamma \sin\left(\frac{\pi}{2}\gamma\right)\right)^2 \right)}} \quad (3.7)$$

Recalling the phase margin specification (3.2),

$$\angle[C(j\omega_{gc})G(j\omega_{gc})] = -\pi + \phi_m$$

Therefore,

$$\tan^{-1}\left(\frac{q_1}{p_1}\right) - \tan^{-1}\left(\frac{q_2}{p_2}\right) - L\omega_{gc} + \tan^{-1}\left(\frac{K_2 \omega_{gc}^\gamma \sin\left(\frac{\pi}{2}\gamma\right)}{1 + K_2 \omega_{gc}^\gamma \cos\left(\frac{\pi}{2}\gamma\right)}\right) = -\pi + \phi_m \quad (3.8)$$

Let,

$$M = \tan\left(-\tan^{-1}\left(\frac{q_1}{p_1}\right) + \tan^{-1}\left(\frac{q_2}{p_2}\right) + L\omega_{gc} - \pi + \phi_m\right) \quad (3.9)$$

From (3.8) and (3.9), we get:

$$\frac{K_2 \omega_{gc}^\gamma \sin\left(\frac{\pi}{2}\gamma\right)}{1 + K_2 \omega_{gc}^\gamma \cos\left(\frac{\pi}{2}\gamma\right)} = M$$

This gives,

$$K_2 = \frac{-M\omega_{gc}^{-\gamma}}{M \cos\left(\frac{\pi}{2}\gamma\right) - \sin\left(\frac{\pi}{2}\gamma\right)} \quad (3.10)$$

Recalling the isodamping condition (3.3):

$$\left(\frac{d(\angle[C(j\omega)G(j\omega)])}{d\omega} \right)_{\omega=\omega_{gc}} = 0$$

Therefore,

$$\begin{aligned} & \frac{p_1 \left(\sum_{i=0}^m (a_i \alpha_i \omega_{gc}^{\alpha_i-1} \sin(\frac{\pi}{2} \alpha_i)) \right) - q_1 \left(\sum_{i=0}^m (a_i \alpha_i \omega_{gc}^{\alpha_i-1} \cos(\frac{\pi}{2} \alpha_i)) \right)}{p_1^2 + q_1^2} \\ & - \frac{p_2 \left(\sum_{k=0}^n (b_k \beta_k \omega_{gc}^{\beta_k-1} \sin(\frac{\pi}{2} \beta_k)) \right) - q_2 \left(\sum_{k=0}^n (b_k \beta_k \omega_{gc}^{\beta_k-1} \cos(\frac{\pi}{2} \beta_k)) \right)}{p_2^2 + q_2^2} \\ & - L + \frac{K_2 \sin(\frac{\pi}{2} \gamma) \gamma \omega_{gc}^{\gamma-1}}{1 + 2K_2 \omega_{gc}^{\gamma} \cos(\frac{\pi}{2} \gamma) + K_2^2 \omega_{gc}^{2\gamma}} = 0 \end{aligned} \quad (3.11)$$

Let,

$$\begin{aligned} N = & \frac{-p_1 \left(\sum_{i=0}^m (a_i \alpha_i \omega_{gc}^{\alpha_i-1} \sin(\frac{\pi}{2} \alpha_i)) \right) + q_1 \left(\sum_{i=0}^m (a_i \alpha_i \omega_{gc}^{\alpha_i-1} \cos(\frac{\pi}{2} \alpha_i)) \right)}{p_1^2 + q_1^2} \\ & + L + \frac{p_2 \left(\sum_{k=0}^n (b_k \beta_k \omega_{gc}^{\beta_k-1} \sin(\frac{\pi}{2} \beta_k)) \right) - q_2 \left(\sum_{k=0}^n (b_k \beta_k \omega_{gc}^{\beta_k-1} \cos(\frac{\pi}{2} \beta_k)) \right)}{p_2^2 + q_2^2} \end{aligned} \quad (3.12)$$

From (3.11) and (3.12), we get,

$$-N + \frac{K_2 \sin(\frac{\pi}{2} \gamma) \gamma \omega_{gc}^{\gamma-1}}{1 + 2K_2 \omega_{gc}^{\gamma} \cos(\frac{\pi}{2} \gamma) + K_2^2 \omega_{gc}^{2\gamma}} = 0$$

Therefore,

$$-K_2 \left(2N \omega_{gc}^{\gamma} \cos\left(\frac{\pi}{2} \gamma\right) - \gamma \sin\left(\frac{\pi}{2} \gamma\right) \omega_{gc}^{\gamma-1} \right) - N - NK_2^2 \omega_{gc}^{2\gamma} = 0 \quad (3.13)$$

Let,

$$H = \left(2N\omega_{gc}^\gamma \cos\left(\frac{\pi}{2}\gamma\right) - \gamma \sin\left(\frac{\pi}{2}\gamma\right) \omega_{gc}^{\gamma-1} \right) \quad (3.14)$$

From (3.13) and (3.14),

$$NK_2^2\omega_{gc}^{2\gamma} + K_2H + N = 0$$

This gives,

$$K_2 = \frac{-H \pm \sqrt{H^2 - 4N^2\omega_{gc}^{2\gamma}}}{2N\omega_{gc}^{2\gamma}} \quad (3.15)$$

On solving (3.7), (3.10), and (3.15) simultaneously, one can obtain the parameters of controller (3.5).

3.4.2 Tuning Expressions for $[PI]^\alpha$ Controller

Similar to the procedure adopted for PI^α and PD^β controllers, the tuning expressions for $[PI]^\alpha$ Controller are obtained as given below:

$$K_i = -\omega_{gc} \tan\left(\frac{-\tan^{-1}\left(\frac{q_1}{p_1}\right) + \tan^{-1}\left(\frac{q_2}{p_2}\right) + L\omega_{gc} - \pi + \phi_m}{\alpha}\right) \quad (3.16)$$

$$K_i = \frac{\alpha \pm \sqrt{\alpha^2 - 4N^2\omega_{gc}^2}}{2N} \quad (3.17)$$

$$K_p = \frac{1}{K} \sqrt{\frac{(p_2^2 + q_2^2)}{(p_1^2 + q_1^2) \left(1 + \left(\frac{K_i}{\omega_{gc}}\right)^2\right)^\alpha}} \quad (3.18)$$

where, p_1, q_1, p_2, q_2 are same as in (3.6). Also, N is as given in (3.12).

On solving (3.16), (3.17), and (3.18) simultaneously, one gets the parameters of

controller (2.43). The derivation is provided in APPENDIX B.1.

3.4.3 Tuning Expressions for $[PD]^\beta$ Controller

Similarly, the tuning expressions for $[PD]^\beta$ Controller are obtained as given below:

$$K_d = \frac{\tan\left(\frac{-\tan^{-1}\left(\frac{q_1}{p_1}\right) + \tan^{-1}\left(\frac{q_2}{p_2}\right) + L\omega_{gc} - \pi + \phi_m}{\beta}\right)}{\omega_{gc}} \quad (3.19)$$

$$K_d = \frac{\beta \pm \sqrt{\beta^2 - 4N^2\omega_{gc}^2}}{2N\omega_{gc}^2} \quad (3.20)$$

$$K_p = \frac{1}{K} \sqrt{\frac{(p_2^2 + q_2^2)}{(p_1^2 + q_1^2) (1 + (K_d\omega_{gc})^2)^\beta}} \quad (3.21)$$

where, p_1, q_1, p_2, q_2 are as given in (3.6). Also, N is same as in (3.12).

On solving (3.19), (3.20), and (3.21) simultaneously, one can obtain the parameters of controller (2.45). The derivation is provided in APPENDIX B.2.

Remark 3.2. *It is important to note that though the Wang-et-al specifications ensure the required positive phase margin at a given gain crossover frequency, they do not guarantee closed loop stability in general. If there occur multiple gain crossover frequencies, such restrictive specifications cannot ensure all the phase margins to be positive. Hence, the generalized derivations presented in this section are useful only for those plants which lead to closed loop stability. Therefore, closed loop stability check is essential after designing the controller for Wang-et-al specifications.*

3.5 Illustration with examples

We illustrate the applicability of the unified controller expressions derived in Section 3.4 with the help of numerical examples in the following subsections.

3.5.1 PI^α and PD^β Controllers

The typical plant structure cases considered for the illustration purpose are:

1. FOPDT [Wang *et al.* (2009b)]
2. Fractional-Order Thermal Process [Petráš *et al.* (2002b)]

The above cases fit in the universal plant structure by selecting the appropriate parameters. The methodology for tuning the controller for universal plant structure is simulated using MATLAB [MATLAB (2010)] and the results are given in Table 3.1.

Table 3.1: Results for PI^α and PD^β Controller

Example	Plant and Specifications	Universal Plant Parameters	Designed Controller
1	$\frac{1}{1+0.4s}e^{-0.01s}$ <p>(FOPDT)</p> $\omega_{gc} = 10 \text{ rad/s}$ $\phi_m = 50^\circ$	$K = 1, L = 0.01,$ $a_0 = 1, \alpha_0 = 0,$ $b_0 = 0.4, \beta_0 = 1,$ $b_1 = 1, \beta_1 = 0$	$2.1208 (1 + 11.0602s^{-0.8732})$ <p>(PI^α Controller)</p>
2	$\frac{1}{0.598+39.69s^{1.26}}$ <p>(Fractional-Order Thermal Process)</p> $\omega_{gc} = 10 \text{ rad/s}, \phi_m = 70^\circ$	$K = 1, L = 0,$ $a_0 = 1, \alpha_0 = 0,$ $b_0 = 0.598, \beta_0 = 0,$ $b_1 = 39.69, \beta_1 = 1.26$	$214.7179 (1 + 2.0862s^{0.0545})$ <p>(PD^β Controller)</p>

For the FOPDT plant considered in Example 1, the Bode plot of open loop TF is shown in Figure 3.2. It is seen from Figure 3.2 that the desired gain crossover frequency, phase margin and isodamping conditions are ensured by the designed controllers. The isodamping condition leads to the flattening of the phase plot locally around gain crossover frequency.

Figure 3.3 presents the unit step response of the closed loop system with variation in the nominal value of plant gain K . It is observed that maximum peak overshoot re-

mains constant irrespective of plant gain variations, thereby illustrating the isodamping condition in time-domain.

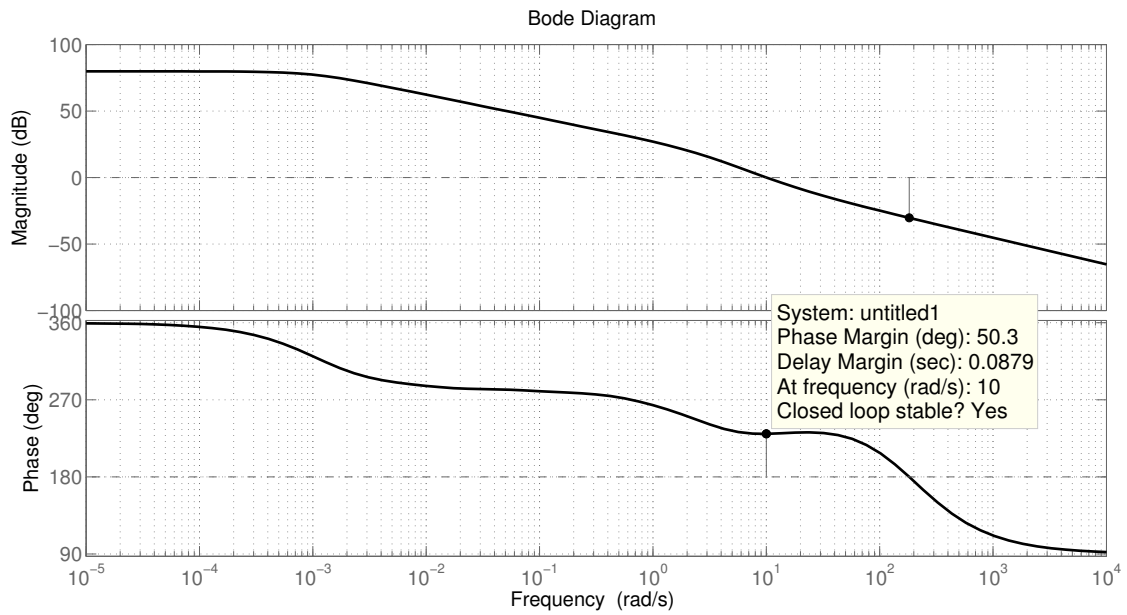


Figure 3.2: Bode Plot (FOPDT) (PI^α Controller)

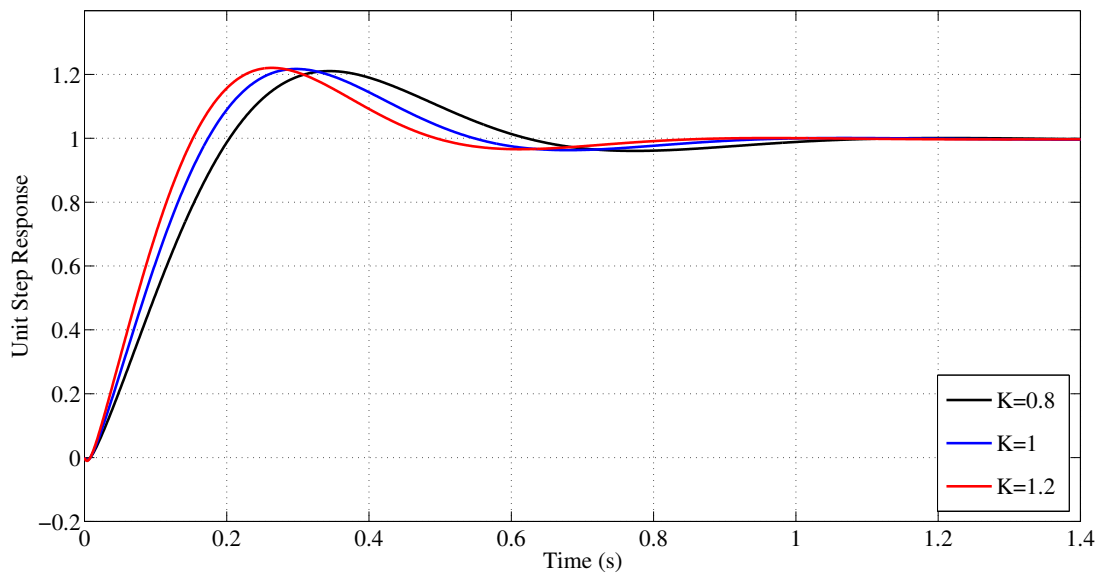


Figure 3.3: Unit Step Response (FOPDT) (PI^α Controller)

For obtaining Figures 3.2 and 3.3, Oustaloup approximation of the FOC is considered. The order of Oustaloup approximation is taken as 7 and it is considered over the frequency range $[0.001, 1000]$ rad/s.

The corresponding results for the fractional-order thermal process which is considered in Example 2 are shown in Figures 3.4 and 3.5. In Example 1, the resulting γ is negative. Hence, the controller is PI^α . On the other hand, the PD^β controllers results for the Example 2 since γ is positive.

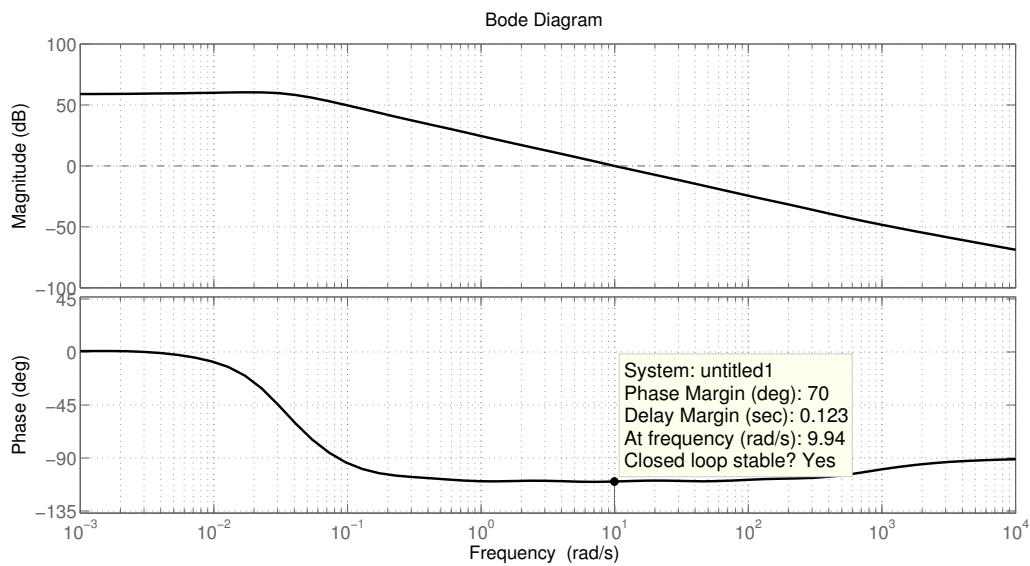


Figure 3.4: Bode Plot (Fractional-Order Thermal Process) (PD^β Controller)

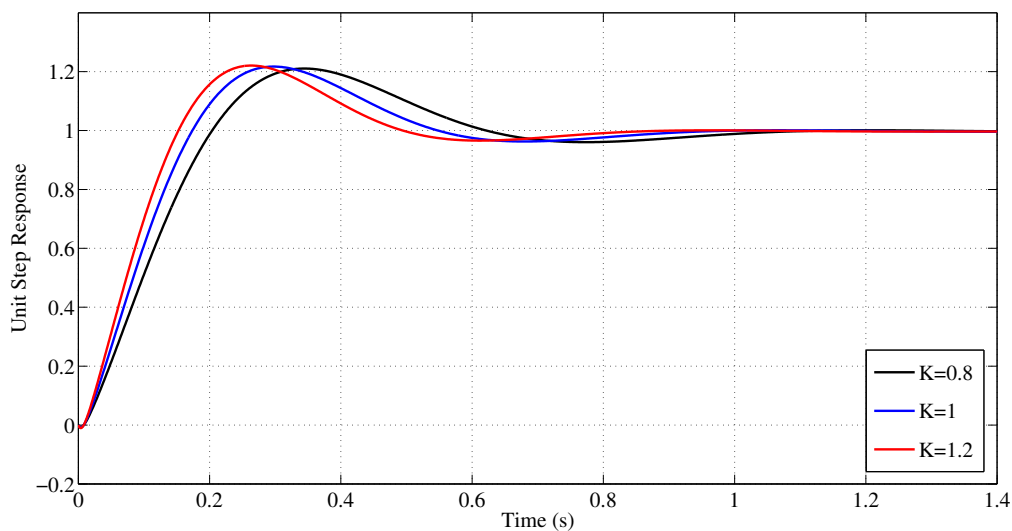


Figure 3.5: Unit Step Response (Fractional-Order Thermal Process) (PD^β Controller)

3.5.2 $[PI]^\alpha$ Controller

The following plant cases are considered for the illustration:

1. Fractional Horsepower Dynamometer [*Luo et al. (2010)*]
2. Velocity Servo System [*Wang et al. (2009a)*]

The results are summarized in Table 3.2. The graphical results for the fractional horsepower dynamometer as considered in Example 1 are shown in Figures 3.6 and 3.7. On the other hand, Figures 3.8 and 3.9 present such results for the velocity servo system considered in Example 2. The plots confirm that the Wang-et-al specifications are met by the tuned $[PI]^\alpha$ controllers.

Table 3.2: Results for $[PI]^\alpha$ Controller

Example	Plant and Specifications	Universal Plant Parameters	Designed Controller
1	$\frac{1}{0.4s^{0.5}+1}$ <p>(Fractional Horsepower Dynamometer)</p> $\omega_{gc} = 10 \text{ rad/s}, \phi_m = 70^\circ$	$K = 1, L = 0,$ $a_0 = 1, \alpha_0 = 0,$ $b_0 = 0.4, \beta_0 = 0.5,$ $b_1 = 1, \beta_1 = 0$	$0.2097 \left(1 + \frac{97.8062}{s}\right)^{1.007}$
2	$\frac{1}{0.4s+1}$ <p>(DC Motor Velocity Servo System)</p> $\omega_{gc} = 10 \text{ rad/s}, \phi_m = 70^\circ$	$K = 1, L = 0,$ $a_0 = 1, \alpha_0 = 0,$ $b_0 = 0.4, \beta_0 = 1,$ $b_1 = 1, \beta_1 = 0$	$2.7482 \left(1 + \frac{18.1507}{s}\right)^{0.5567}$

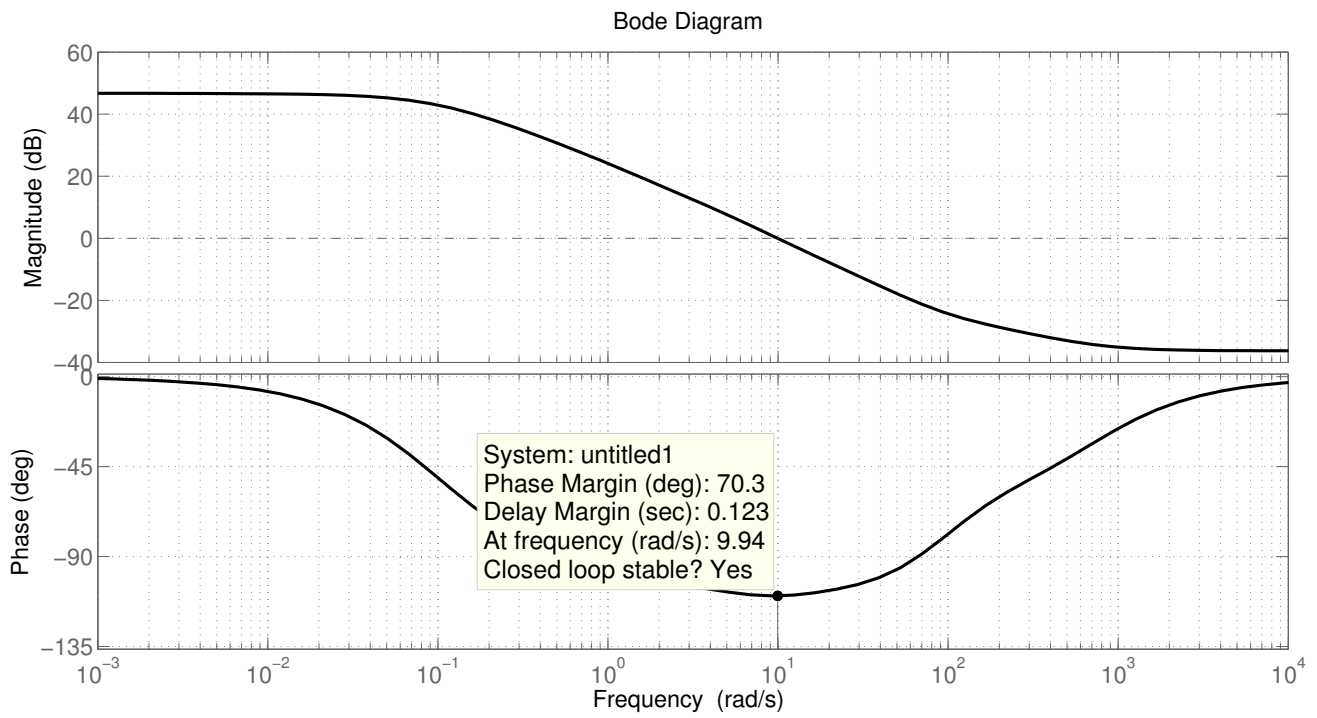


Figure 3.6: Bode Plot (Fractional Horsepower Dynamometer) ($[PI]^\alpha$ Controller)

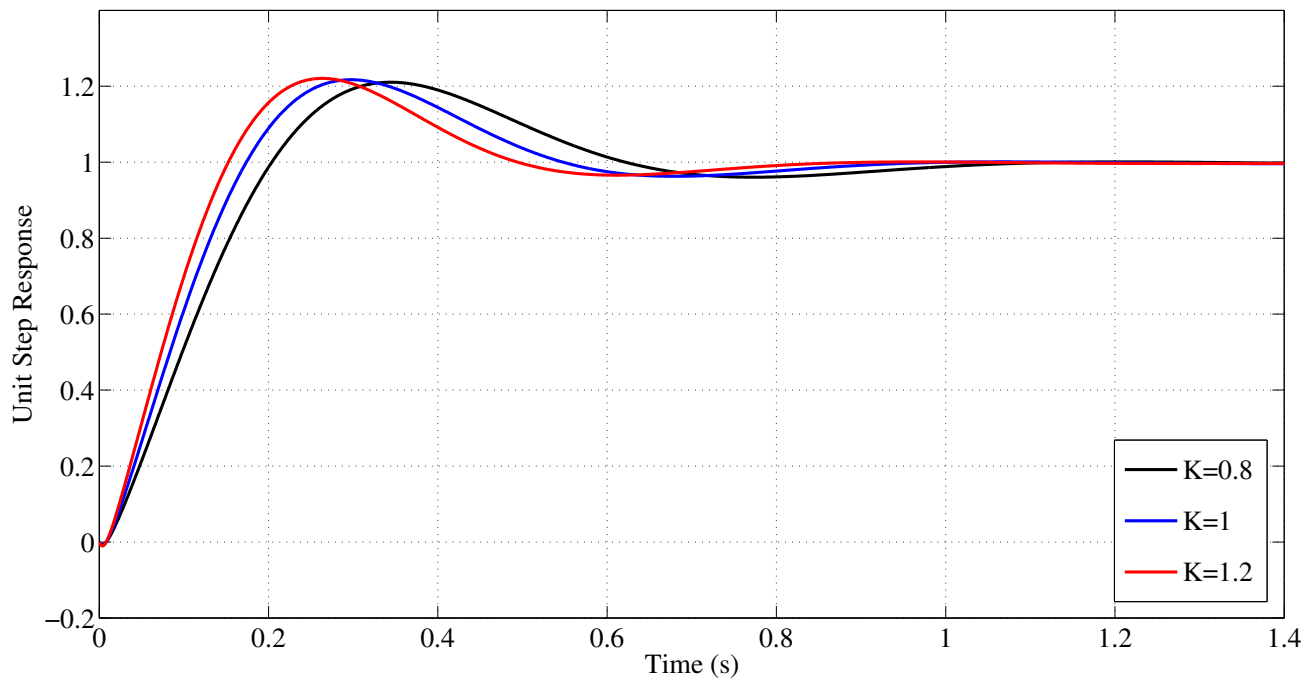


Figure 3.7: Unit Step Response (Fractional Horsepower Dynamometer) ($[PI]^\alpha$ Controller)

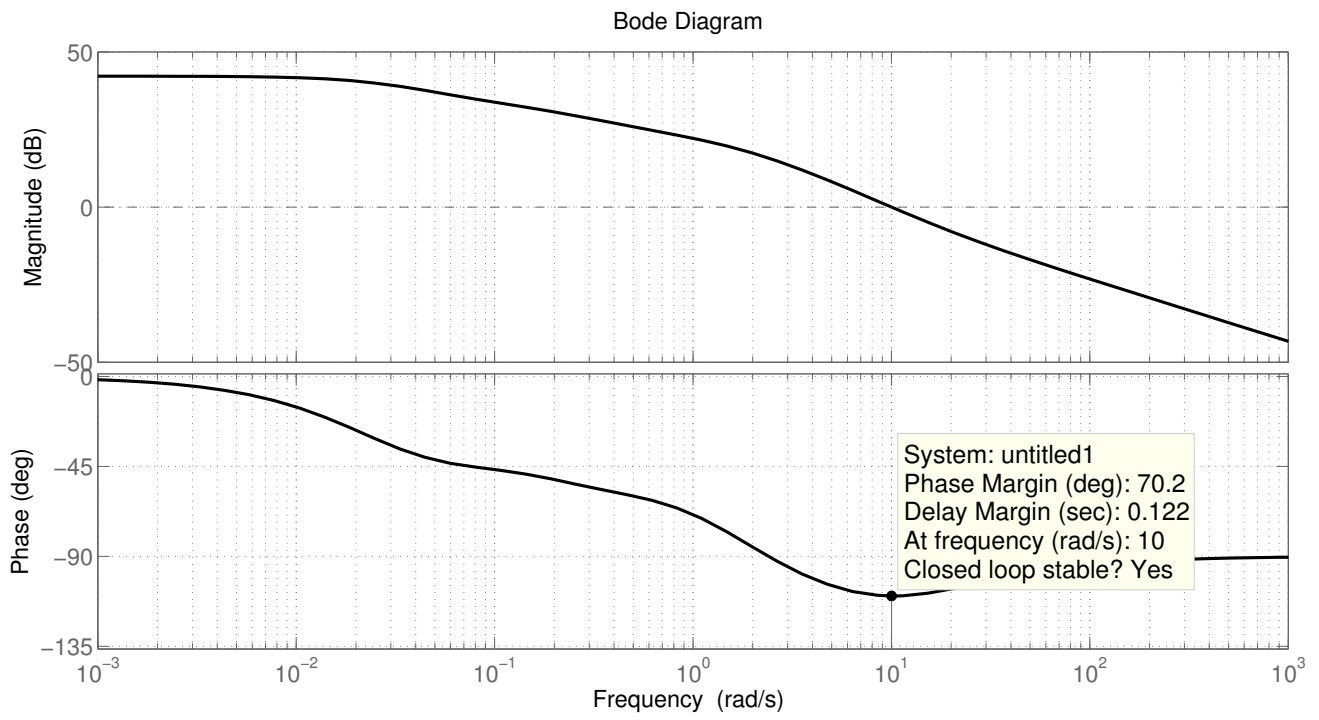


Figure 3.8: Bode Plot (Velocity Servo System) ($[PI]^\alpha$ Controller)

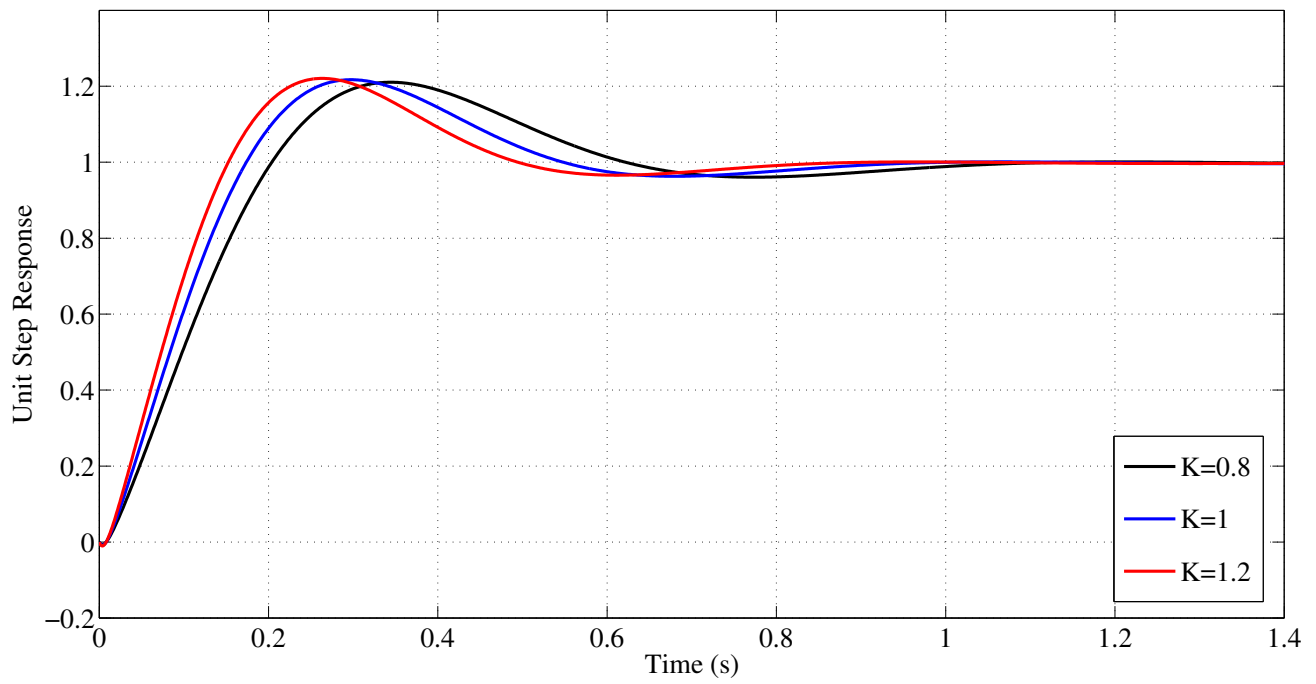


Figure 3.9: Unit Step Response (Velocity Servo System) ($[PI]^\alpha$ Controller)

3.5.3 $[PD]^\beta$ Controller

The following plant cases are considered for the illustration:

1. Fractional-Order Thermal Process [Petráš et al. (2002b)]
2. Position Servo System [Li and Chen (2008)], [Luo and Chen (2009b)]

The results are summarized in Table 3.3. The graphical results for the fractional-order thermal process of Example 1 are shown Figures 3.10 and 3.11. On the other hand, Figures 3.12 and 3.13 present such results for position servo system considered in Example 2. It is observed from these plots that the designed $[PD]^\beta$ controllers meet the required set of specifications.

Table 3.3: Results for $[PD]^\beta$ Controller

Example	Plant and Specifications	Universal Plant Parameters	Designed Controller
1	$\frac{1}{39.69s^{1.26}+0.598}$ (Fractional-Order Thermal Process) $\omega_{gc} = 0.5 \text{ rad/s}$ $\phi_m = 70^\circ$	$K = 1, a_0 = 1, \alpha_0 = 0,$ $b_0 = 39.69, \beta_0 = 1.26,$ $b_1 = 0.598, \beta_1 = 0,$ $L = 0$	$16.2769 (1 + 0.6484s)^{0.0824}$
2	$\frac{1}{s(0.4s+1)}$ (DC Motor Position Servo System) $\omega_{gc} = 10 \text{ rad/s}$ $\phi_m = 70^\circ$	$K = 1, a_0 = 1, \alpha_0 = 0,$ $b_0 = 0.4, \beta_0 = 2,$ $b_1 = 1, \beta_1 = 1, L = 0$	$16.7780 (1 + 0.2992s)^{0.7826}$

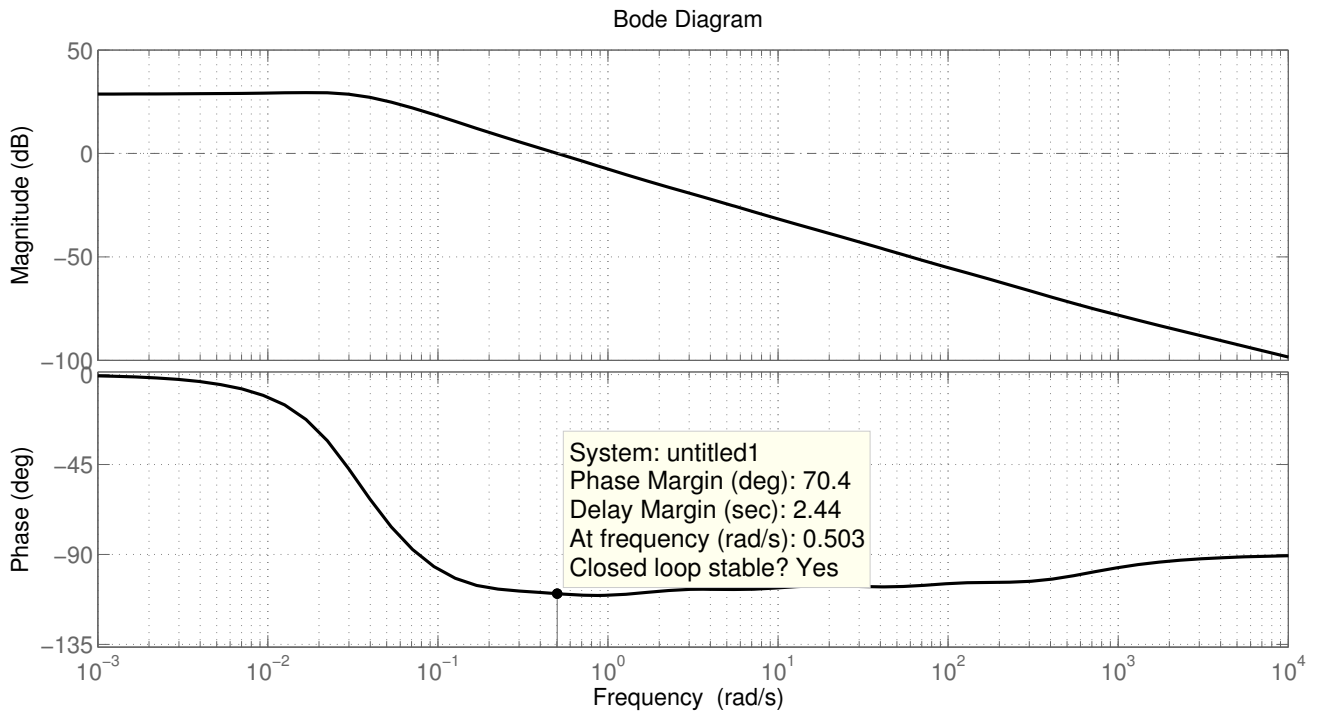


Figure 3.10: Bode Plot (Fractional-Order Thermal Process) ($[PD]^\beta$ Controller)

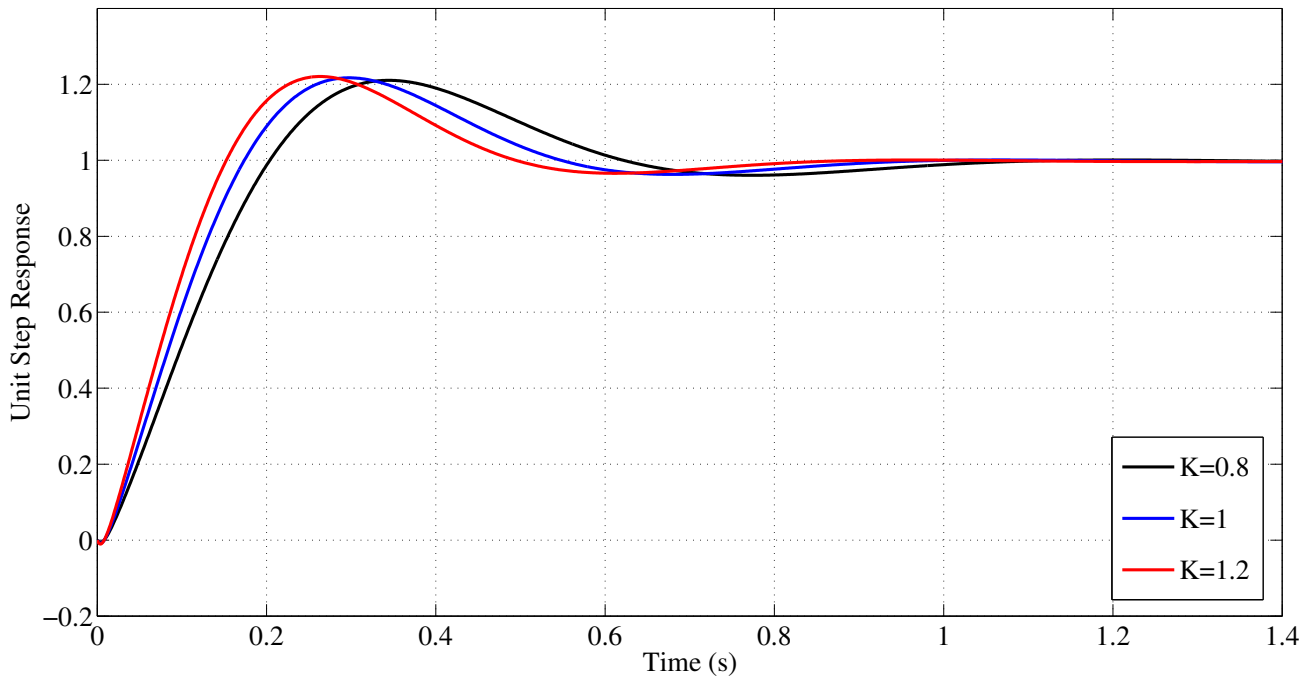


Figure 3.11: Unit Step Response (Fractional-Order Thermal Process) ($[PD]^\beta$ Controller)

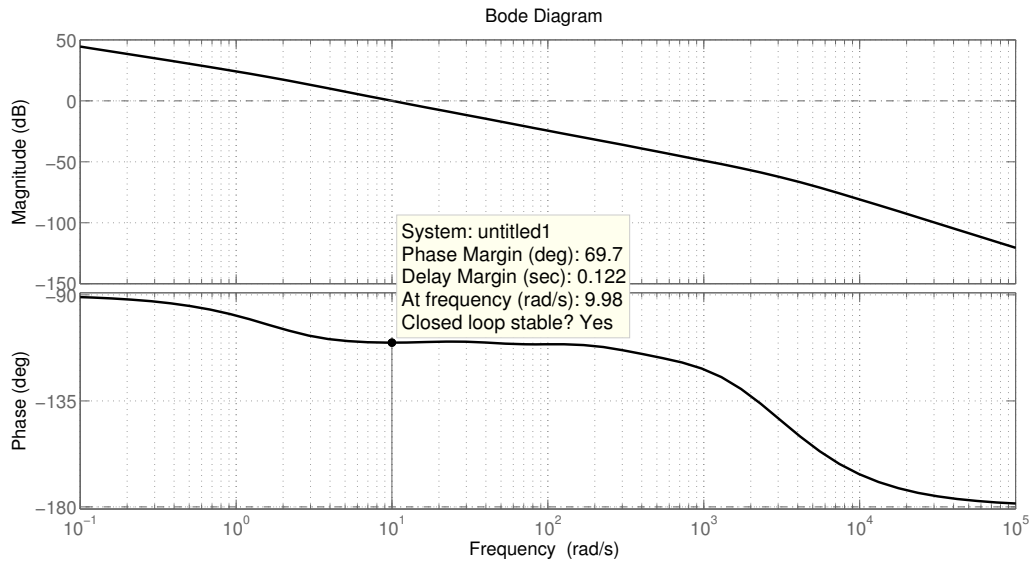


Figure 3.12: Bode Plot (Position Servo System) ($[PD]^\beta$ Controller)

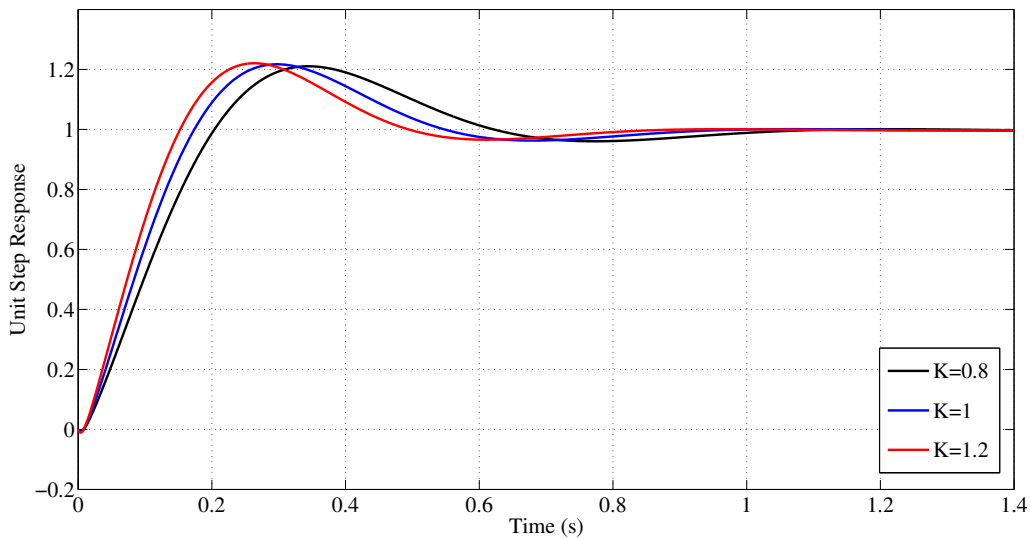


Figure 3.13: Unit Step Response (Position Servo System) ($[PD]^\beta$ Controller)

3.6 Summary

In this chapter, we derived unified tuning expressions for three-parameter FOCs such as PI^α , PD^β , $[PD]^\beta$, and $[PI]^\alpha$ for meeting Wang-et-al specifications. A universal plant structure was proposed which can accommodate any integer and fractional-order TF with appropriate choice of parameters. The usefulness of the tuning expressions was demonstrated with several integer and fractional-order plants.

CHAPTER 4

Limit Cycle Performance of Fractional-Order Controllers Meeting Wang-et-al Specifications

4.1 Introduction

In the previous chapter, a unified design of three-parameter Fractional-Order Controllers (FOCs) was considered for Linear Time-Invariant (LTI) plants so as to meet Wang-et-al specifications. The present chapter focuses on the observation of limit cycle performance of FOCs for a plant containing separable nonlinearity. First, an elementary servo plant model consisting of static backlash nonlinearity is considered. The FOCs such as PI^α , $[PI]^\alpha$ and the integer PID controller are designed for the Transfer Function (TF) of such plants to meet Wang-et-al specifications. The limit cycle performances of the designed controllers are analyzed by means of closed loop nonlinear simulation as well as Describing Function (DF) method. It turns out that FOCs are superior over integer PID in limit cycle suppression. Additionally, such superior performance of FOCs is also observed for the experimental set-up of Precision Modular Servo.

4.2 Control of Servo System with Gears

In this section, we concentrate on a plant which contains a separable nonlinearity. The FOCs are first tuned for the TF of such plants (i.e. without nonlinearity) to meet Wang-et-al specifications. Later, the limit cycle performance of such controllers is analyzed in the presence of plant nonlinearity.

Let us consider a servo system with gears [Gopal (2012)] as shown in Figure 4.1. The mathematical model of the plant consists of a TF, $G(s) = \frac{K}{s(s+a)}$ of the amplifier-motor combination and a static backlash nonlinearity between gear 1 and gear 2. Figure 4.2 shows closed loop control scheme consisting of controller $C(s)$ and the servo-system containing backlash.

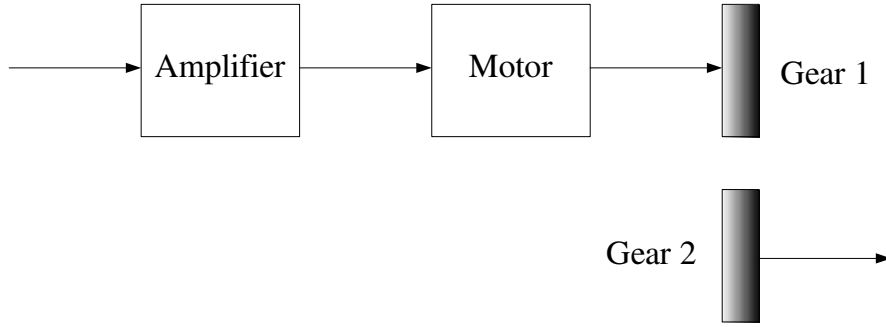


Figure 4.1: A Servo System with Gears

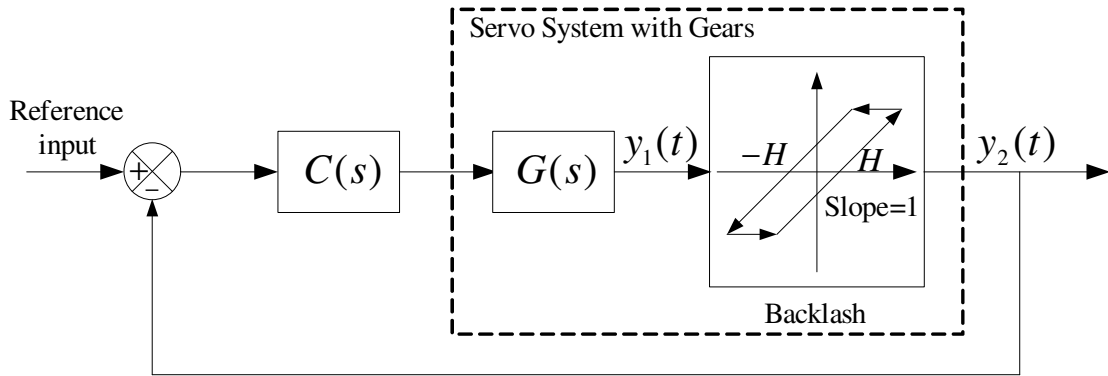


Figure 4.2: Closed Loop Control Scheme

4.2.1 Controller Design for Wang-et-al Specifications

In this subsection, we design the controller $C(s)$ for plant TF $G(s)$ to meet Wang-et-al specifications (3.1), (3.2), and (3.3). For the design purpose, we consider FOCs such as PI^α (2.42) and $[PI]^\alpha$ (2.43). Later, these FOCs will be compared with the integer-order controllers for their limit cycle performances in the presence of plant nonlinearity.

Usually, the FOCs are compared with their integer-order counterparts. Therefore, one has to compare PI^α or $[PI]^\alpha$ controllers with the integer PI . However, it is necessary to select controllers having three parameters (Integer PI has two parameters) as the number of Wang-et-al specifications are three. It is also important to note that while designing PI^α or $[PI]^\alpha$ controllers if the resultant α is not equal to 1, it implies that the integer PI solution does not exist. This inherently shows the superiority of fractional PI over integer PI .

In the present chapter, for the additional comparison with PI^α and $[PI]^\alpha$, we consider three-parameter integer PID controller which has the TF, $K_p \left(1 + \frac{K_i}{s} + K_d s\right)$.

Let the numerical details for plant be $K = 5, a = 0.7, H = 0.05$. The designed controllers for $\phi_m = 50^\circ$ and $\omega_{gc} = 0.5$ rad/s are summarized in Table 4.1. For designing FOCs, the unified tuning expressions developed in Chapter 3 are utilized. The unified tuning expressions for integer PID controller are provided in the APPENDIX C.

Table 4.1: Resultant Designed Controllers

Controller Type	Designed Controller
PID	$0.0858 \left(1 + \frac{0.1385}{s} + 0.3978s \right)$
PI^α	$0.0855 \left(1 + \frac{0.0400}{s^{0.9707}} \right)$
$[PI]^\alpha$	$0.0857 \left(1 + \frac{0.0415}{s} \right)^{0.9408}$

4.2.2 Performance of Loop Transfer Function

For the verification of Wang-et-al performance of designed $PID, PI^\alpha,$ and $[PI]^\alpha$ controllers, the Nyquist plots of the open loop TF are obtained for every case and are superimposed as shown in Figure 4.3.

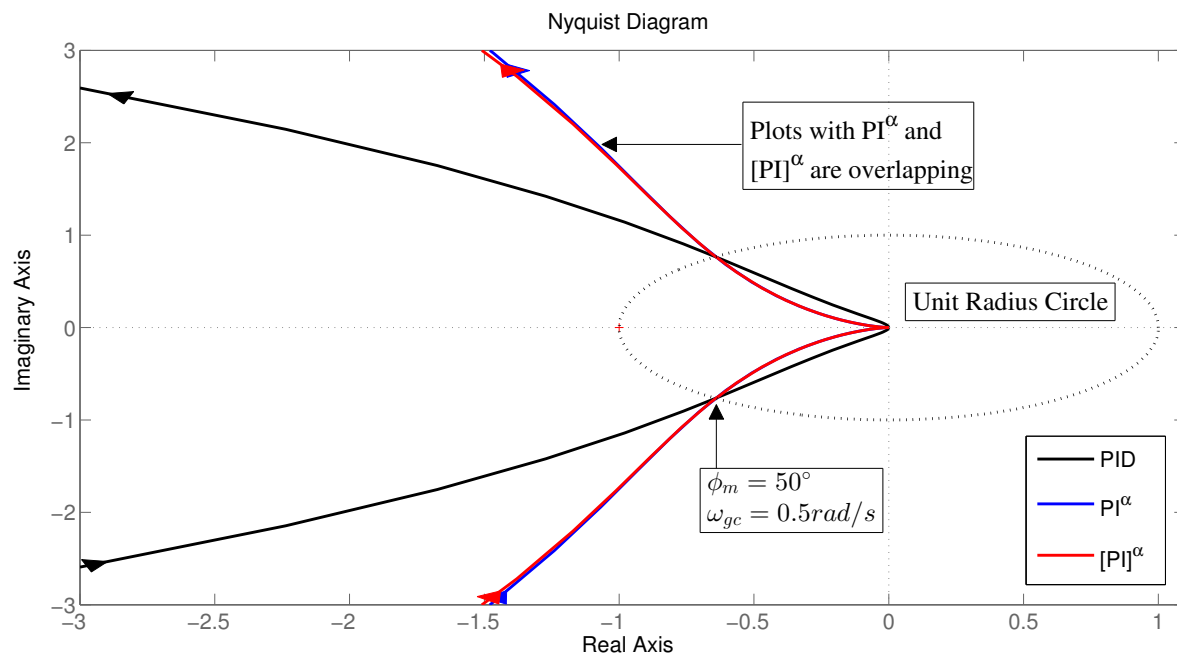


Figure 4.3: Superimposed Nyquist Plots of Loop TFs with $PID, PI^\alpha, [PI]^\alpha$

It is seen in Figure 4.3 that the designed controllers meet the desired ϕ_m and ω_{gc} . In addition, the phase angles for Nyquist plots do not change much for the frequencies local to ω_{gc} . This ensures the isodamping condition.

4.3 Limit Cycle Performance of Controllers

Since the designed PI^α , $[PI]^\alpha$, and PID controllers meet desired Wang-et-al specifications, it creates a common platform to investigate and compare their limit cycle suppression abilities in the presence of static nonlinearity. The analysis of their limit cycle performances is carried out using following methods:

1. Closed Loop Nonlinear Simulation
2. Describing Function Method

4.3.1 Closed Loop Nonlinear Simulation

The designed controllers given in Table 4.1 are tested for their closed loop step response performance in the presence of nonlinearity. For the step input of magnitude 0.1, the limit cycle responses $y_1(t)$ for PID , PI^α , and $[PI]^\alpha$ controllers are superimposed as presented in Figure 4.4. The corresponding sustained periodic oscillations in the system response $y_2(t)$ are shown in Figure 4.5. Recall that in Figure 4.2, $y_1(t)$ represents output of $G(s)$ whereas $y_2(t)$ is output of backlash nonlinearity. The Oustaloup [Oustaloup et al. (2000)] approximated fractional order term is considered for numerical simulation with the order 9 and frequency range [0.001, 1000] rad/s.

The limit cycle amplitude (X_0) and sustained oscillation amplitude (A) are obtained from Figure 4.4 and 4.5 respectively and are presented in Table 4.2. From the Table 4.2, it is seen that the FOCs (i.e. PI^α and $[PI]^\alpha$) produce nearly 20% reduction in the limit cycle amplitude as compared to the integer controller (PID). Consequently, approximately 70% reduction in the sustained oscillation amplitudes is observed with FOCs when compared with the integer PID .

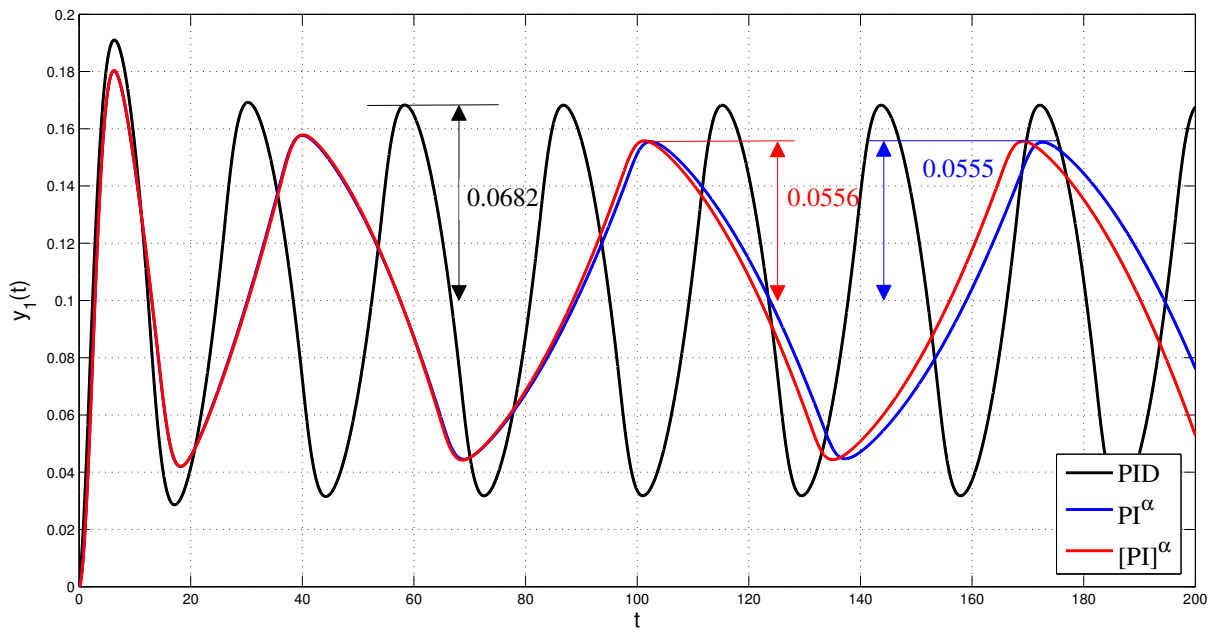


Figure 4.4: Limit Cycles with PID , PI^α , and $[PI]^\alpha$ Controllers

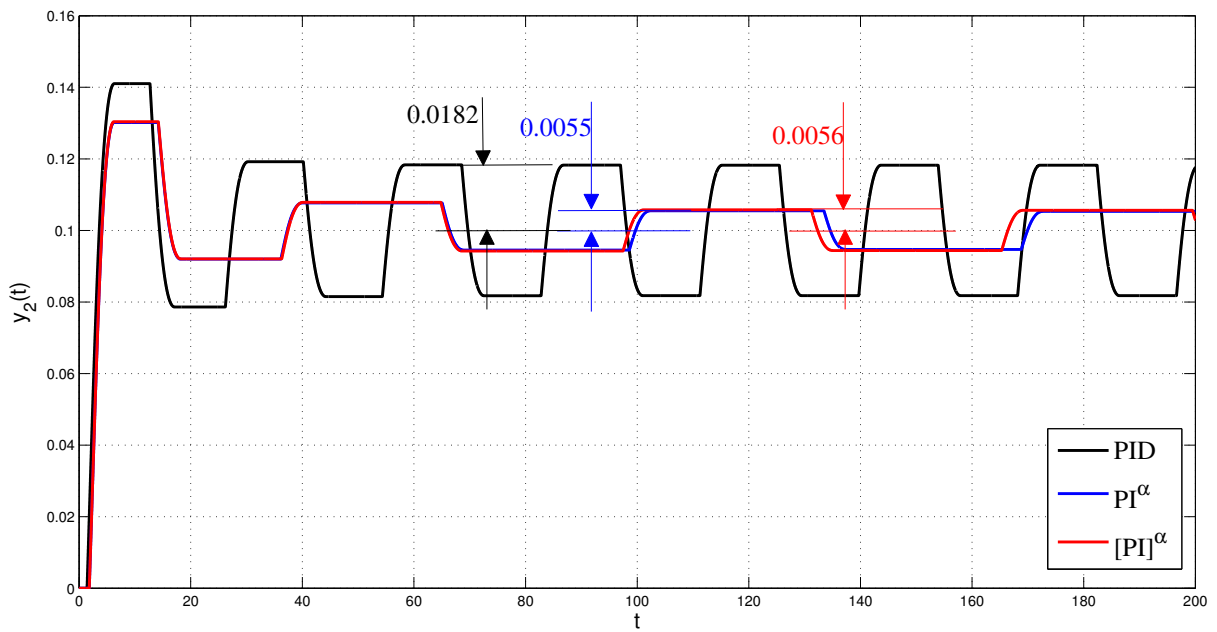


Figure 4.5: Sustained Oscillations in the Plant Output with PID , PI^α , and $[PI]^\alpha$ Controllers

4.3.2 Describing Function Analysis

To confirm the performance of above designed controllers in the presence of nonlinearity, DF analysis is performed. In this method, the Nyquist plot of the linear part of the system and the negative inverse of the DF of the nonlinearity are drawn in the complex plane. The intersection of these curves gives approximate limit-cycle details [Khalil and Grizzle (2002)].

The static backlash nonlinearity in the servo-system has following DF [Gopal (2012)]:

$$N(X) = \frac{1}{\pi} \left(\frac{\pi}{2} + \beta + \frac{1}{2} \sin(2\beta) - j \cos^2 \beta \right) \quad (4.1)$$

where, $\beta = \sin^{-1} \left(1 - \frac{2H}{X} \right)$.

In order to get the limit cycle amplitude X_0 and frequency ω_0 , the following relationship must hold true:

$$-\frac{1}{N(X)}_{X=X_0} = L(s)_{s=j\omega_0} \quad (4.2)$$

where, $L(s) = G(s)C(s)$.

The equation (4.2) is solved graphically in which the point of intersection of the curves of $-\frac{1}{N(X)}$ and $L(j\omega)$ gives the limit cycle details, X_0 and ω_0 . The curve of $L(j\omega)$ is superimposed on the the curve of $-\frac{1}{N(X)}$ for PID , PI^α and $[PI]^\alpha$ cases, as shown in Figures 4.6, 4.7, and 4.8 respectively. One can observe from these Figures that the locations of crossing points between the curves of $-\frac{1}{N(X)}$ and $L(j\omega)$ with different controllers are distinct, which leads to corresponding limit cycle performances. A detailed discussion on this point is pursued later in Section 5.2.2 of Chapter 5.

The limit cycle amplitude (X_0) and output sustained oscillation amplitude ($A = X_0 - H$) are summarized in Table 4.2. From the Table 4.2, it is seen that the FOCs produce significant reduction (nearly 20%) in the limit cycle amplitude as compared to the integer controller. Subsequently, it results into a reduction of nearly 66% in sustained oscillation amplitude in the plant response with FOCs. This is close to 70% as observed previously in the closed loop nonlinear simulation. The difference in the results with closed loop nonlinear simulation and DF method is due to approximation of nonlinearity in the latter case.

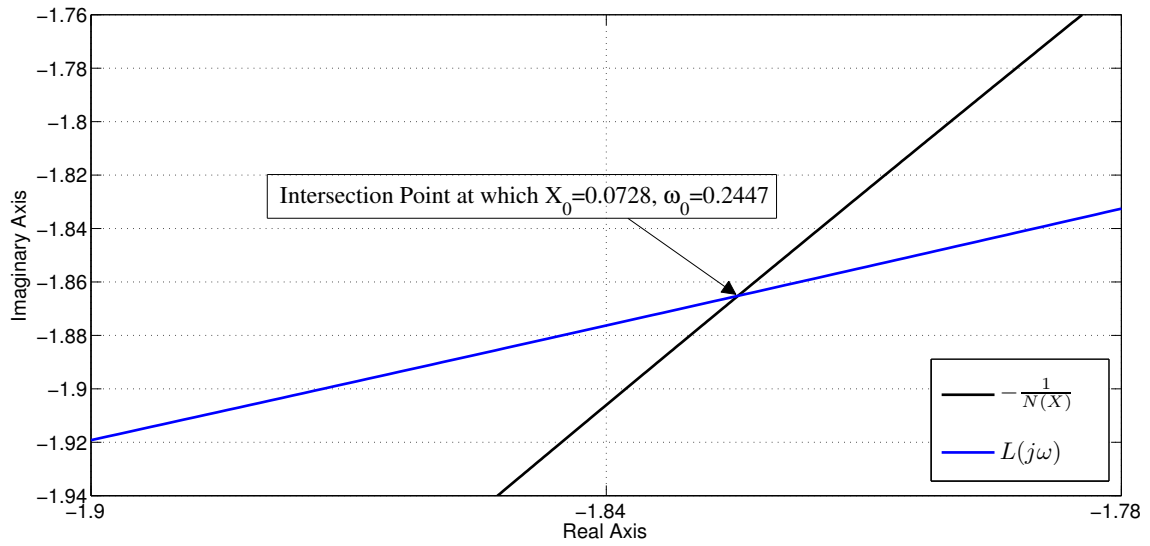


Figure 4.6: Computation of Limit Cycle Details: *PID* Case

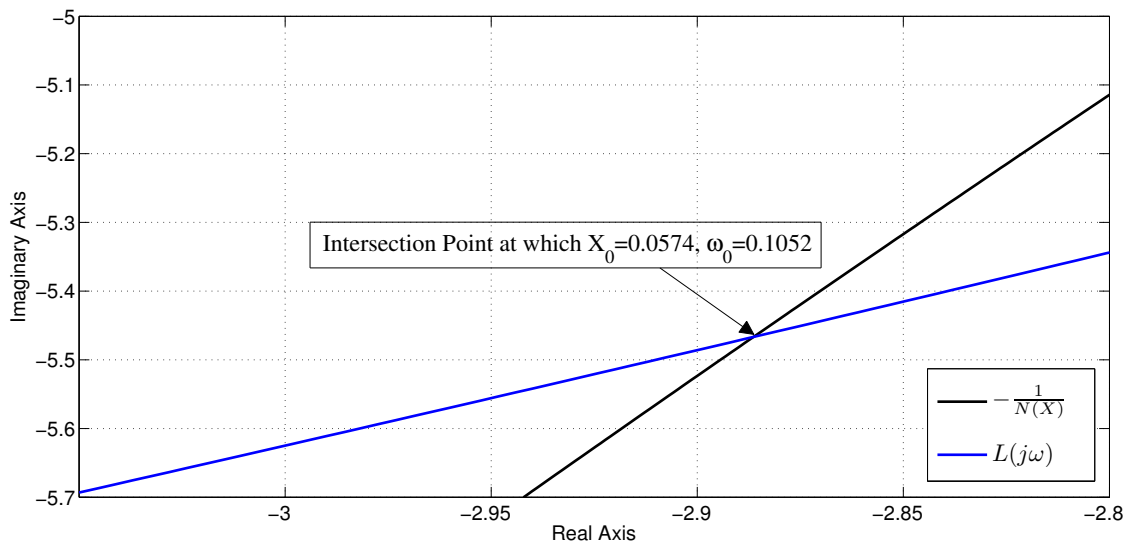


Figure 4.7: Computation of Limit Cycle Details: PI^α Case

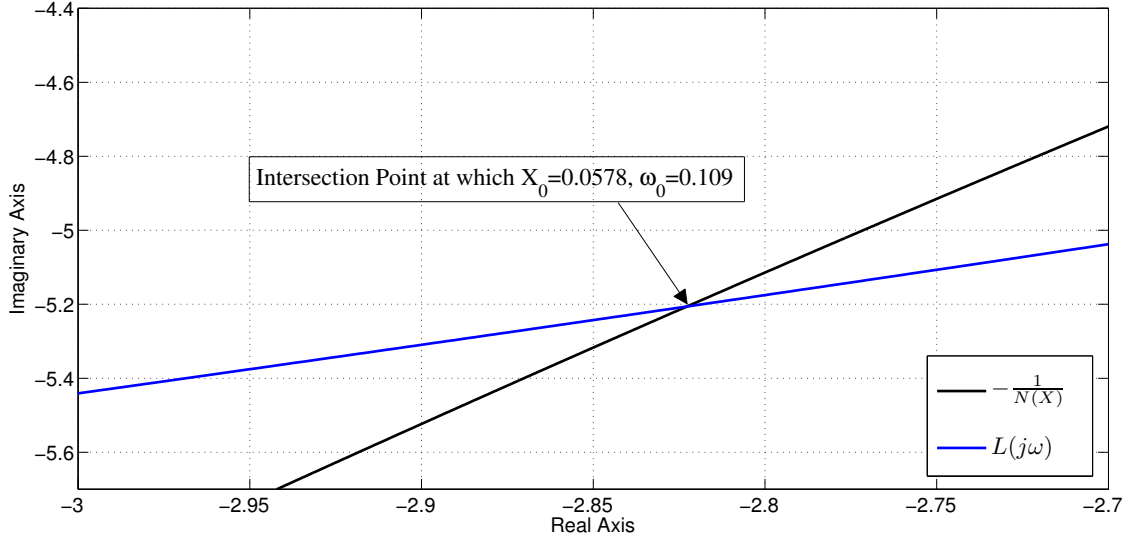


Figure 4.8: Computation of Limit Cycle Details: $[PI]^\alpha$ Case

Table 4.2: Controller Performance in the Presence of Nonlinearity

Analysis Method	Parameter	PID	PI^α	($\%$) Reduction	
				with PI^α over PID	with $[PI]^\alpha$ over PID
Closed Loop Simulation	X_0	0.0682	0.0555	18.6217	0.0556
	A	0.0182	0.0055	69.7802	0.0056
Describing Function	X_0	0.0728	0.0574	21.1538	0.0578
	A	0.0228	0.0074	67.5439	0.0078

4.4 Control of Precision Modular Servo Set-up

Similar to the discussion in Sections 4.2 and 4.3, we examine the possible superiority of FOCs over integer-order controllers in limit cycle suppression for an experimental set-up of Precision Modular Servo (PMS) developed by Feedback Instruments, UK. *[Manual (33-927S)]*

4.4.1 Plant Description

The PMS set-up consists of DC Motor, Digital Encoder, Power Supply, Pre-Amplifier, Servo-Amplifier, and Analogue Control Interface units as shown in Figure 4.9. The set-up allows testing of designed controllers in real time using MATLAB/SIMULINK environment [MATLAB (2010)] in Hardware-in-Loop configuration.

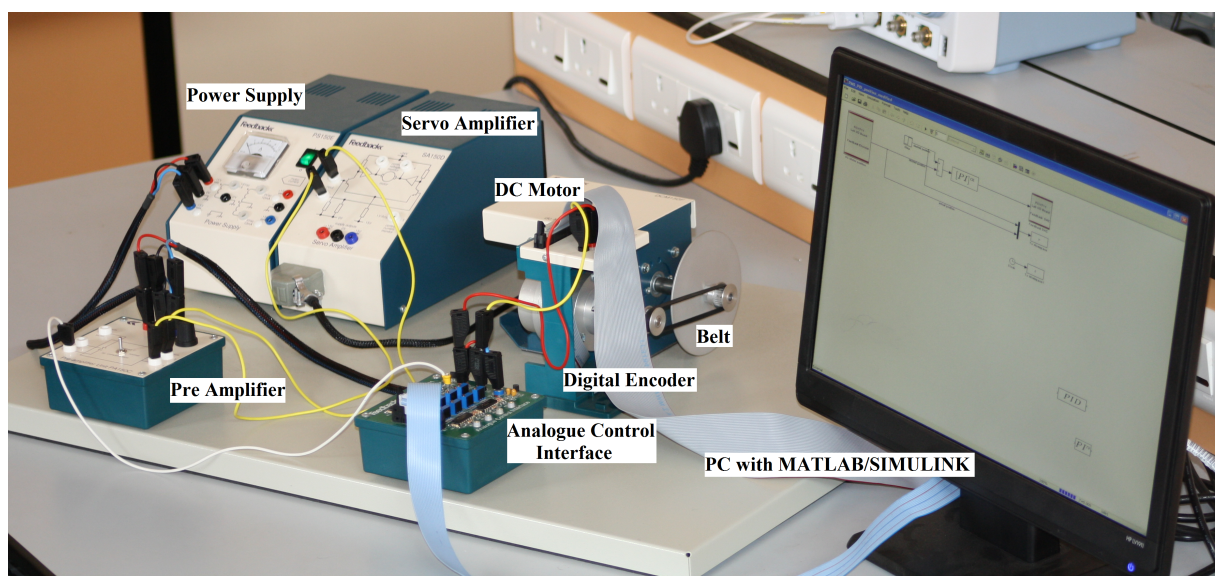


Figure 4.9: Pictorial View of the Precision Modular Servo Set-up

Mathematical model of the PMS system is nonlinear due to presence of elements such as saturation limits in the Pre-Amplifier and Servo-Amplifier stages, friction in the Motor, static backlash due to clearance in the belt. The belt connects Motor shaft to Digital Encoder.

For the controller design nonlinearity is neglected and the following TF model of the system is considered, which relates pre-amplifier input voltage to the voltage equivalent of DC Motor shaft angular position [Manual (33-927S)]:

$$G(s) = \frac{KK_t}{s(JLs^2 + (RJ + dL)s + (dR + K_bK_t))} \quad (4.3)$$

The numerical details of the plant [Manual (33-927S)] are given in Table 4.3.

Table 4.3: List of Parameters

Symbol	Description	Value	Unit
J	Moment of Inertia	140e-7	kgm ²
K_t	Torque Constant	0.052	Nm/A
K_b	Electromotive Force Constant	0.057	Vs/rad
d	Linear Approximation of Viscous Friction	1e-6	Nms/rad
R	Resistance	2.5	Ω
L	Inductance	2.5	mH
K	Amplifier Gain	9.6	—

4.4.2 Designed Controllers

By adopting a procedure similar to one discussed in Section 4.2, the controllers PID , PI^α , and $[PI]^\alpha$ are designed for the PMS set-up to satisfy Wang et al specifications ($\phi_m = 70^\circ$, $\omega_{gc} = 10$ rad/s). The resultant controllers are summarized in Table 4.4.

Table 4.4: Designed Controllers

Controller Type	Designed Controller
PID	$0.05816 \left(1 + \frac{1.795}{s} - 0.0056s \right)$
PI^α	$0.0454 \left(1 + \frac{1.375}{s^{0.5237}} \right)$
$[PI]^\alpha$	$0.0524 \left(1 + \frac{13.7567}{s} \right)^{0.2459}$

4.4.3 Performance of Loop Transfer Function

The performance of the designed loop TF is analyzed by considering the Nyquist plots of corresponding loop TFs as shown in Figure 4.10. As seen in Figure 4.10, the designed controllers meet the required ϕ_m and ω_{gc} specifications along with the isodamping condition. This creates a common platform for comparing their limit cycle performances with the real set-up.

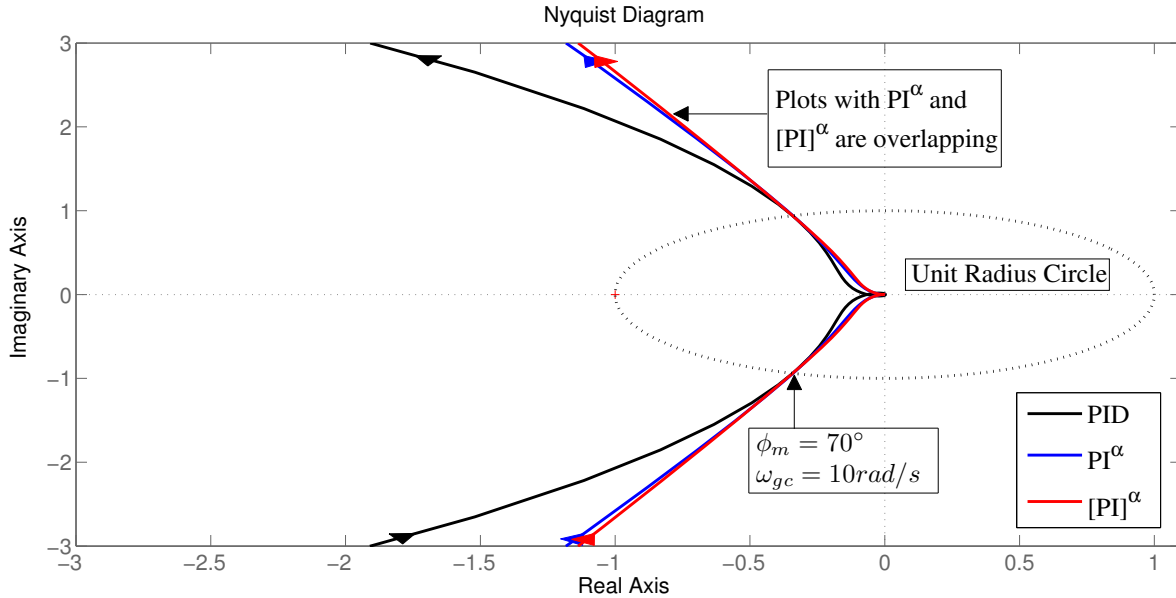


Figure 4.10: Superimposed Nyquist Plots for Loop TFs with PID , PI^α , and $[PI]^\alpha$ Controllers

4.5 Limit Cycle Performance with Laboratory Experimental Set-up

The designed controllers shown in Table 4.4 are tested for their closed loop response with the real plant using hardware-in-loop configuration. The real time responses obtained for step command input of amplitude 10 with the various controllers are shown in Figure 4.11. The zoomed view of the selected portion of Figure 4.11 is shown in Figure 4.12.

The controllers produce undesirable sustained oscillations in the plant output response due to existence of stable limit cycles. The sustained oscillation amplitudes in the closed loop response for PID , PI^α , and $[PI]^\alpha$ controllers as observed in Figure 4.12 are presented in Table 4.5. From the Table 4.5, it is seen that FOCs produce more than 60% reduction in these amplitudes as compared to integer PID .

Thus, the experimental results with PMS set-up suggest that the FOCs PI^α , $[PI]^\alpha$ are significantly better over the integer PID in their limit cycle performance. Additional confirmation of these results using DF method has not been performed due to unavailability of exact nonlinear mathematical model for the PMS set-up.

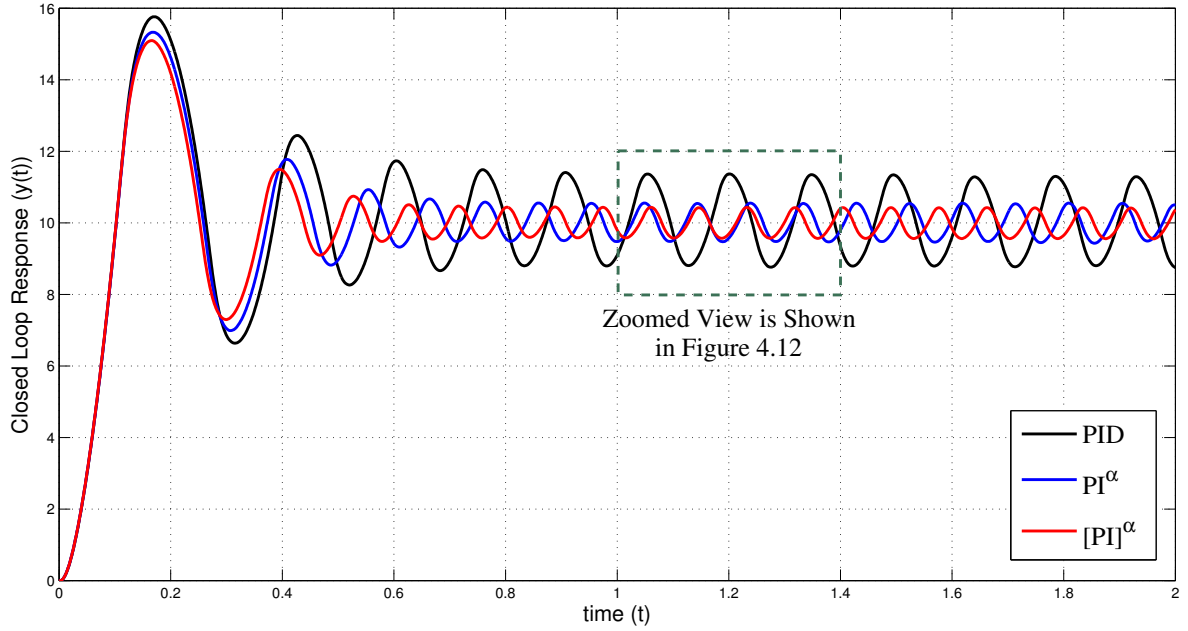


Figure 4.11: Sustained Oscillations with PID , PI^α , and $[PI]^\alpha$ Controllers

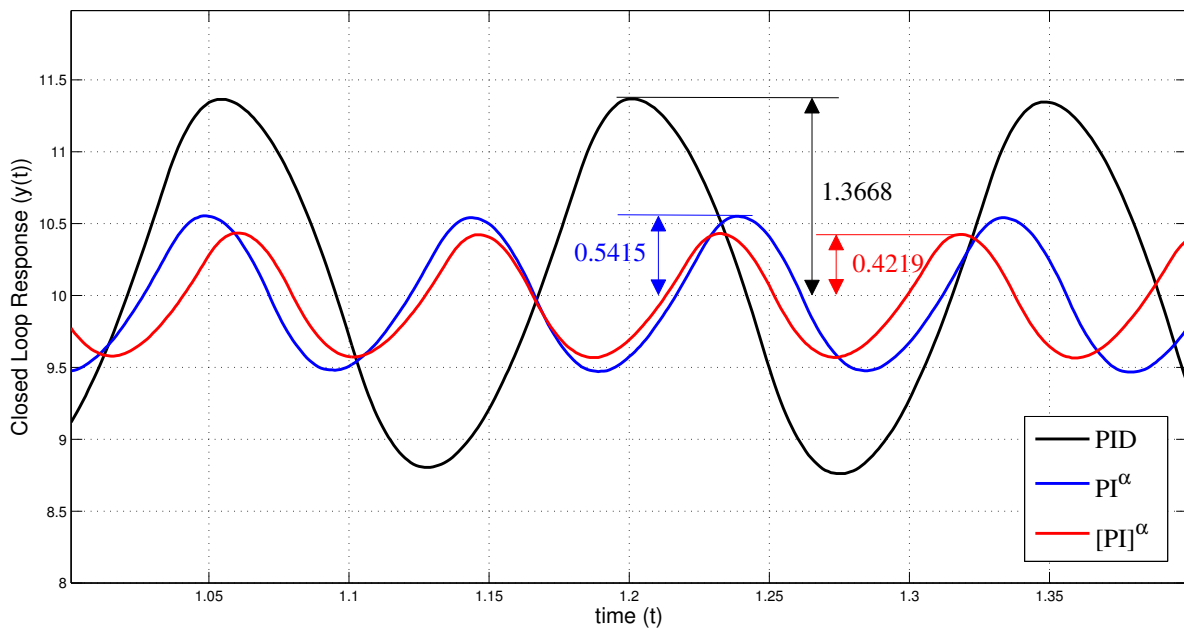


Figure 4.12: Zoomed View From Figure 4.11

Table 4.5: Sustained Oscillation Amplitudes with Various Controllers

PID	PI^α	(%) Reduction with PI^α over PID	$[PI]^\alpha$	(%) Reduction with $[PI]^\alpha$ over PID
1.3668	0.5415	60.382	0.4219	69.132

4.6 Summary

In this chapter, three-parameter FOCs such as PI^α and $[PI]^\alpha$ and integer PID were considered for an elementary servo plant containing a static backlash nonlinearity. The controllers were designed to meet Wang-et-al specifications for the plant TF and subsequently their limit cycle performances in the presence of plant nonlinearity were observed. The results obtained by means of closed loop simulation as well as DF analysis exhibited a better limit cycle performance with FOCs as compared to the integer PID . Such observations were also made for the experimental PMS set-up.

Overall, the results presented in this chapter hinted towards the capability of FOCs in producing the better limit cycle performance than the integer-order controllers. We present a more detailed assessment in this direction in the next chapter.

CHAPTER 5

Limit Cycle Performance of Fractional-Order Controllers for Plants with Backlash and Relay Nonlinearities

5.1 Introduction

For plants containing separable nonlinearity, the closed loop control system usually produces undesirable sustained periodic oscillations in the plant output response owing to the existence of stable limit cycles [Gopal (2012)]. In the previous chapter, we noticed a superior limit cycle performance by Fractional-Order Controllers (FOCs) over integer-order controllers for such plants when they were designed to meet Wang-et-al specifications. In the present chapter, we aim at a more detailed study in this direction by specifically targeting the limit cycle performance for the suppression of sustained oscillation amplitudes at the controller design stage. For this purpose, we consider two types of plant models, namely, plant with backlash and plant with relay. In each case, certain optimization based controller design frameworks are formulated. Subsequently, the FOCs are tuned and compared with their integer-order counterparts.

5.2 FOCs for Plants with Backlash Nonlinearity

Let us consider the schematics shown in Figure 5.1 which consists of a controller $C(s)$ and a plant having a Transfer Function (TF) $G(s)$ in cascade with a static nonlinearity.

For designing $C(s)$, it is desired to incorporate the nonlinearity in terms of its Describing Function (DF). The DF approximates the nonlinearity by neglecting higher harmonics relative to the first harmonic at its output. Therefore, it is essential that the linear part of the designed system along the loop (i.e. $C(s)G(s)$) provides sufficiently strong low pass filtering effects [Gopal (2012)]. In general, such requirement is satisfied when the loop is shaped to meet standard control specifications. However, one

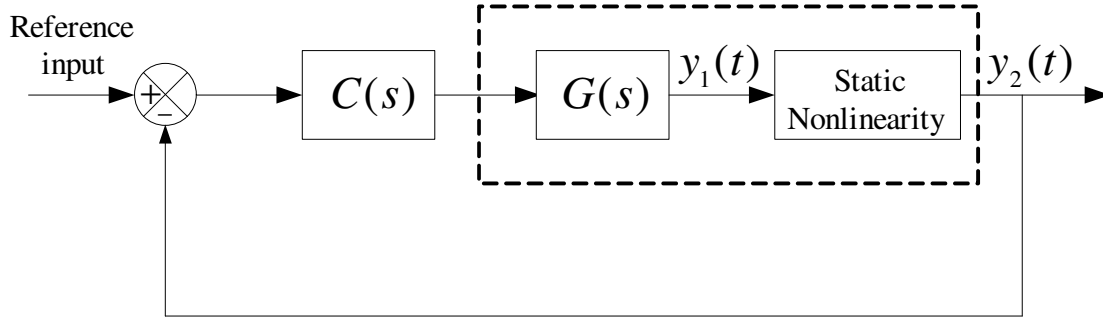


Figure 5.1: Closed Loop Control System Schematics

needs to perform the closed loop simulation of the designed control system containing separable nonlinearity so as to confirm that the desired performance is sufficiently met. Additionally, we focus on the most common class of nonlinear loops for which there occurs only one intersection between the Nyquist plot of $C(s)G(s)$ and the negative inverse of DF to form a stable limit cycle point¹.

Under above conditions, the controller design is formulated as a constrained optimization problem as presented in the next subsection.

5.2.1 Optimization Problem for Limit Cycle Minimization

We formulate the following constrained optimization problem for meeting desirable limit cycle and transient performance:

$$\underset{(\text{Controller Parameters}, \omega, X)}{\text{Minimize}} \quad X$$

subject to:

1. Nyquist Condition for Limit Cycle Existence [Gopal (2012)]:

$$-\frac{1}{N(X)} = [C(s)G(s)]_{s=j\omega} \quad (5.1)$$

Where, $N(X)$ denotes DF of the separable nonlinearity in the plant. X denotes limit cycle amplitude, i.e. the peak amplitude of signal $y_1(t)$ (refer Figure 5.1) in the steady state.

¹The stability of the limit cycle point is essential for the sustained oscillations to be produced in the output response in the presence of nonlinearity.

2. Gain Crossover Frequency (ω_{gc}) Specification:

$$|C(j\omega_{gc})G(j\omega_{gc})| = 1 \quad (5.2)$$

3. Phase Margin (ϕ_m) Specification:

$$\angle[C(j\omega_{gc})G(j\omega_{gc})] = -\pi + \phi_m \quad (5.3)$$

The above optimization problem designs the control system to satisfy certain steady state and transient requirements of the plant output response as explained below:

1. Steady State Requirements

For the schematics shown in Figure 5.1, the minimization of X leads to the minimization of amplitude of sustained oscillations occurring in the steady state of the signal $y_2(t)$ for certain nonlinearities such as static backlash, dead-zone, etc. Of these, the static backlash case is of high practical importance which occurs commonly in the servo-systems with gears. A few other nonlinearities falling in this class have been given in [Sridhar (1960)] .

2. Transient Requirements

The extra performance specifications such as gain crossover frequency and phase margin are forced to capitalize on the degree of freedom available with the parameters of optimization. It is important to note that these loop TF specifications cannot incorporate nonlinearity effects. However, they are still useful to some extent in shaping the transient response of the plant output in the presence of nonlinearity.

5.2.2 Graphical Interpretation of the Optimization Problem

On solving the proposed optimization problem, one obtains a controller $C(s)$ which meets the desired (ω_{gc}, ϕ_m) specifications and produces limit cycles with least amplitude X . In the present subsection, we interpret such optimization problem graphically. The graphical interpretation must consider the following points:

1. The optimization problem is constructed for the class of nonlinear loops which produces only one *stable* limit cycle point. For the stability of limit cycles, it is essential that the plot of $-\frac{1}{N(X)}$ seen in the increasing direction of X crosses the given Nyquist curve seen in the increasing direction of ω from right to left (i.e. from unstable region to stable region) [Khalil and Grizzle (2002)].
2. Minimization of X can be explained graphically by comparing the limit cycle performances of two loops $L_1(s) = C_1(s)G(s)$ and $L_2(s) = C_2(s)G(s)$, which meet the common (ω_{gc}, ϕ_m) specifications.

Based on above discussion, we sketch Figure 5.2 which superimposes following curves:

- (i) $-\frac{1}{N(X)}$ plot of the nonlinearity
- (ii) Nyquist plots of loop TFs $L_1(s) = C_1(s)G(s)$ and $L_2(s) = C_2(s)G(s)$ (of controllers $C_1(s)$ and $C_2(s)$ respectively)

The arrow in the Nyquist plots indicates increasing ω direction. The arrow in $-\frac{1}{N(X)}$ plot shows increasing X direction.

In Figure 5.2, Nyquist plots of L_1 and L_2 pass through a fixed phase margin (ϕ_m) point in complex plane at ω_{gc} (refer point ①). Apart from the point ①, the Nyquist plots are separated from each other in general. Due to such separation, the plot of $-\frac{1}{N(X)}$ superimposed on this diagram crosses different Nyquist plots at distinct points (points ② and ③). The relative positions of the crossing points for Nyquist plots play an important role in deciding the superiority of the controller in limit cycle suppression. The following proposition is stated to give a sufficient condition for finding the superior controller in limit cycle minimization for the schematics shown in Figure 5.1:

Proposition 5.1. *In Figure 5.2, for the given $-\frac{1}{N(X)}$ plot seen in the increasing direction of X , if the crossing point of Nyquist plot for L_1 (i.e. point ②) occurs before the crossing point for L_2 (i.e. point ③), then the C_1 is better over C_2 in limit cycle suppression.*

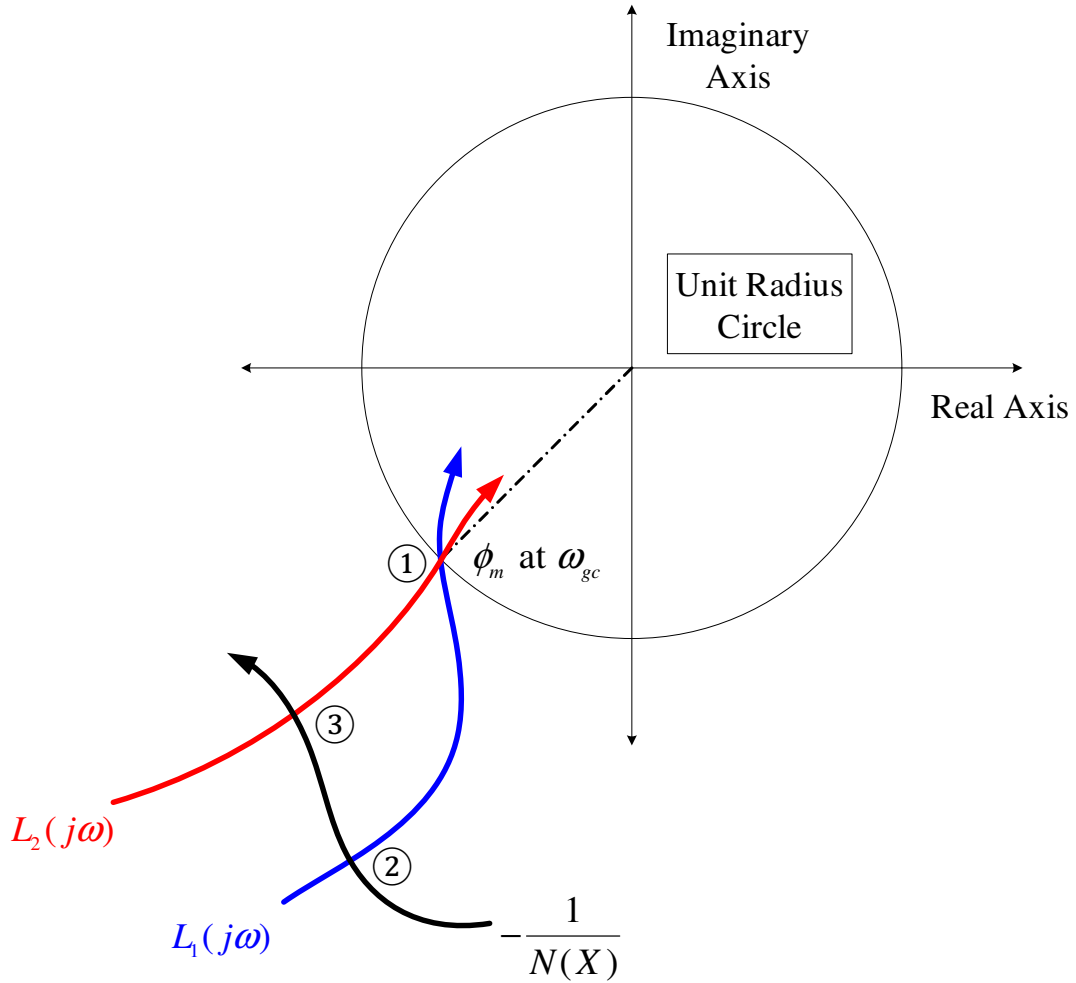


Figure 5.2: Graphical Interpretation of Optimization Problem

Proof. At point (2), the Nyquist condition [Gopal (2012)] leads to following relation:

$$-\frac{1}{N(X_1)} = [C_1(s)G(s)]_{s=j\omega_1} \quad (5.4)$$

Where, X_1 and ω_1 are limit cycle amplitude and frequency respectively.

Similarly, we get the following relation at point (3):

$$-\frac{1}{N(X_2)} = [C_2(s)G(s)]_{s=j\omega_2} \quad (5.5)$$

Where, X_2 and ω_2 are limit cycle amplitude and frequency respectively.

Since, the arrow direction for the curve $-\frac{1}{N(X)}$ is in increasing direction of X , we

have:

$$X_1 < X_2 \quad (5.6)$$

Therefore, it is clear from (5.4), (5.5), and (5.6) that C_1 is better over C_2 in limit cycle suppression. \square

Based on the above discussion, we draw the following remarks:

Remark 5.1. *Optimization problem proposed in Section 5.2.1 results into a controller that produces least X in addition to meeting (ω_{gc}, ϕ_m) specifications. Based on its graphical interpretation as presented in Figure 5.2, such controller is $C_1(s)$ which is better in limit cycle suppression over any other $C_2(s)$ as per Proposition 5.1.*

Remark 5.2. *The Proposition 5.1 is further useful for graphically comparing the limit cycle performance of FOCs with their integer-order counterparts when they are tuned based on the optimization problem proposed in Section 5.2.1.*

5.2.3 Demonstration with a Servo System Containing Static Backlash

For illustrating design and comparison of controllers under limit cycle suppression property, it is necessary to consider a suitable plant case having a TF and a single separable nonlinearity in cascade. Let us recall the servo-system with gears presented in Chapter 4.

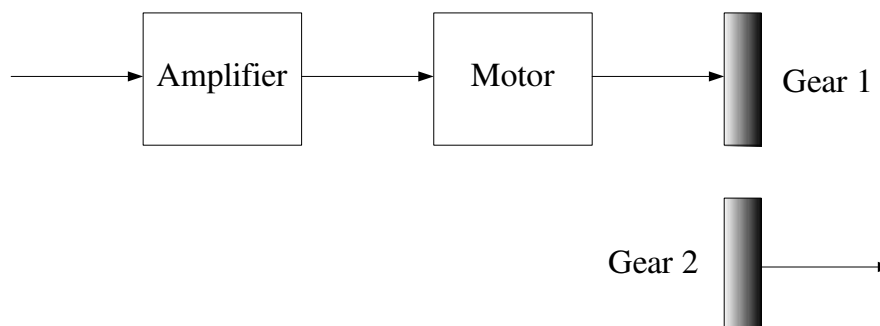


Figure 5.3: A Servo System with Gears (Recalled from Figure 4.1)

Also recalling the discussion in Section 4.2, the mathematical model of such plant consists of a TF, $G(s) = \frac{K}{s(s+a)}$ of the amplifier-motor combination and a static backlash

nonlinearity between gear 1 and gear 2. The closed loop control scheme consisting of controller $C(s)$ and the servo-system with gears is shown in the Figure given below:

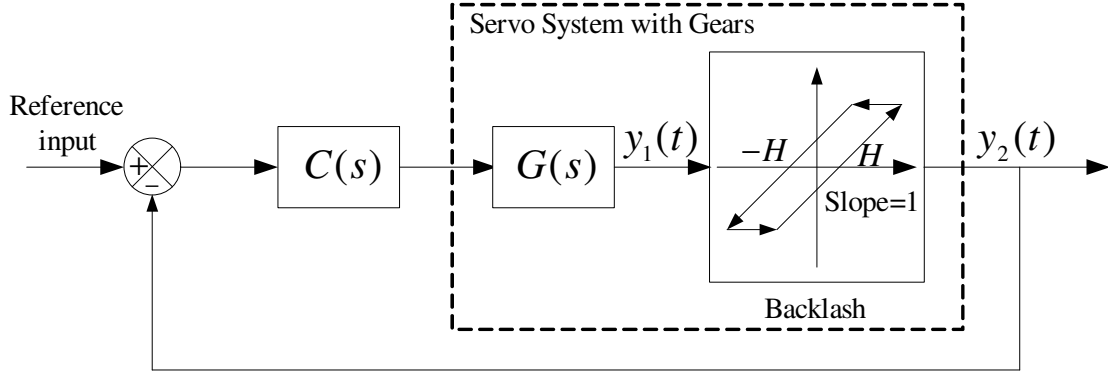


Figure 5.4: Closed Loop Control Scheme (Recalled from Figure 4.2)

The backlash nonlinearity in the servo-system has following DF [Gopal (2012)]:

$$N(X) = \frac{1}{\pi} \left(\frac{\pi}{2} + \beta + \frac{1}{2} \sin(2\beta) - j \cos^2 \beta \right) \quad (5.7)$$

where, $\beta = \sin^{-1} \left(1 - \frac{2H}{X} \right)$.

It is desired to design and compare FOCs and their integer-order counterparts for the control scheme shown in Figure 5.4 under the optimization problem discussed in Section 5.2.1. The following controllers are selected:

- Integer PI and Fractional PI (i.e. PI^α , $[PI]^\alpha$).
- Integer PID and Fractional PID (i.e. $PI^\alpha D^\beta$).

For illustration purpose, the following numerical values are selected for plant parameters and design specifications: $K = 5$, $a = 0.7$, $H = 0.05$, $\phi_m = 50^\circ$, $\omega_{gc} = 0.5$ rad/s. Also, the bounds of controller parameters are fixed as follows: $K_p \in (0, 1]$, $K_i \in (0, 1]$, $K_d \in (0, 1]$, $\alpha \in (0, 1)$, $\beta \in (0, 1)$. In the chosen bounds for K_d , 0 is not included to maintain the separate identity of PID and PI controllers while tuning.

5.2.4 Solution to Constrained Optimization Problem

In general, the optimization problem formulated in Section 5.2.1 is non-convex in nature which is difficult to solve analytically. Hence, a numerical approach is preferred.

However, it usually leads to the sub-optimal solutions due to existence of local minima. Therefore, it becomes necessary to solve the problem repeatedly with sufficiently large number of randomly selected initial guesses.

The `fmincon()` solver available in MATLAB [MATLAB (2010)] is used for this purpose which simulates Interior-point algorithm. For each controller case, ten random initial guesses are taken and the corresponding converged values are preserved. Best among the ten (i.e. the one with least X) is selected for the performance analysis. The simulation results for controllers PI , PI^α , $[PI]^\alpha$, PID , and $PI^\alpha D^\beta$ are presented in Tables 5.1-5.5 respectively.

Table 5.1 presents results for Integer PI controller. The controller producing least X among 10 ($K_p = 0.0858$, $K_i = 0.039$, $\omega = 0.1091$, $X = 0.0578$) is chosen as highlighted in Table 5.1. The selected controller is further analyzed for the stability of limit cycle using the graphical approach as will be explained in section 5.2.5. If the limit cycle nature is found *unstable*, selected controller is discarded and the new selection is made from the remaining ones as per the least X criterion. Similarly, the selected PI^α , $[PI]^\alpha$, PID , and $PI^\alpha D^\beta$ controllers have been highlighted in Tables 5.2-5.5 respectively.

5.2.5 Performance Analysis Using Graphical Interpretation

In the present subsection, we compare the performances of FOCs and their integer-order counterparts to determine the superior controllers on the basis of Remark 5.2.

Figure 5.5 shows the Nyquist plots for loop TFs with the designed integer PI and PI^α , $[PI]^\alpha$ controllers over which the plot of $-\frac{1}{N(X)}$ is superimposed. (The selected PI , PI^α , and $[PI]^\alpha$ controllers have been highlighted in the Tables 5.1, 5.2, and 5.3 respectively.) The crossing points between $-\frac{1}{N(X)}$ and $C(j\omega)G(j\omega)$ (refer points \textcircled{A} , \textcircled{B} , and \textcircled{C} for PI , PI^α , and $[PI]^\alpha$ cases respectively) give the following limit cycle details:

- At point \textcircled{A} (PI case), $X = 0.0578$, $\omega = 0.1091$.
- At point \textcircled{B} (PI^α case), $X = 0.0504$, $\omega = 0.0075$.
- At point \textcircled{C} ($[PI]^\alpha$ case), $X = 0.0505$, $\omega = 0.011$.

Table 5.1: Design of Integer PI Controller

Random Initial Guess				Converged Value			
K_p	K_i	ω	X	K_p	K_i	ω	X
0.8530	0.6221	0.3510	0.5132	0.0858	0.0390	0.1091	0.0578
0.4018	0.0760	0.2399	0.1233	0.0858	0.0390	0.1091	0.0578
0.1839	0.2400	0.4173	0.0497	0.0858	0.0390	0.1091	0.0578
0.9027	0.9448	0.4909	0.4893	0.0384	1.0000	0.4825	0.1001
0.3377	0.9001	0.3692	0.1112	0.0380	1.0000	0.5196	0.0750
0.5470	0.2963	0.7447	0.1890	0.0858	0.0390	0.1091	0.0578
0.6868	0.1835	0.3685	0.6256	0.0858	0.0390	0.1091	0.0578
0.7802	0.0811	0.9294	0.7757	0.0858	0.0390	0.1091	0.0578
0.4868	0.4359	0.4468	0.3063	0.0858	0.0390	0.1091	0.0578
0.5085	0.5108	0.8176	0.7948	0.0858	0.0390	0.1091	0.0578

Table 5.2: Design of PI^α Controller

Random Initial Guess					Converged Value				
K_p	K_i	α	ω	X	K_p	K_i	α	ω	X
0.6443	0.3786	0.8116	0.5328	0.3507	0.0801	0.0745	0.5533	0.0487	0.0528
0.9390	0.8759	0.5502	0.6225	0.5870	0.0792	0.0829	0.5083	0.0430	0.0524
0.2077	0.3012	0.4709	0.2305	0.8443	0.0742	0.1425	0.3347	0.0235	0.0512
0.1948	0.2259	0.1707	0.2277	0.4357	0.0747	0.1359	0.3469	0.0247	0.0513
0.3111	0.9234	0.4302	0.1848	0.9049	0.0534	0.5658	0.1298	0.0075	0.0504
0.9797	0.4389	0.1111	0.2581	0.4087	0.0768	0.1100	0.4075	0.0311	0.0517
0.5949	0.2622	0.6028	0.7112	0.2217	0.0553	0.5128	0.1377	0.0079	0.0504
0.1174	0.2967	0.3188	0.4242	0.5079	0.0708	0.1922	0.2678	0.0173	0.0509
0.0855	0.2625	0.8010	0.0292	0.9289	0.0733	0.1555	0.3134	0.0214	0.0511
0.7303	0.4886	0.5785	0.2373	0.4588	0.0779	0.0967	0.4503	0.0360	0.0520

Table 5.3: Design of $[PI]^\alpha$ Controller

Random Initial Guess					Converged Value				
K_p	K_i	α	ω	X	K_p	K_i	α	ω	X
0.9063	0.8797	0.8178	0.2607	0.5944	0.0821	0.7408	0.0797	0.0115	0.0506
0.0225	0.4253	0.3127	0.1615	0.1788	0.0849	0.1643	0.2453	0.0777	0.0545
0.4229	0.0942	0.5985	0.4709	0.6959	0.0852	0.1323	0.3011	0.0885	0.0554
0.6999	0.6385	0.0336	0.0688	0.3196	0.0840	0.3227	0.1359	0.0356	0.0518
0.5309	0.6544	0.4076	0.8200	0.7184	0.0848	0.1945	0.2099	0.0675	0.0538
0.9686	0.5313	0.3251	0.1056	0.6110	0.0828	0.5606	0.0924	0.0160	0.0508
0.6761	0.2891	0.6718	0.6951	0.0680	0.0820	0.7702	0.0783	0.0110	0.0505
0.7788	0.4235	0.0908	0.2665	0.1537	0.0849	0.1669	0.2417	0.0768	0.0545
0.2810	0.4401	0.5271	0.4574	0.8754	0.0844	0.2463	0.1702	0.0519	0.0527
0.5181	0.9436	0.6377	0.9577	0.2407	0.0830	0.5270	0.0960	0.0174	0.0508

Table 5.4: Design of Integer PID Controller

Random Initial Guess					Converged Value				
K_p	K_i	K_d	ω	X	K_p	K_i	K_d	ω	X
0.4587	0.6619	0.7703	0.3502	0.662	0.0858	0.1307	0.3667	0.2375	0.0718
0.4162	0.8419	0.8329	0.2564	0.6135	0.0858	0.0697	0.1229	0.1631	0.0628
0.5822	0.5407	0.8699	0.2648	0.3181	0.0858	0.0474	0.0335	0.1252	0.0592
0.1192	0.9398	0.6456	0.4795	0.6393	0.0383	1.0000	0.0100	0.3398	0.0951
0.5447	0.6473	0.5439	0.7210	0.5225	0.0858	0.1522	0.4529	0.2566	0.0746
0.9937	0.2187	0.1058	0.1097	0.0636	0.0858	0.088	0.1959	0.1892	0.0656
0.4046	0.4484	0.3658	0.7635	0.6279	0.0858	0.0547	0.0626	0.1383	0.0604
0.7720	0.9329	0.9727	0.1920	0.1389	0.0858	0.1652	0.5046	0.2668	0.0763
0.6963	0.0938	0.5254	0.5303	0.8611	0.0858	0.1646	0.5023	0.2663	0.0762
0.4849	0.3935	0.6714	0.7413	0.5201	0.0858	0.0891	0.2002	0.1907	0.0658

Table 5.5: Design of $PI^\alpha D^\beta$ Controller

Random Initial Guess							Converged Value						
K_p	K_i	K_d	α	β	ω	X	K_p	K_i	K_d	α	β	ω	X
0.6967	0.5828	0.8154	0.879	0.9889	0.0005	0.8654	0.0551	0.3644	0.5335	0.5499	0.5952	0.1535	0.0603
0.6126	0.99	0.5277	0.4795	0.8013	0.2278	0.4981	0.0437	0.5445	0.4762	0.3060	0.2605	0.0468	0.0525
0.9009	0.5747	0.8452	0.7386	0.586	0.2467	0.6664	0.0425	0.5485	0.4498	0.2238	0.0959	0.0195	0.0510
0.0835	0.6260	0.6609	0.7298	0.8908	0.9823	0.7690	0.0640	0.2680	0.6950	0.8718	0.6348	0.2509	0.0739
0.5814	0.9283	0.5801	0.017	0.1209	0.8627	0.4843	0.0604	0.2533	0.4183	0.6216	0.5171	0.1490	0.0602
0.8449	0.2094	0.5523	0.6299	0.032	0.6147	0.3624	0.0612	0.323	0.3013	0.4337	0.7682	0.0983	0.0557
0.0495	0.4896	0.1925	0.1231	0.2055	0.1465	0.1891	0.0536	0.4004	0.4753	0.4741	0.5866	0.1243	0.0577
0.0427	0.6352	0.2819	0.5386	0.6952	0.4991	0.5358	0.0592	0.3355	0.3483	0.4581	0.6860	0.1097	0.0565
0.4452	0.1239	0.4904	0.8530	0.8739	0.2703	0.2085	0.0493	0.1529	0.6527	0.6562	0.0729	0.0863	0.0554
0.5650	0.6403	0.4170	0.2060	0.9479	0.0821	0.1057	0.0563	0.3650	0.4662	0.5077	0.6388	0.1375	0.0588

It is observed from the above values that the FOCs minimize X better than integer-order controllers. The nature of the limit cycle shown in Figure 5.5 is *stable* in each cases. This can be depicted by seeing Nyquist curve in the increasing direction of ω and noticing that its crossing by $-\frac{1}{N(X)}$ plot in the increasing direction of X is from right to left (i.e. from unstable region to stable region). Therefore, the selected PI , PI^α , and $[PI]^\alpha$ controllers are acceptable.

It can also be seen from the plot (and the subsequent zoomed view in Figure 5.6) that the required phase margin ($\phi_m = 50^\circ$) and gain crossover frequency ($\omega_{gc} = 0.5$ rad/s) are met by the designed controllers. Furthermore, for the given $-\frac{1}{N(X)}$ plot seen in the increasing direction of X , crossing points for FOC cases (i.e. points (B) and (C)) occur *before* the crossing point for integer controller (i.e. point (A)). This confirms the better limit cycle suppression capabilities of FOCs.

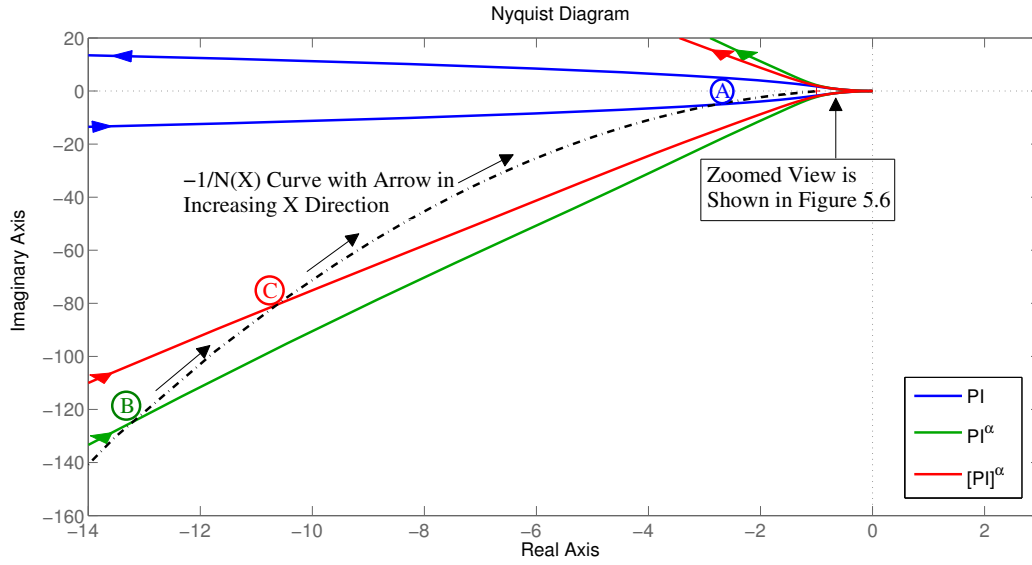


Figure 5.5: Points Ⓑ and Ⓒ occur before point Ⓐ for $-\frac{1}{N(X)}$ plot seen in the arrow direction indicating superiority of PI^α and $[PI]^\alpha$ over PI

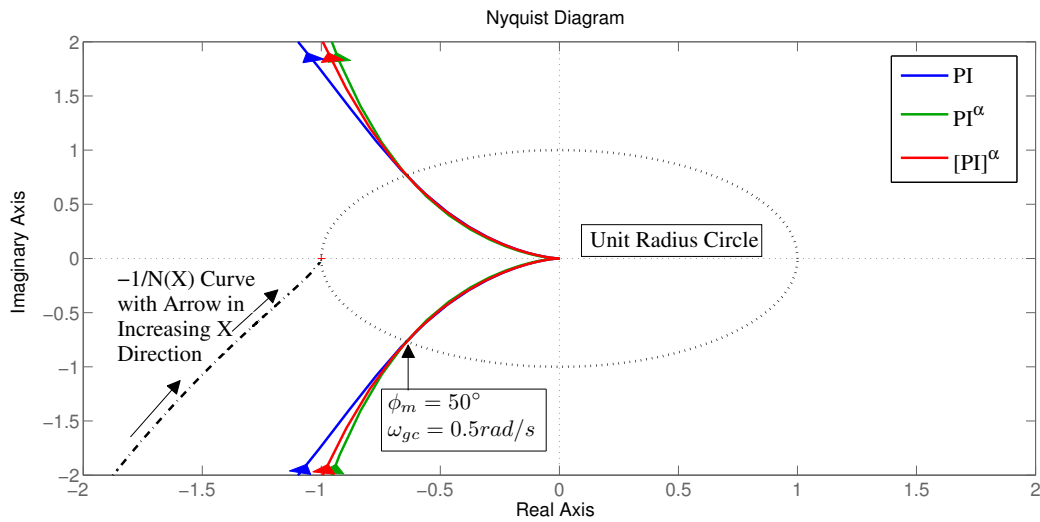


Figure 5.6: Zoomed view of Figure 5.5: fractional and integer PI meeting required phase margin and gain crossover frequency

Similar results are observed with the designed integer and fractional PID controllers as shown in Figure 5.7. (The selected PID and $PI^\alpha D^\beta$ controllers have been highlighted in Tables 5.4 and 5.5 respectively.) The corresponding zoomed view is shown in Figure 5.8.

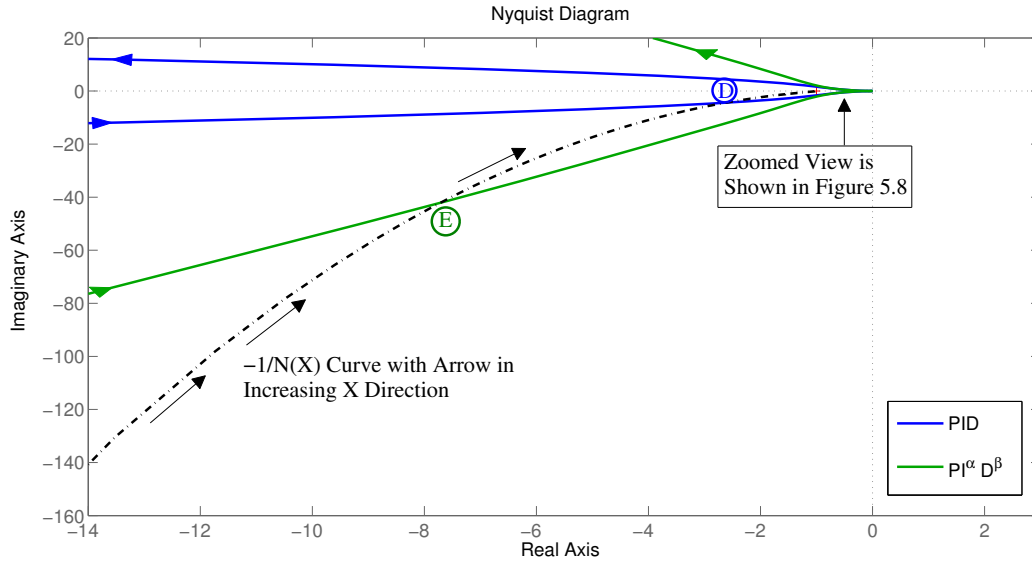


Figure 5.7: Point \textcircled{E} occurs before point \textcircled{D} for $-\frac{1}{N(X)}$ plot seen in the arrow direction indicating superiority of $PI^\alpha D^\beta$ over PID

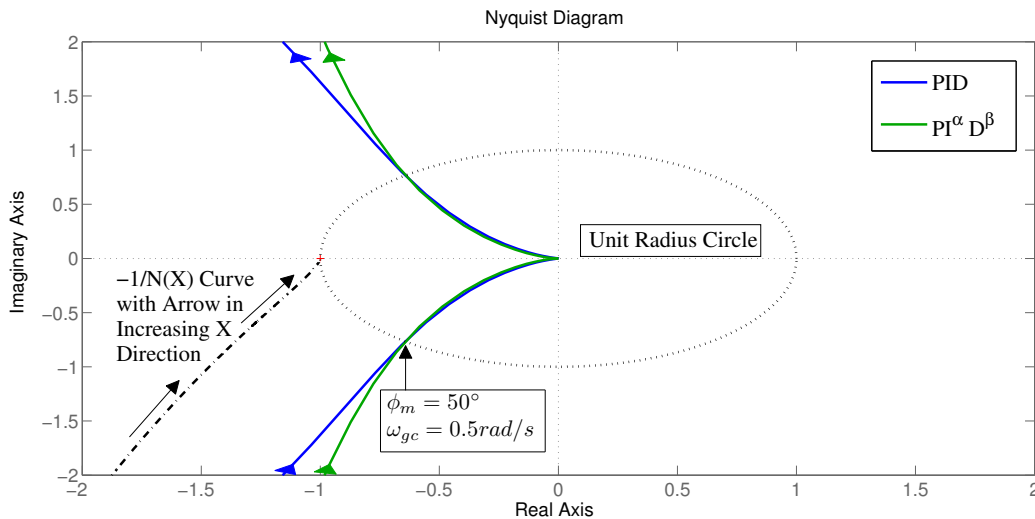


Figure 5.8: Zoomed view of Figure 5.7: fractional and integer PID meeting required phase margin and gain crossover frequency

The crossing point details as observed in Figure 5.7 are:

- At point \textcircled{D} (PID case), $X = 0.0592, \omega = 0.1252$.
- At point \textcircled{E} ($PI^\alpha D^\beta$ case), $X = 0.051, \omega = 0.0195$.

Stable limit cycles produce sustained oscillations in the plant output. The relation between limit cycle amplitude (X) and corresponding sustained oscillation amplitude

(Y) for static backlash nonlinearity [Gopal (2012)] is given as: $Y = X - H$. The details of X and corresponding Y for each controller case are consolidated in Table 5.6. (The Table 5.6 has been given in Section 5.2.7.)

5.2.6 Performance Analysis Using Closed Loop Simulation in the Presence of Plant Nonlinearity

In this subsection, we simulate the closed loop control system to obtain its step response in the presence of plant nonlinearity. For this purpose, a SIMULINK patch-up is constructed for the control scheme shown in Figure 5.4 and a step signal of magnitude 0.1 is given as an input. For FOCs, the Oustaloup approximation is considered with order 9 and frequency range $[0.001, 1000]$ rad/s.²

The limit cycles (refer signal $y_1(t)$ in Figure 5.4) obtained in the closed loop simulation with integer and fractional PI controllers are shown in Figure 5.9.

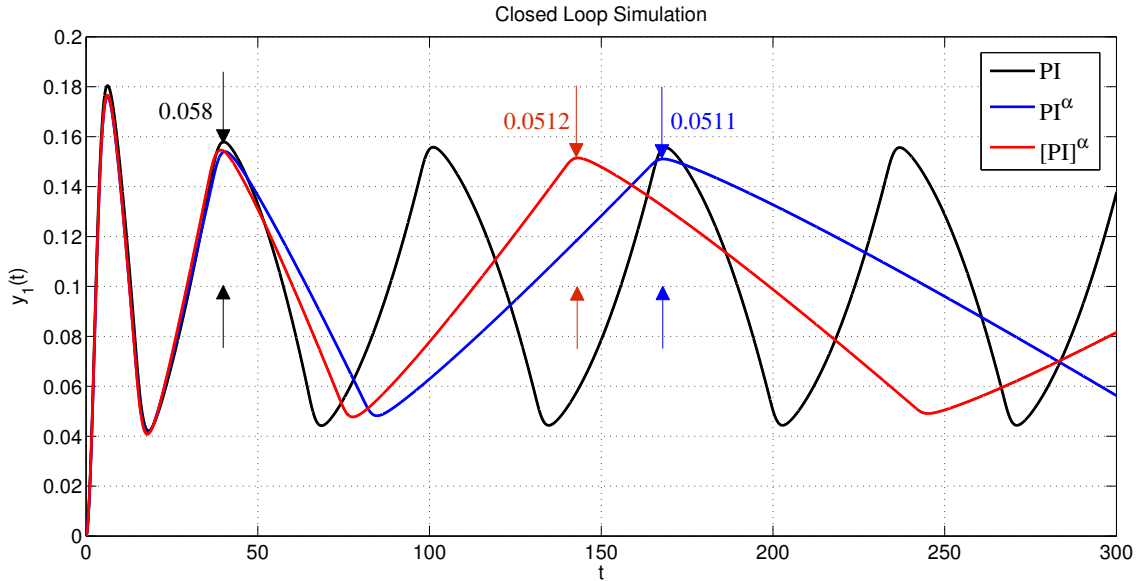


Figure 5.9: Limit Cycles with PI , PI^α , and $[PI]^\alpha$ Controllers

It is seen in the Figure 5.9 that PI^α and $[PI]^\alpha$ controllers produce lesser amplitude limit cycles as compared to integer PI . This corresponds to lesser amplitude sustained oscillations (refer signal $y_2(t)$ in Figure 5.4) as shown in Figure 5.10.

²If the desired control specifications are met, it confirms the low pass filtering property of the linear part of the designed loop which is an essential requirement for replacing nonlinearity by its DF.

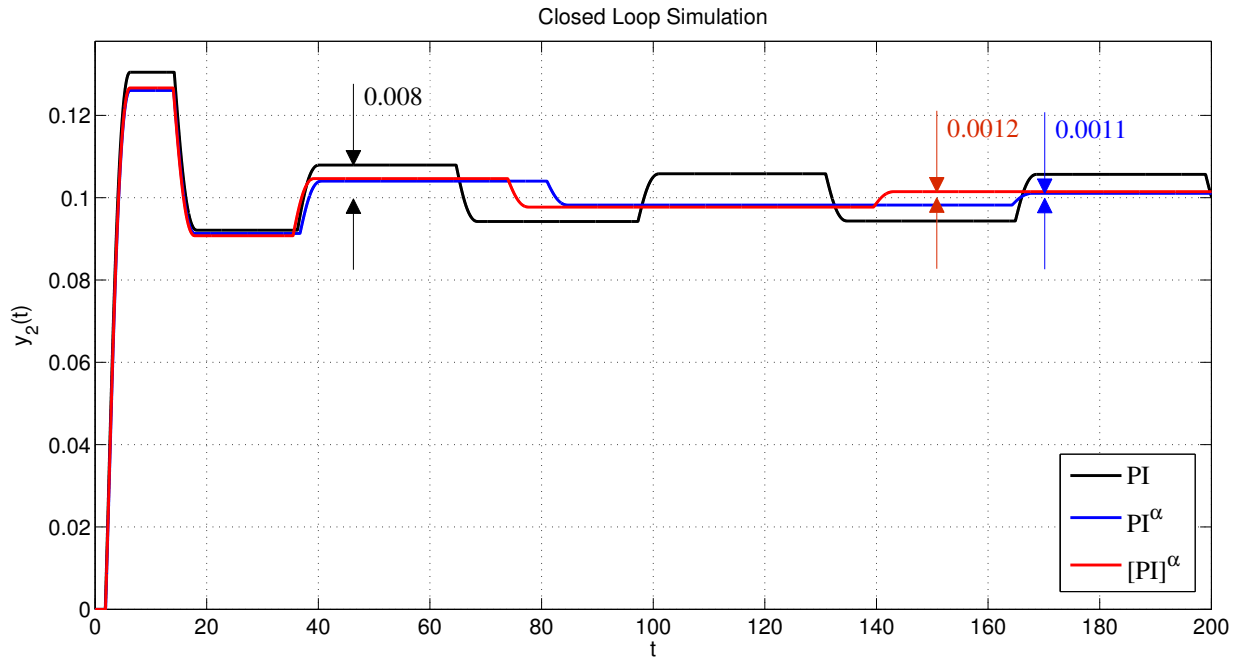


Figure 5.10: Sustained Oscillations with PI , PI^α , and $[PI]^\alpha$ Controllers

Such similar fractional superiority for PID case is shown in Figures 5.11 and 5.12.

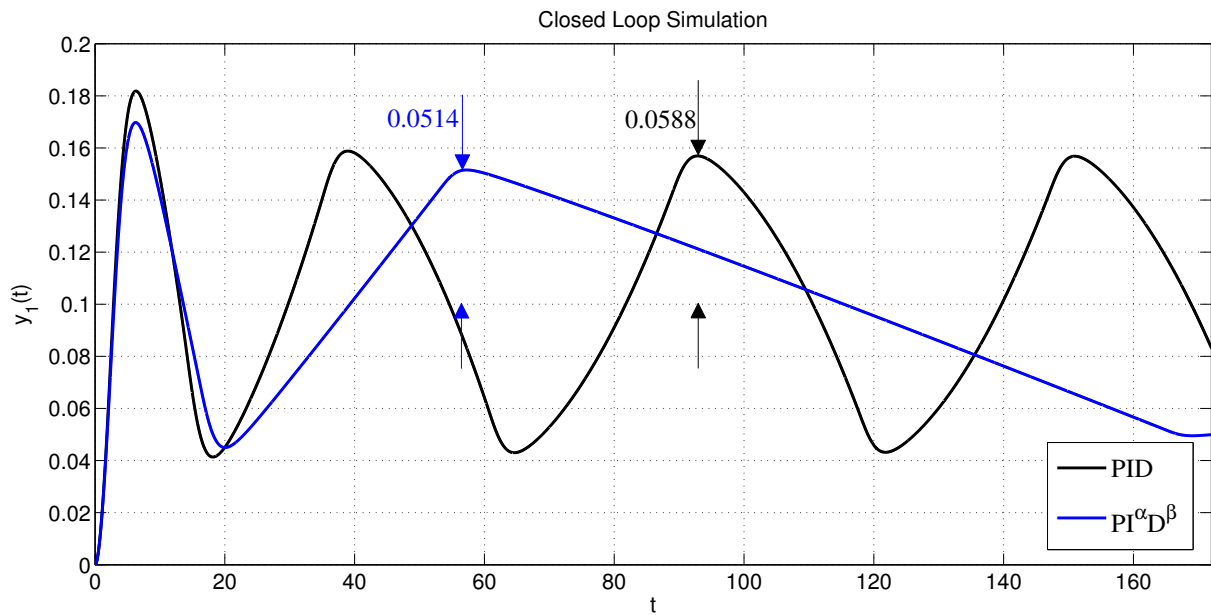


Figure 5.11: Limit Cycles with PID and $PI^\alpha D^\beta$ Controllers

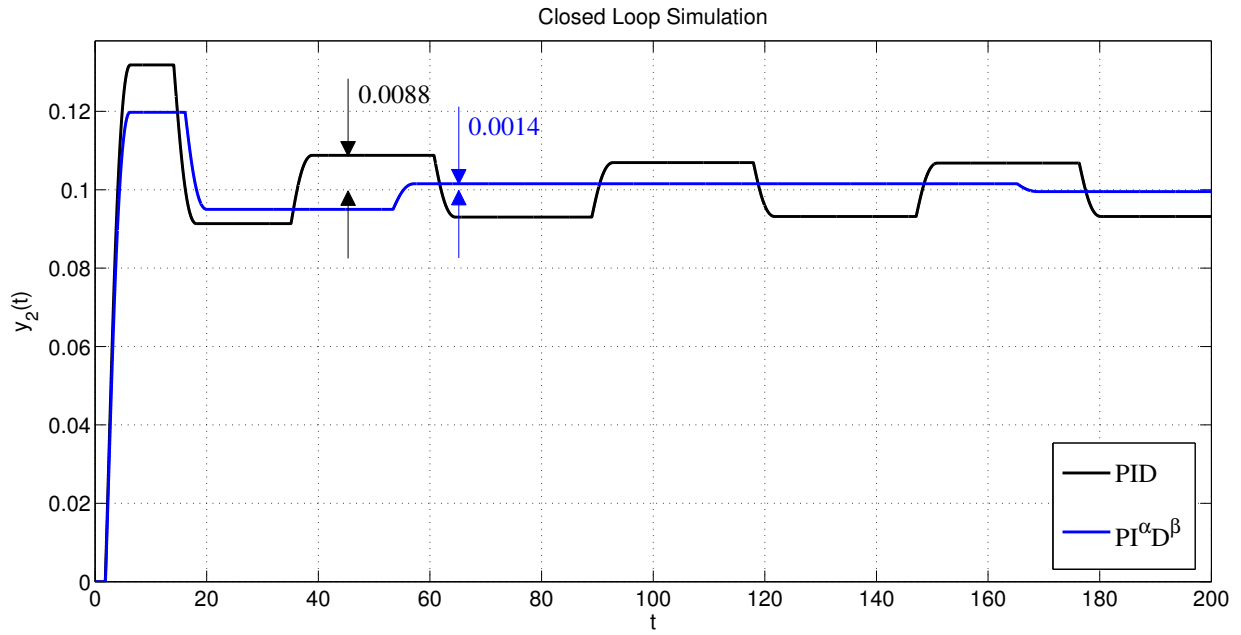


Figure 5.12: Sustained Oscillations with PID and $PI^\alpha D^\beta$ Controllers

The numerical values of amplitudes of limit cycles and sustained oscillations are presented in Table 5.6.

5.2.7 Comparison between FOCs and their Integer-Order Counterparts

Table 5.6 consolidates the results obtained using graphical interpretation as well as closed loop simulation. The results presented in Table 5.6 are further analyzed to compare FOCs with their integer-order counterparts. Such a comparison for integer and fractional PI controllers is presented in Table 5.7. It can be observed in Table 5.7 that there is a significant reduction in the limit cycle amplitudes (around 12%) with fractional PI controllers when compared with integer PI . Correspondingly, the sustained oscillations are suppressed to a large extent (more than 85%) with PI^α and $[PI]^\alpha$ controllers than the integer PI .

Similarly, the comparison between integer and fractional-order PID controller is given in Table 5.8. It is seen in Table 5.8 that $PI^\alpha D^\beta$ outperforms integer PID in the suppression of limit cycles and sustained oscillations.

Table 5.6: Details of Limit Cycle and Sustained Oscillation Amplitudes

Controller	Graphical Interpretation		Closed Loop Simulation	
	Limit Cycle Amplitude	Sustained Oscillation Amplitude	Limit Cycle Amplitude	Sustained Oscillation Amplitude
PI	0.0578	0.0078	0.058	0.008
PI^α	0.0504	0.0004	0.0511	0.0011
$[PI]^\alpha$	0.0505	0.0005	0.0512	0.0012
PID	0.0592	0.0092	0.0588	0.0088
$PI^\alpha D^\beta$	0.051	0.001	0.0514	0.0014

Table 5.7: Superiority of PI^α and $[PI]^\alpha$ over Integer PI

Approach	Amplitudes	PI	PI^α	(%) Reduction with PI^α over PI	$[PI]^\alpha$	(%) Reduction with $[PI]^\alpha$ over PI
Graphical Interpretation	Limit Cycle	0.0578	0.0504	12.8028	0.0505	12.6298
	Sustained Oscillations	0.0078	0.0004	94.8718	0.0005	93.5897
Closed Loop Simulation	Limit Cycle	0.058	0.0511	11.8966	0.0512	11.7241
	Sustained Oscillations	0.008	0.0011	86.25	0.0012	85

Table 5.8: Superiority of $PI^\alpha D^\beta$ over Integer PID

Approach	Amplitudes	PID	$PI^\alpha D^\beta$	(%) Reduction with $PI^\alpha D^\beta$ over PID
Graphical Interpretation	Limit Cycle	0.0592	0.051	13.8514
	Sustained Oscillations	0.0092	0.001	89.1304
Closed Loop Simulation	Limit Cycle	0.0588	0.0514	12.5850
	Sustained Oscillations	0.0088	0.0014	84.0909

Thus, we designed and compared FOCs with their integer-order counterparts for the plant containing backlash nonlinearity. In the next section, we consider plants with relay nonlinearity and analyze the performance of FOCs.

5.3 FOCs for Plants with Relay Nonlinearity

Let us consider a plant having a TF $G(s)$ in cascade with a relay nonlinearity. The closed loop control schematics containing such a plant and controller $C(s)$ is shown in Figure 5.13. Mathematically, the relay nonlinearity in Figure 5.13 is given by the following relation:

$$y_2(t) = \begin{cases} M, & \text{if } y_1(t) \geq 0 \\ -M, & \text{if } y_1(t) < 0 \end{cases} \quad (5.8)$$

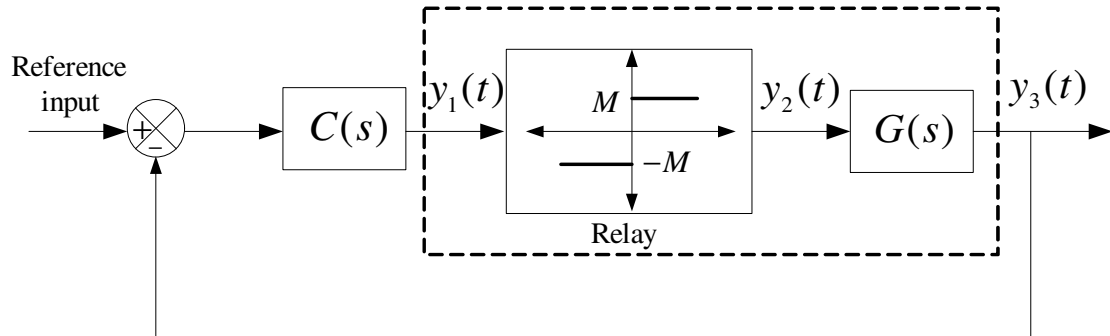


Figure 5.13: Closed Loop Control Schematics

For the nonlinear control loop shown in Figure 5.13, we intend to construct the controller design framework which leads to a desirable transient as well as steady state performance at the plant output. For this purpose, we first discuss a few basics on relay nonlinearity in the context of limit cycles as follows:

5.3.1 Relay Nonlinearity and Stable Limit Cycles

Let us consider a sketch drawn in Figure 5.14 which shows the superposition of:

1. $-\frac{1}{N(X)}$ curve, where $N(X) = \frac{4M}{\pi X}$ is the DF of relay nonlinearity [Gopal (2012)].

2. Nyquist plot of loop TF, $L(s) = C(s)G(s)$.

In Figure 5.14, the arrow of the Nyquist plot indicates increasing ω direction ($\omega \in [0, \infty)$). The arrow in $-\frac{1}{N(X)}$ plot shows increasing X direction. Also, the limit cycle point \textcircled{A} is the intersection point between Nyquist plot and $-\frac{1}{N(X)}$ curve.

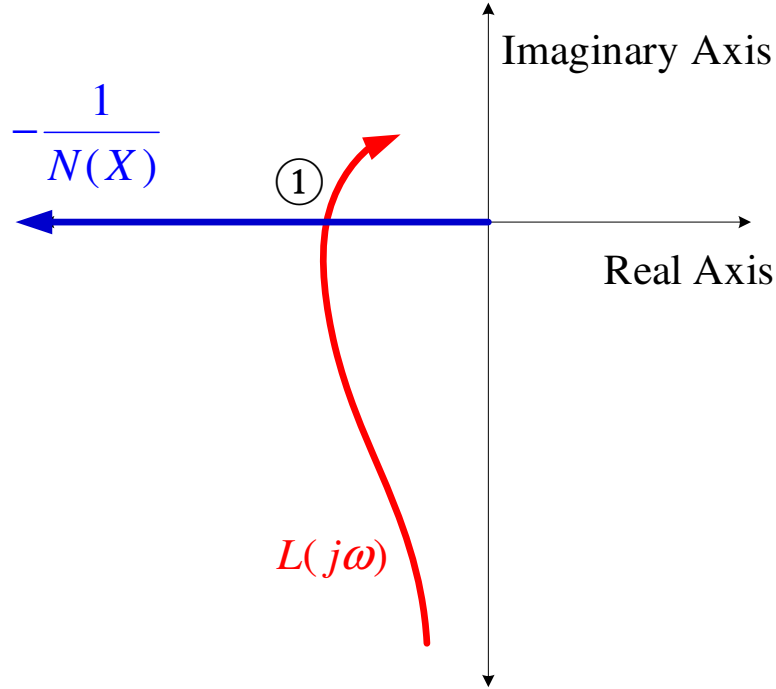


Figure 5.14: Stability of Limit Cycles for Relay Nonlinearity

In Figure 5.14, Nyquist plot of $L(s)$ intersects $-\frac{1}{N(X)}$ curve only once, thereby resulting into a single limit cycle point. Usually, the nonlinear control loops shown in Figure 5.13 fall into a class which leads to such single limit cycle point³. Therefore, currently we focus on such class nonlinear loops.

For closed loop system shown in Figure 5.13, sustained oscillations are observed in output ($y_3(t)$), if the nature of limit cycle point is *stable*. The occurrence and stability of limit cycles for the relay nonlinearity case is ensured if the following conditions by loop TF $L(s)$:

1. Nyquist Condition [Gopal (2012)] for Limit Cycle Existence

$$\left[-\frac{1}{N(X)} \right]_{X=X_0} = [L(j\omega)]_{\omega=\omega_0} \quad (5.9)$$

³[Oliveira et al. (2003)] also focuses on such a specific case.

where, ω_0 is the limit cycle frequency at point ① in rad/s. X_0 denotes the limit cycle amplitude.

2. Tsytkin's Condition [Tsytkin (1955)] for Stability of Limit Cycle

For stability of limit cycle, it is essential that for the given Nyquist curve seen in its arrow direction, the $-\frac{1}{N(X)}$ curve in its arrow direction crosses from right to left (i.e. from unstable region to stable region) [Khalil and Grizzle (2002)]. For relay nonlinearity case, the $-\frac{1}{N(X)}$ curve is along the negative real axis. Therefore, for ensuring the stability of limit cycles, the Nyquist curve must cut $-\frac{1}{N(X)}$ in the direction as shown in Figure 5.14. Mathematically, this leads to the following condition [Tsytkin (1955)]:

$$\left[\frac{d}{d\omega} (Im(L(j\omega))) \right]_{\omega=\omega_0} > 0 \quad (5.10)$$

Next, we show the usefulness of above conditions in developing a controller design framework which shapes the limit cycles in a desirable way. Additionally, we constrain the controller to meet specified gain crossover frequency, phase margin, and closed loop stability condition.

5.3.2 Controlling Transient Behaviour using Describing Function

Usually, DFs are used to estimate the amplitude and frequency of limit cycles. In the present subsection, we discuss their usefulness for controlling the transient behavior of the closed loop system.

To design controller $C(s)$ for the closed loop schematics shown in Figure 5.13, one neglects nonlinearity and considers the plant TF $G(s)$. In other words, the nonlinearity is considered as a gain of 1 during design. For the designed control system, at a certain step reference amplitude A , if we assume the signal at the input of nonlinearity to roughly take a shape of sine wave with peak amplitude P such that $N(P) = 1$, then the closed loop system with and without nonlinearity behaves *equally* during the transient phase. Therefore, the transient meets the desired performance in the presence of nonlinearity for such a reference input.

The above concept can be extended for a general P , when $N(P)$ is not necessarily

1. For such P , one can design the controller for $N(P)G(s)$. Therefore, for a particular amplitude A of the step reference, the input to the nonlinearity takes form of a sine wave with amplitude P and the designed transient performance is satisfied in the presence of plant nonlinearity. We further illustrate this point for the numerical example under consideration in Subsection 5.3.9.

Thus, one needs to consider the loop TF $C(s)N(P)G(s)$ for meeting desired transient performance.

Remark 5.3. *It can be noted that for any other $P_1 \neq P$, the corresponding controller $C_1(s)$ meeting the same loop performance can be obtained in the following way:*

$$C(s)N(P)G(s) = C_1(s)N(P_1)G(s) \implies C_1(s) = \frac{C(s)N(P)}{N(P_1)}$$

5.3.3 Proposed Closed Loop Stability Conditions

To ensure the closed loop stability, necessary conditions need to be evaluated. For this purpose, let us consider the sketch shown in Figure 5.15 which shows the Nyquist plot of loop TF $C(s)N(P)G(s)$.

From Figure 5.15, gain margin in dB is expressed as: $GM_{dB} = 20 \cdot \log_{10} \left(\frac{1}{a} \right)$. Therefore, for $GM_{dB} > 0$, one requires $a < 1$. Furthermore, we have the following condition at phase crossover frequency ω_{pc} : $\angle[C(j\omega_{pc})N(P)G(j\omega_{pc})] = -\pi$.

Relay nonlinearity does not introduce any phase shift, which results into its DF $N(P)$ being a real quantity ($N(P) = \frac{4M}{\pi P}$), i.e. $\angle N(P) = 0$. It is also noticed from Figure 5.14 and the condition (5.9) that $\angle[C(j\omega_0)G(j\omega_0)] = -\pi$. Therefore, one can conclude that the limit cycle frequency ω_0 and phase crossover frequency ω_{pc} are equal for the case of relay nonlinearity. i.e.,

$$\omega_0 = \omega_{pc} \tag{5.11}$$

From Figure 5.15, we have,

$$a = |C(j\omega_{pc})N(P)G(j\omega_{pc})| = N(P) |C(j\omega_{pc})G(j\omega_{pc})| \tag{5.12}$$

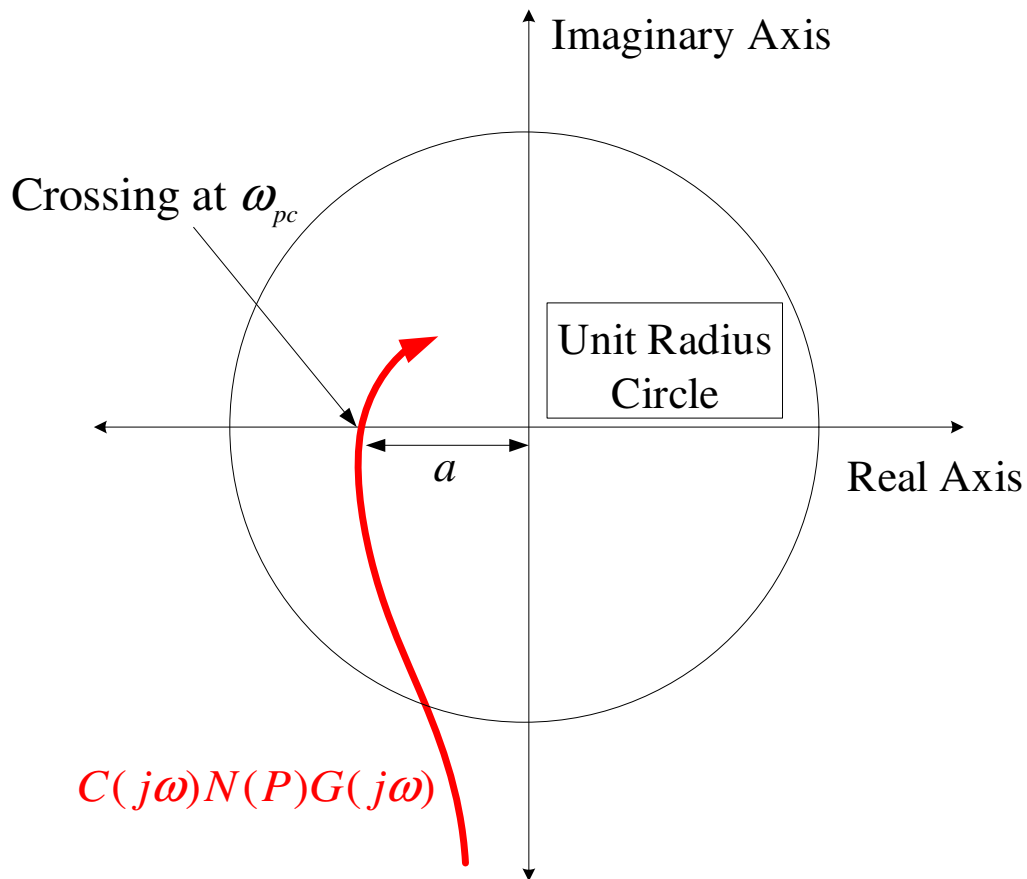


Figure 5.15: Condition for Closed Loop Stability

because, $N(P)$ is a positive real quantity.

Recall (5.9):

$$\left[-\frac{1}{N(X)} \right]_{X=X_0} = [L(j\omega)]_{\omega=\omega_0} = [C(j\omega)G(j\omega)]_{\omega=\omega_0}$$

On taking modulus on both the sides and simplifying, one gets:

$$1 = N(X_0) |C(j\omega_0)G(j\omega_0)| \tag{5.13}$$

Using (5.11), (5.12), and (5.13), the condition $a < 1$ implies that:

$$N(P) < N(X_0)$$

Therefore,

$$X_0 < P \quad (5.14)$$

Thus, we obtain the condition (5.14) in terms of X_0 and P for positive gain margin. For the closed loop stability, it is clear that the positive phase and gain margins are necessary along with the following relation between phase crossover frequency (ω_{pc}) and gain crossover frequency (ω_{gc}):

$$\omega_{pc} > \omega_{gc}$$

Since, $\omega_0 = \omega_{pc}$ (refer (5.11)), we get,

$$\omega_0 > \omega_{gc} \quad (5.15)$$

The conditions (5.14) and (5.15) are necessary for closed loop stability.

Remark 5.4. Using (5.11), (5.12), and (5.13), we get $a = \frac{N(P)}{N(X_0)}$. Therefore,

$$GM_{dB} = 20 \cdot \log_{10} \left(\frac{1}{a} \right) = 20 \cdot \log_{10} \left(\frac{N(X_0)}{N(P)} \right) = 20 \cdot \log_{10} \left(\frac{4M}{N(P)\pi X_0} \right) \quad (5.16)$$

In (5.16), as X_0 decreases, GM_{dB} increases. Hence, any controller which minimizes X_0 is also useful in maximizing GM_{dB} for plants with relay nonlinearity.

5.3.4 Maximization of Limit Cycle Frequency

In Figure 5.13, if we consider the signal $y_1(t)$ of the form $X_0 \sin(\omega_0 t)$, then $y_2(t)$ is a square-wave signal having frequency ω_0 and amplitudes M and $-M$ during ON and OFF-time respectively. For such $y_2(t)$, the plant TF $G(s)$ usually produces a response $y_3(t)$ which increases and decreases monotonically during the ON and OFF-time of $y_2(t)$ respectively. This is the case with many plants such as type-0 first order, type-1 second order, type-1 third order, etc. For such plants, the peak amplitude of $y_3(t)$ is

decided by the frequency of $y_2(t)$, i.e. ω_0 . For instance, if the frequency ω_0 is high (i.e. time period is less), ON and OFF times are less. Therefore, $y_3(t)$ reaches lesser peak value.

Based on the above discussion, we note that if the limit cycle frequency ω_0 is maximized, it minimizes the peak amplitude of $y_3(t)$, which is the amplitude of sustained oscillations. Therefore, for reducing amplitude of sustained oscillations, one can consider maximization⁴ of ω_0 (or minimization of $\frac{1}{\omega_0}$) as an objective function.

5.3.5 Loop Performance Specifications

In addition to meeting desirable limit cycle performance, we also constrain the controller to meet specifications such as gain crossover frequency and phase margin. As discussed previously, loop under consideration for such specifications is $C(s)N(P)G(s)$.

- Gain Crossover Frequency (ω_{gc}):

$$|C(j\omega_{gc})N(P)G(j\omega_{gc})| = 1$$

- Phase Margin (ϕ_m):

$$\angle[C(j\omega_{gc})N(P)G(j\omega_{gc})] = -\pi + \phi_m$$

Due to above loop performance specifications, the sketch presented in Figure 5.15 is modified as shown in Figure 5.16.

⁴For practical applications, there is an upper limit on ω_0 as one cannot allow relay to toggle beyond a certain rate. Therefore, maximization of ω_0 needs to be considered within such bound.

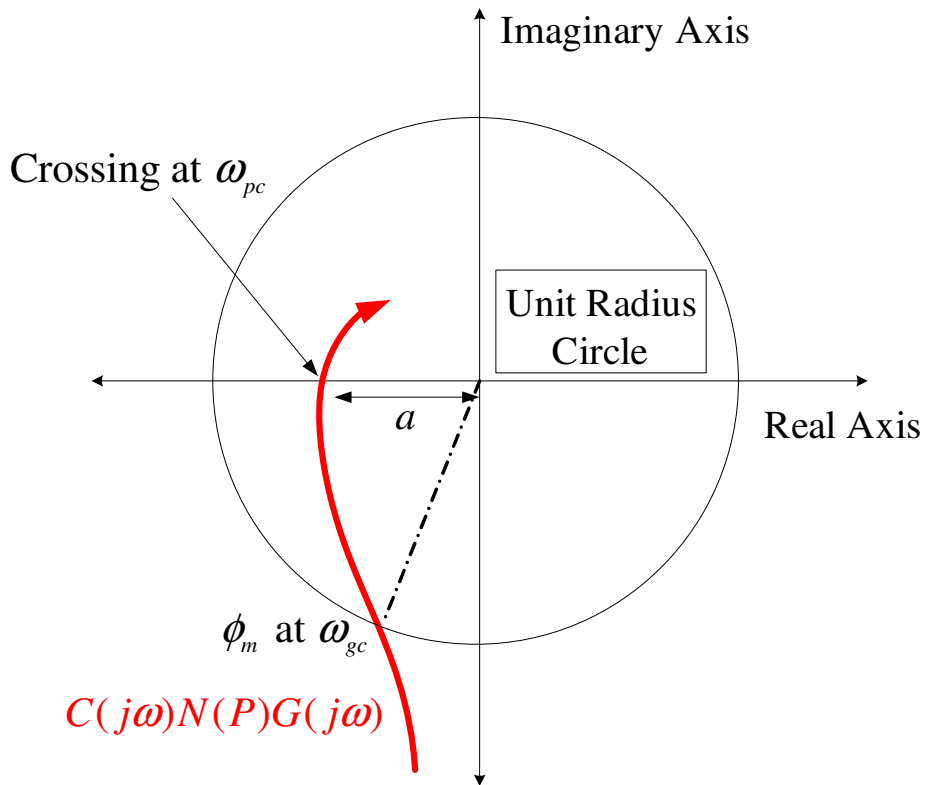


Figure 5.16: Nyquist plot of $C(s)N(P)G(s)$ with Performance Specifications and Closed Loop Stability

5.3.6 Optimization Problem for Controller Design

Based on the discussions made in Subsections 5.3.1-5.3.5, we construct the following constrained optimization problem for the controller design:

$$\text{Minimize}_{(\text{Controller Parameters, } \omega_0, X_0)} \left(X_0 + \frac{1}{\omega_0} \right)$$

subject to:

1. Occurrence and Stability of Limit Cycles:

(i) Nyquist Condition for Limit Cycle Existence:

$$\left[-\frac{1}{N(X)} \right]_{X=X_0} = [L(j\omega)]_{\omega=\omega_0} \quad (5.17)$$

(ii) Stability of Limit Cycle Condition:

$$\left[\frac{d}{d\omega} (\text{Im}(L(j\omega))) \right]_{\omega=\omega_0} > 0 \quad (5.18)$$

2. Performance Specifications:

(i) Gain Crossover Frequency (ω_{gc}):

$$|C(j\omega_{gc})N(P)G(j\omega_{gc})| = 1 \quad (5.19)$$

(ii) Phase Margin (ϕ_m):

$$\angle[C(j\omega_{gc})N(P)G(j\omega_{gc})] = -\pi + \phi_m \quad (5.20)$$

(iii) Condition for Positive Gain Margin:

$$X_0 < P \quad (5.21)$$

(iv) Condition on ω_0 and ω_{gc} :

$$\omega_0 > \omega_{gc} \quad (5.22)$$

In the above described optimization problem, constraints (5.17) and (5.18) guarantee the occurrence and stability of limit cycles. The equations (5.19)-(5.22) shape the loop to meet desirable performance. The objective function $\left(X_0 + \frac{1}{\omega_0}\right)$ is considered to ensure the minimization of X_0 as well as $\frac{1}{\omega_0}$.

Remark 5.5. *Under the special case, when $N(P) = 1$, $C(S)N(P)G(s) = C(s)G(s)$. Therefore, one can visualize limit cycle and performance shaping in a single sketch as shown in Figure 5.17.*

Next, we demonstrate the application of optimization problem presented in the current subsection to design a PI^α controller for a type-1 motion control plant containing relay nonlinearity.

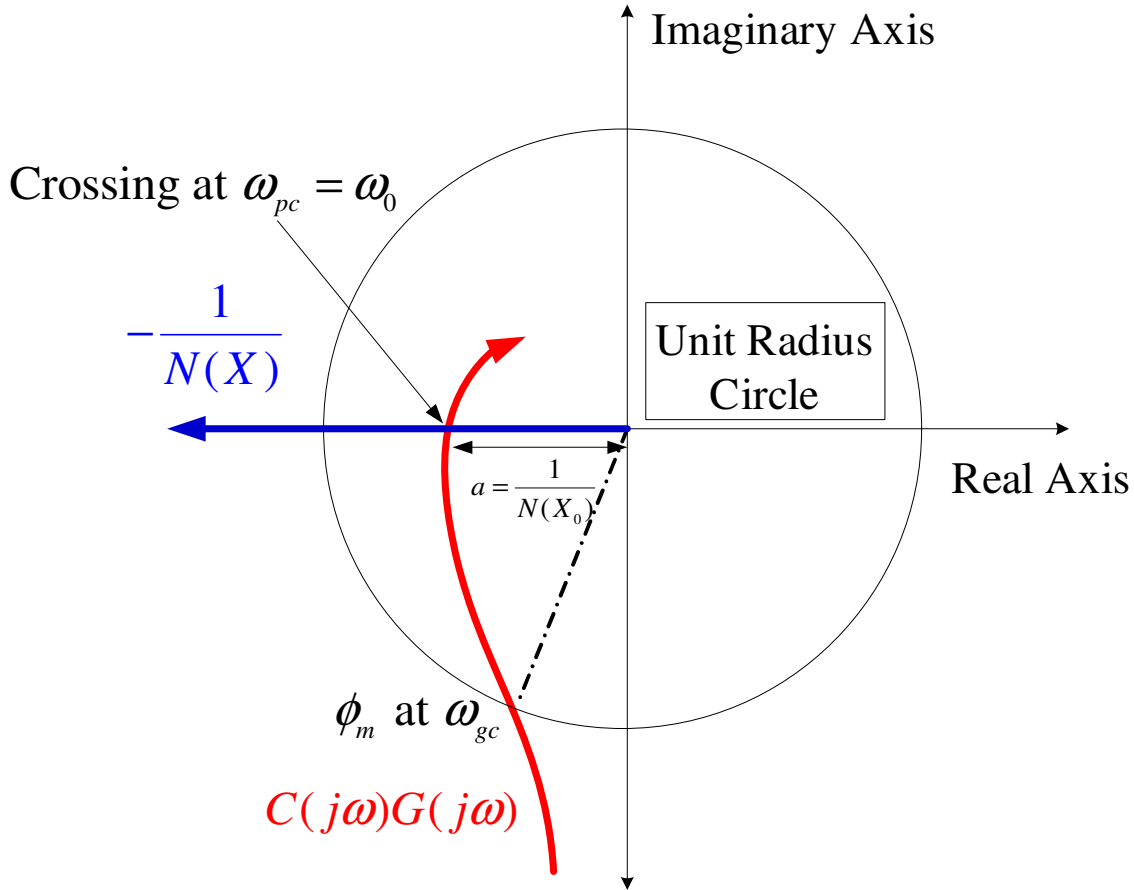


Figure 5.17: Limit Cycle and Loop Performance Together when $N(P) = 1$

5.3.7 Application: PI^α Controller Design

Let us consider a plant consisting of relay nonlinearity in cascade with a TF $G(s) = \frac{K}{s(s+b)}$. The TF $G(s)$ satisfies the required monotonicity property as discussed in Section 5.3.4. For the design purpose, a PI^α controller is considered. Since the PI^α controller takes the form of integer PI when $\alpha = 1$, on considering PI^α controller, one also takes into account the possibility of integer PI as a solution.

Tsytkin's Condition of limit cycle stability (5.10) for the loop TF $L(s) = C(s)G(s)$ in the present case leads to following inequality (refer APPENDIX D for derivation):

$$\begin{aligned} & [(\omega^3 + b^2\omega) \left(K_i(1 - \alpha)\omega^{-\alpha} \sin\left(\frac{\pi}{2}\alpha\right) + bK_i\alpha\omega^{-\alpha} \cos\left(\frac{\pi}{2}\alpha\right) \right) - \\ & \left(\frac{K_i}{\omega^{\alpha-1}} \sin\left(\frac{\pi}{2}\alpha\right) - b \left(1 + \frac{K_i}{\omega^\alpha} \cos\left(\frac{\pi}{2}\alpha\right) \right) \right) (3\omega^2 + b^2)]_{\omega=\omega_0} > 0 \end{aligned} \quad (5.23)$$

For demonstration, let the numerical values be: $K = 5, b = 0.7, M = 1, \omega_{gc} = 0.5$ rad/s, $\phi_m = 50^\circ = \frac{5\pi}{18}$ rad. The bounds for α are selected as $(0, 1]$ so as to include PI controller (for which $\alpha = 1$) as a possible candidate for solution. Also, for convenience, P is taken as $\frac{4M}{\pi}$ so that $N(P) = 1$. Therefore, one may refer Figure 5.17 to visualize the controller design problem graphically. The selected intervals for optimization parameters are as follows:

- $K_p \in [0.01, 1], K_i \in [0.01, 1], \alpha \in [0.01, 1]$.
- $\omega_0 \in (0.5, 11.7769]$.

Recalling (5.22), $\omega_0 > \omega_{gc}$. Since, $\omega_{gc} = 0.5$, lower bound is taken as 0.5. The upper bound 11.7769 is an arbitrarily chosen number for the demonstration.

- $X_0 \in [0, 1.15]$ (Recalling (5.21), $X_0 < P$. Since, $P = \frac{4M}{\pi} = 1.2732$, upper bound for X_0 is chosen as 1.15.)

For solving the optimization problem, `fmincon()` solver available in MATLAB is used which realizes the interior point algorithm. For each controller case, 20 random initial guesses are taken and the corresponding converged values are preserved. Best among the 20 (i.e. the one with least $(X_0 + \frac{1}{\omega_0})$) is selected for the performance analysis. At the end of the simulation, we obtain: $K_p = 0.0532, K_i = 0.5711, \alpha = 0.1291, \omega_0 = 11.7728, X_0 = 0.0034$. Thus, the resultant controller is a non-integer order (fractional) PI with $\alpha = 0.1291$.

5.3.8 Graphical Performance Analysis of Designed Controller

For graphically analyzing the performance of designed PI^α controller, its Oustaloup approximation is considered. The order of Oustaloup approximation is taken as 9 and is considered over $[0.001, 1000]$ rad/s. For the discussion hereafter, $L(s)$ denotes the product of $G(s)$ and Oustaloup approximation of $C(s)$.

Figure 5.18 shows Nyquist plot of $L(s)$ over which $-\frac{1}{N(X)}$ curve is superimposed. The zoomed view of the selected portion of Figure 5.18 is shown in Figure 5.19.

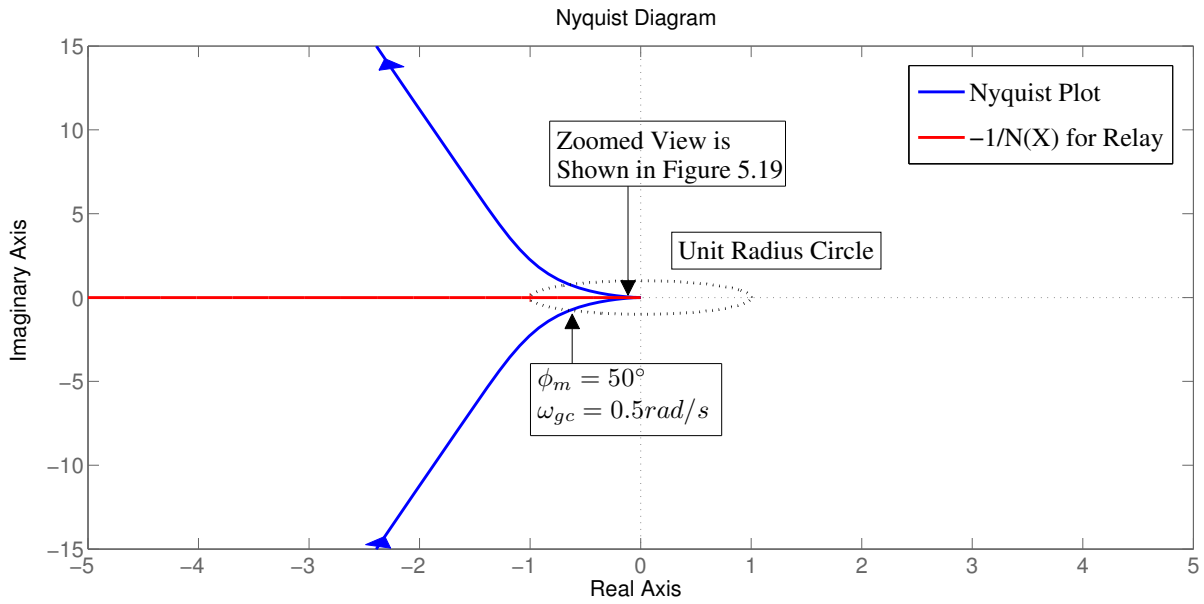


Figure 5.18: Performance Analysis using Graph

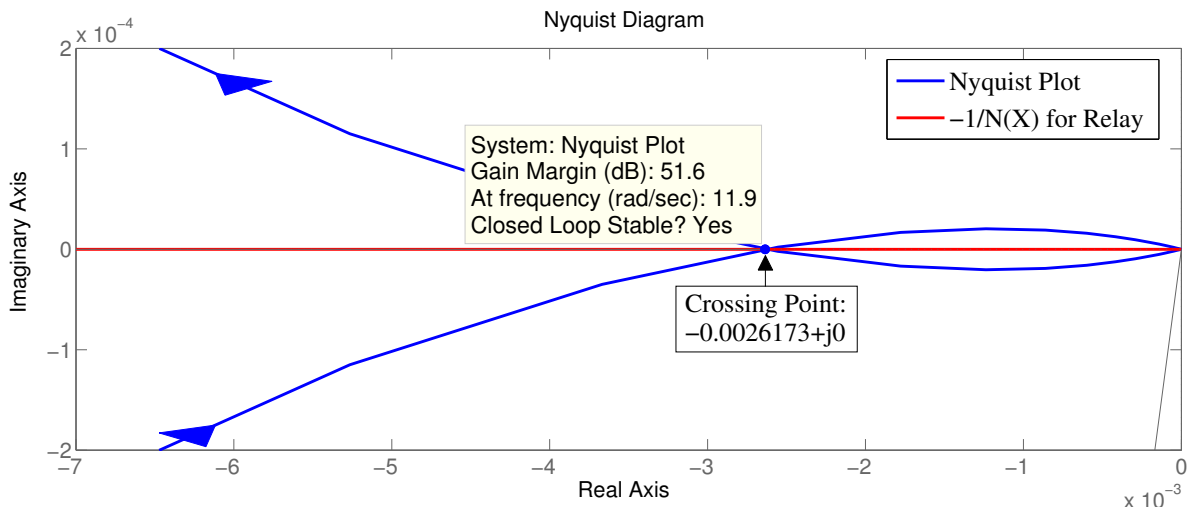


Figure 5.19: Zoomed View of Figure 5.18

As seen from Figure 5.19, there is a *single* crossing point between $-\frac{1}{N(X)}$ and $L(j\omega)$, which is $-0.0026173 + j0$. Therefore,

$$-\frac{1}{N(X)}_{X=X_0} = -\frac{\pi X_0}{4M} = -0.0026173$$

The above leads to $X_0 = 0.0033$. This value matches with the one obtained after solving optimization (i.e. $X_0 = 0.0034$). Furthermore, from the expression (5.16), we get $GM_{dB} = 51.7279$.

Gain margin seen from Figure 5.19 is 51.6 dB which closely matches to the above value, thereby confirming correctness of (5.16). Also, one can see from Figure 5.19 that crossing point occurs at frequency, $\omega_0 = \omega_{pc} = 11.9$ rad/s. This value is very near to the $\omega_0 = 11.7728$ rad/s obtained as a result of optimization.

Thus, it is seen that Nyquist plot of shaped $L(j\omega)$ with $\omega \in [0, \infty)$ meets the requirement of stable limit cycles as well as desired phase margin and gain crossover frequency. One can also see from Figure 5.19 that the closed loop system is stable.

5.3.9 Verification of Limit Cycles with Closed Loop Simulation

A SIMULINK patch-up is constructed for the schematics shown in Figure 5.13 to verify the limit cycle details using closed loop simulation. A step reference input of magnitude 16 is given to the patch-up and consequently the limit cycles are observed ($y_1(t)$) as shown in shown in Figure 5.20. Corresponding to such limit cycles, closed loop response ($y_3(t)$) shows sustained oscillations in the steady state as shown in Figure 5.21.

Figure 5.21 also shows the closed loop response obtained without relay nonlinearity. It must be noted that for fractional-order term, its Oustaloup approximation is considered. The order of approximation is taken as 9 and is considered over $[0.001, 1000]$ rad/s.

It is observed in Figure 5.20 that $P = 1.2834$ for which $N(P) = 0.9921 \approx 1$. Since we designed the controller to meet loop performance for $N(P) = 1$, the transient responses for this reference with linear and nonlinear simulation match closely as can be seen from Figure 5.21.

For step amplitudes other than 16, however, $N(P) \neq 1$. Therefore, transients with linear and nonlinear simulation deviate from each other as the step amplitude drifts from 16. Thus, the controller sufficiently meets the desired transient performance in the presence of relay only for a range of step amplitudes around 16.

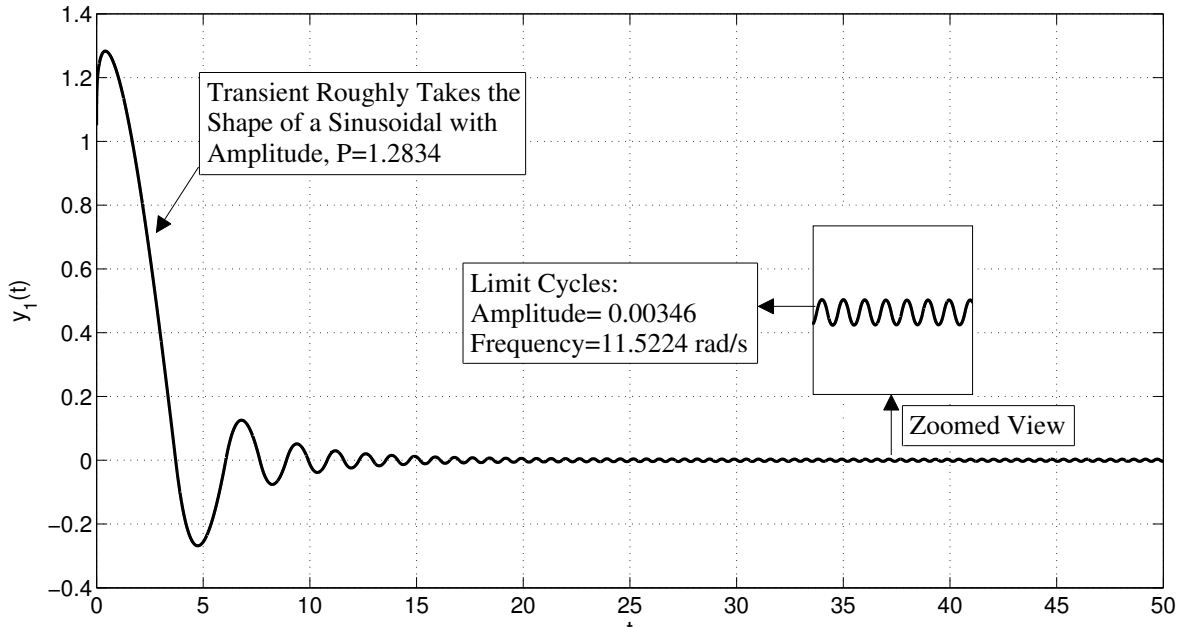


Figure 5.20: Limit Cycles

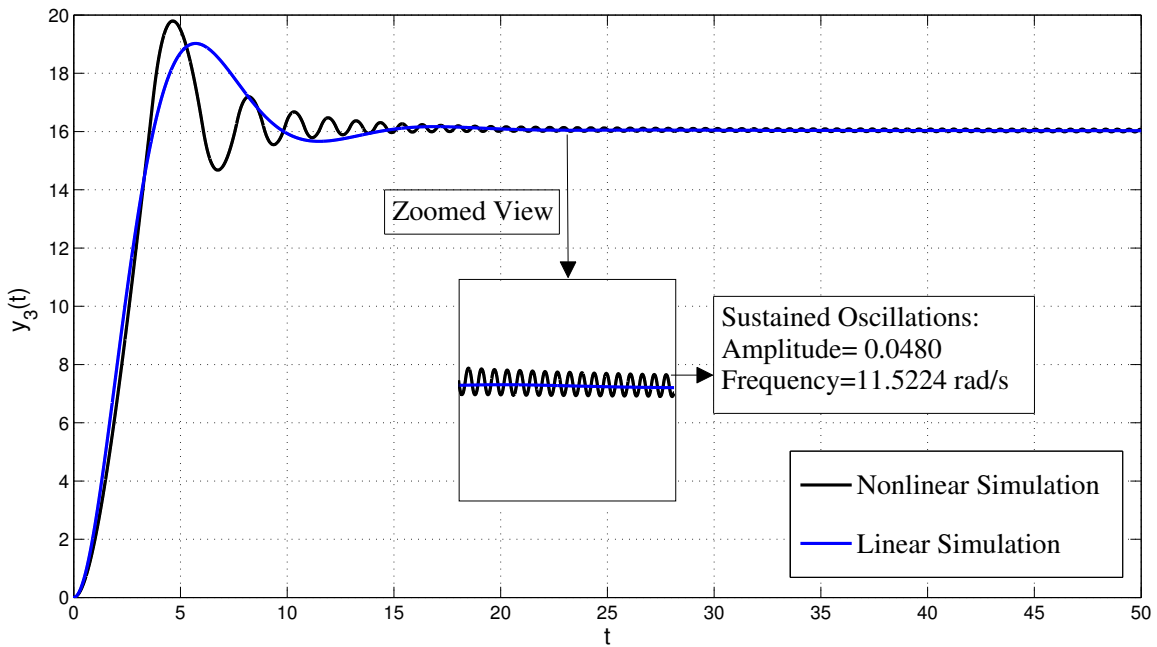


Figure 5.21: Closed Loop Response

Limit cycle performance for the given loop, however, must remain same for all the reference values since it is independent of input signal amplitude. As seen from Figure 5.20, the limit cycles have following details: $X_0 = 0.00346$, $\omega_0 = 11.5224$. The values are very close to those obtained with DF approach. Sustained oscillations in the steady state of the closed loop response due to such limit cycles are seen in Figure 5.21.

Table 5.9 summarizes the limit cycle details obtained from optimization results, graphical analysis, and closed loop simulation. It is seen in Table 5.9 that the results are close to each other, which confirms the correctness of our design. It is important to note that the optimization results are obtained with the irrational form PI^α controller whereas the graphical analysis and closed loop simulation considers Oustaloup approximation. Furthermore, graphical analysis is performed using DF of nonlinearity, while the closed loop simulation takes original nonlinearity into account. Therefore, small differences are expected in the limit cycle details when obtained from different sources.

Table 5.9: Limit Cycle Details

Source	X_0	ω_0
Optimization Results	0.0034	11.7728
Graphical Analysis	0.0033	11.9
Closed Loop Simulation	0.00346	11.5224

5.4 Summary

This chapter considered two plants, one with backlash and the other containing relay nonlinearity and consequently developed controller design frameworks for such plants in order to achieve desired limit cycle performance. The demonstration in each case was made by designing FOCs and their superiority in this aspect over their integer-order controllers was claimed. The design frameworks made an efficient use of DF of the nonlinearity and verified the intended performance using closed loop nonlinear simulations.

CHAPTER 6

Development of Asymptotic Bode Plots for Fractional-Order Controllers

6.1 Introduction

Bode plot [Bode (1940)], [Bode (1945)] plays an important role in the control theory for graphically visualizing the frequency behavior of a Transfer Function (TF). Generally, software tools such as MATLAB, SCILAB, etc. are used for obtaining an accurate Bode plot as it involves significant amount of computational efforts. However, one can sketch a good straight-line approximation of the exact Bode plot known as asymptotic Bode plot [Dorf and Bishop (2011)] by doing a few simple calculations. Asymptotic Bode plots are useful for quick manual analysis of the designed control system with a reasonable degree of accuracy [DiStefano et al. (1967)]. They are also important for understanding the role of each parameter of the given TF in deciding the shape of its Bode response [Gajdošík and Žáková (2011)].

The procedures to sketch asymptotic Bode plots of *integer-order* TFs are well established in the existing theory [Benjamin (1995)], [Dorf and Bishop (2011)]. On the other hand, development of such plots for fractional-order TFs has not received much attention in the literature. A brief mention is found in [Monje et al. (2004b)], [Chen and Vinagre (2010)] about asymptotic plots in the context of fractional-order lead compensator. In the present chapter, we develop asymptotic magnitude and phase Bode plots for the Fractional-Order Controllers (FOCs) such as PI^α , $[PI]^\alpha$, PD^β , $[PD]^\beta$, and $PI^\alpha D^\beta$. We further show the construction of such plots for general fractional commensurate order TFs. The identification of fractional-order TF from a given asymptotic magnitude Bode plot is illustrated. The usefulness of asymptotic magnitude and phase Bode plots for the manual analysis of a designed fractional-control loop is also presented in detail.

6.2 Asymptotic Magnitude Bode Plots for Fractional-Order Controllers

In earlier chapters, it was discussed that the FOCs such as PI^α , $[PI]^\alpha$, PD^β , $[PD]^\beta$, and $PI^\alpha D^\beta$ possess irrational form TF. In the present section, we develop their asymptotic magnitude Bode plots. The plots can be useful in understanding the magnitude versus frequency characteristics of these FOCs by determining the role of their parameters α , β , etc. For this purpose, we introduce a few basic fractional-order terms given in Table 6.1, where $K, a, a_1, a_2 \in \mathbb{R}$ and $\alpha, \beta \in \mathbb{R}_{>0}$.

Table 6.1: Basic Fractional-Order Terms

Sr. No.	Term Description	TF ($T(s)$)
1	Constant Gain	K
2	Fractional Zero	$s^\alpha + a$
3	Fractional Pole	$\frac{1}{s^\alpha + a}$
4	Fractional Zero at Origin	s^α
5	Fractional Pole at Origin	$\frac{1}{s^\alpha}$
6	Fractional [Zero]	$(s + a)^\alpha$
7	Fractional [Pole]	$\frac{1}{(s+a)^\alpha}$
8	Fractional Double-Term Zero	$s^{\alpha+\beta} + a_1 s^\alpha + a_2$
9	Fractional Double-Term Pole	$\frac{1}{s^{\alpha+\beta} + a_1 s^\alpha + a_2}$

First, we explain the development of asymptotic magnitude Bode plots for terms namely, constant gain, fractional zero, and fractional double-term pole. Later, such plots are obtained for the remaining terms.

6.2.1 Constant Gain

It is easy to see that for the constant gain TF $T(s) = K$, the magnitude $|T(j\omega)|_{dB} = 20\log_{10}|K|, \forall \omega$. Therefore, to draw magnitude Bode plot of constant gain, one just has to sketch a horizontal line at $20\log_{10}|K|$. In Bode plot, x -axis represents frequency (ω)

in rad/s on a logarithmic scale and y -axis represents magnitude in dB on a linear scale.

6.2.2 Fractional Zero

The TF of fractional zero is given by $T(s) = (s^\alpha + a)$. Substituting $s = j\omega$ (where, $\omega \in \mathbb{R}_{\geq 0}$) results into:

$$T(j\omega) = (j\omega)^\alpha + a$$

Therefore, the magnitude in dB is given by,

$$|T(j\omega)|_{dB} = 20 \log_{10} \left(a^2 + \omega^{2\alpha} + 2a\omega^\alpha \cos \left(\frac{\pi\alpha}{2} \right) \right)^{\frac{1}{2}}$$

In the sum $(a^2 + \omega^{2\alpha} + 2a\omega^\alpha \cos(\frac{\pi\alpha}{2}))$, the term a^2 dominates at lower frequencies whereas the term $\omega^{2\alpha}$ dominates at higher frequencies. For the intended approximation, we choose the corner frequency (or break frequency) ω_{cr} such that these terms are equal, that is,

$$a^2 = \omega^{2\alpha} |_{\omega=\omega_{cr}}$$

From which, one obtains the corner frequency,

$$\omega_{cr} = |a|^{\frac{1}{\alpha}}$$

Thus, the following approximation of the magnitude is obtained:

1. For $\omega \leq \omega_{cr}$,

$$|T(j\omega)|_{dB} = 20 \log_{10} (a^2)^{\frac{1}{2}} = 20 \log_{10} |a|$$

2. For $\omega > \omega_{cr}$,

$$|T(j\omega)|_{dB} = 20 \log_{10} (\omega^{2\alpha})^{\frac{1}{2}} = 20\alpha \log_{10} \omega$$

Based on the above discussion, we lay down the following procedure to construct the asymptotic magnitude plot for $(s^\alpha + a)$ shown in Figure 6.1:

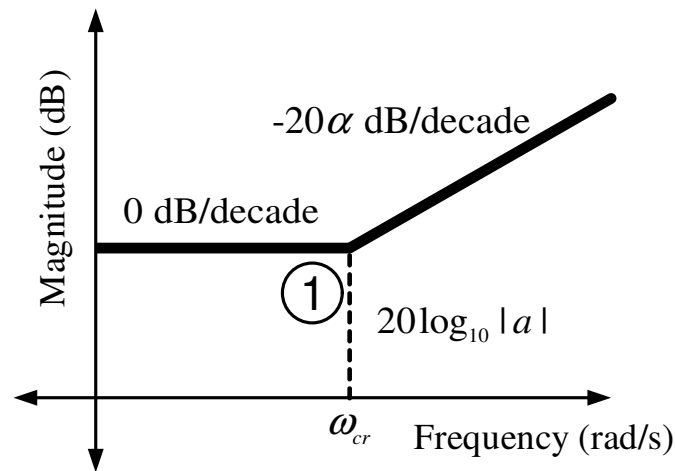


Figure 6.1: Asymptotic Magnitude Bode Plot for Fractional Zero

Procedure

1. Compute the corner frequency $\omega_{cr} = |a|^{\frac{1}{\alpha}}$ and locate point ① at magnitude $20 \log_{10} |a|$.
2. Draw a line with slope 0 dB/decade for $\omega \leq \omega_{cr}$, and a line with slope 20α dB/decade for $\omega > \omega_{cr}$ as shown in Figure 6.1.

6.2.3 Fractional Double-Term Pole

The TF of fractional double-term pole is given by $T(s) = \frac{1}{(s^{\alpha+\beta} + a_1 s^\alpha + a_2)}$. Substituting $s = j\omega$ (where, $\omega \in \mathbb{R}_{\geq 0}$) leads to:

$$T(j\omega) = \frac{1}{(j\omega)^{\alpha+\beta} + a_1 (j\omega)^\alpha + a_2}$$

The decibel magnitude of $T(j\omega)$ is given by,

$$|T(j\omega)|_{dB} = -20\log_{10} \left(\omega^{2(\alpha+\beta)} + a_1^2\omega^\alpha + a_2^2 + 2a_1\omega^{2\alpha+\beta}\cos\left(\frac{\pi\beta}{2}\right) + 2a_2\omega^{\alpha+\beta}\cos\left(\frac{\pi(\alpha+\beta)}{2}\right) + 2a_1a_2\omega^\alpha\cos\left(\frac{\pi\alpha}{2}\right) \right)^{\frac{1}{2}}$$

In the sum $\left(\omega^{2(\alpha+\beta)} + a_1^2\omega^\alpha + a_2^2 + 2a_1\omega^{2\alpha+\beta}\cos\left(\frac{\pi\beta}{2}\right) + 2a_2\omega^{\alpha+\beta}\cos\left(\frac{\pi(\alpha+\beta)}{2}\right) + 2a_1a_2\omega^\alpha\cos\left(\frac{\pi\alpha}{2}\right) \right)$, the term a_2^2 dominates at lower frequencies whereas the term $\omega^{2(\alpha+\beta)}$ dominates at higher frequencies. For the approximation purpose, the corner frequency ω_{cr} is chosen such that the dominant terms are equal,

$$a_2^2 = [\omega^{2(\alpha+\beta)}]_{\omega=\omega_{cr}}$$

Therefore, one gets the corner frequency,

$$\omega_{cr} = |a_2|^{\frac{1}{(\alpha+\beta)}}$$

Hence, the following magnitude approximation is obtained:

1. For $\omega \leq \omega_{cr}$:

$$|T(j\omega)|_{dB} = -20\log_{10}|a_2|$$

2. For $\omega > \omega_{cr}$:

$$|T(j\omega)|_{dB} = -20\log_{10}|\omega^{(\alpha+\beta)}| = -20(\alpha + \beta)\log_{10}\omega$$

From the discussion above, following procedure is stated to sketch asymptotic magnitude Bode plot for fractional double-term pole $\frac{1}{(s^{\alpha+\beta} + a_1s^\alpha + a_2)}$ shown in Figure 6.2:

Procedure

1. Compute the corner frequency $\omega_{cr} = |a_2|^{\frac{1}{(\alpha+\beta)}}$ and locate point ① at magnitude $-20\log_{10}|a_2|$.
2. Draw a line with slope 0 dB/decade for $\omega \leq \omega_{cr}$, and a line with slope $-20(\alpha+\beta)$ dB/decade for $\omega > \omega_{cr}$ as shown in Figure 6.2.

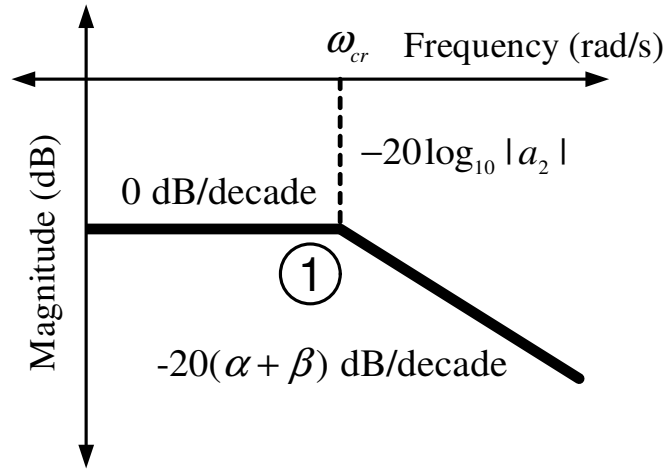


Figure 6.2: Asymptotic Magnitude Bode Plot for Fractional double-term Pole

Similarly, one can obtain such plots for terms: $\frac{1}{s^\alpha + a}$, s^α , $\frac{1}{s^\alpha}$, $(s + a)^\alpha$, $\frac{1}{(s+a)^\alpha}$ and $s^{\alpha+\beta} + a_1 s^\alpha + a_2$. The results are summarized in Table 6.2.

Remark 6.1. *It can be observed in Table 6.2 that since the TFs of fractional zero and fractional pole are reciprocal of each other, their magnitude plots are mirror images of each other with respect to ω -axis. This is also true for pairs such as fractional pole and zero at origin, fractional [pole] and [zero], fractional double-term pole and zero.*

Table 6.2: Asymptotic Magnitude Bode Plots for Remaining Basic Fractional-Order Terms

Term	Corner Frequency	Asymptotic Magnitude Bode Plot
Fractional Pole, $\frac{1}{s^\alpha + a}$	$\omega_{cr} = a ^{\frac{1}{\alpha}}$	
Fractional Zero at Origin, s^α	—	
Fractional Pole at Origin, $\frac{1}{s^\alpha}$	—	
Fractional [Zero], $(s + a)^\alpha$	$\omega_{cr} = a $	
Fractional [Pole], $\frac{1}{(s+a)^\alpha}$	$\omega_{cr} = a $	
Fractional Double-Term Zero, $(s^{\alpha+\beta} + a_1 s^\alpha + a_2)$	$\omega_{cr} = a_2 ^{\frac{1}{(\alpha+\beta)}}$	

6.2.4 Asymptotic Magnitude Bode Plots for Fractional-Order Controllers

In the present subsection, the asymptotic magnitude Bode plots of basic fractional-order terms are used to obtain such plots for FOCs, PI^α , $[PI]^\alpha$, PD^β , $[PD]^\beta$, and $PI^\alpha D^\beta$.

Let us consider PI^α controller which has the following TF:

$$\begin{aligned} C(s) &= K_p \left(1 + \frac{K_i}{s^\alpha} \right) \\ &= (K_p) (s^\alpha + K_i) \left(\frac{1}{s^\alpha} \right) \end{aligned} \quad (6.1)$$

As observed in (6.1), PI^α TF is expressed as a product of TFs of constant gain, fractional zero and fractional pole at origin. Therefore, the magnitude of PI^α in dB can be obtained by adding the magnitudes (in dB) of its constituent terms. This means that the asymptotic magnitude Bode plot of PI^α can be obtained by *adding* such plots of its constituent elements as shown in Table 6.3.

Similarly, one can develop the asymptotic magnitude Bode plots for $[PI]^\alpha$, PD^β , $[PD]^\beta$, and $PI^\alpha D^\beta$ controllers as summarized in Table 6.4.

Table 6.3: Asymptotic Magnitude Bode Plot for PI^α Controller

Term	Corner Frequency	Asymptotic Magnitude Bode Plot
Constant Gain, K_p	—	
Fractional Zero, $s^\alpha + K_i$	$\omega_{cr} = K_i ^{\frac{1}{\alpha}}$	
Fractional Pole at Origin, $\frac{1}{s^\alpha}$	—	

By adding the above plots, one gets:

PI^α Controller $= K_p \left(1 + \frac{K_i}{s^\alpha}\right)$ $= (K_p) (s^\alpha + K_i) \left(\frac{1}{s^\alpha}\right)$	$\omega_{cr} = K_i ^{\frac{1}{\alpha}}$	
---	--	--

Table 6.4: Asymptotic Magnitude Bode Plots for Other FOCs

Controller	Corner Frequency	Asymptotic Magnitude Bode Plot
$[PI]^\alpha$ $K_p \left(1 + \frac{K_i}{s}\right)^\alpha$ $= K_p (s + K_i)^\alpha \left(\frac{1}{s^\alpha}\right)$	$\omega_{cr} = K_i $	
PD^β $= K_p (1 + K_d s^\beta)$ $= K_p K_d \left(s^\beta + \frac{1}{K_d}\right)$	$\omega_{cr} = \left \frac{1}{K_d}\right ^{\frac{1}{\beta}}$	
$[PD]^\beta$ $= K_p (1 + K_d s)^\beta$ $= K_p K_d^\beta \left(s + \frac{1}{K_d}\right)^\beta$	$\omega_{cr} = \left \frac{1}{K_d}\right $	
$PI^\alpha D^\beta$ $= K_p \left(1 + \frac{K_i}{s^\alpha} + K_d s^\beta\right)$ $= K_p K_d \left(s^{\alpha+\beta} + \frac{s^\alpha}{K_d} + \frac{K_i}{K_d}\right) \frac{1}{s^\alpha}$	$\omega_{cr} = \left \frac{K_i}{K_d}\right ^{\frac{1}{(\alpha+\beta)}}$	

6.3 Asymptotic Phase Bode Plots for Fractional-Order Controllers

In this section, asymptotic phase Bode plots are developed for FOCs such as PI^α , $[PI]^\alpha$, PD^β , $[PD]^\beta$, and $PI^\alpha D^\beta$. For this purpose, let us consider the basic fractional-order terms presented in Table 6.1, where, $K \in \mathbb{R}$, $a, a_1, a_2 \in \mathbb{R}_{\neq 0}$ and $\alpha, \beta \in \mathbb{R}_{>0}$.

6.3.1 Phase Characteristics of Basic Fractional-Order Terms

In this subsection, we discuss the phase properties of the basic terms. The bounds of α and β are $(0, \infty)$ as specified earlier. However, considering that the target TFs are FOCs, the bounds of α and β are restricted to the interval $(0, 1)$ for the further discussion.

The terms in Table 6.1 are now considered one by one for their phase characteristics.

1. Constant Gain

The TF of constant gain is given by $T(s) = K$. For $K \geq 0$, the angle $\angle T(j\omega) = 0^\circ$. On the other hand, when $K < 0$, the angle $\angle T(j\omega)$ is 180° .

2. Fractional Zero

The TF of fractional zero is $T(s) = s^\alpha + a$. Substituting $s = j\omega$ (where, $\omega \in \mathbb{R}_{\geq 0}$) results into,

$$\begin{aligned} T(j\omega) &= (j\omega)^\alpha + a \\ &= \omega^\alpha e^{j\frac{\pi}{2}\alpha} + a \\ &= \left[\omega^\alpha \cos\left(\frac{\pi}{2}\alpha\right) + a \right] + j \left[\omega^\alpha \sin\left(\frac{\pi}{2}\alpha\right) \right] \end{aligned}$$

Therefore, one gets the phase angle,

$$\angle T(j\omega) = \tan^{-1} \left(\frac{\omega^\alpha \sin\left(\frac{\pi}{2}\alpha\right)}{\omega^\alpha \cos\left(\frac{\pi}{2}\alpha\right) + a} \right)$$

For the given phase function, its asymptotic approximation is drawn using straight lines by considering its extreme frequency behaviors. The approximation holds

good if the phase function behaves *monotonically* while changing from one level to another when ω goes from 0 to ∞ . A detailed discussion on this issue has been made in APPENDIX E. Based on the discussion in APPENDIX E.1, there are two cases:

(i) $a > 0$

- For $\omega = 0$, $\angle T(j\omega) = 0 \text{ rad} = 0^\circ$
- For $\omega \rightarrow \infty$, $\angle T(j\omega) = \frac{\pi\alpha}{2} \text{ rad} = (90\alpha)^\circ$

(ii) $a < 0$

- For $\omega = 0$, $\angle T(j\omega) = \pi \text{ rad} = 180^\circ$
- For $\omega \rightarrow \infty$, $\angle T(j\omega) = \frac{\pi\alpha}{2} \text{ rad} = (90\alpha)^\circ$

3. Fractional Pole

Fractional pole has TF $T(s) = \frac{1}{s^\alpha + a}$, which is inverse of the TF of fractional zero.

Therefore, the phase angle of fractional pole $\angle T(j\omega)$ is given by,

$$\begin{aligned}\angle T(j\omega) &= \angle \left[\frac{1}{(j\omega)^\alpha + a} \right] = -\angle [(j\omega)^\alpha + a] \\ &= -[\text{angle for fractional zero}]\end{aligned}$$

4. Fractional Zero at Origin

For the TF of fractional zero at origin $T(s) = s^\alpha$, $T(j\omega)$ equals $(j\omega)^\alpha = \omega^\alpha e^{j\frac{\pi}{2}\alpha}$.

Therefore, phase angle $\angle T(j\omega) = \frac{\pi}{2}\alpha \text{ rad} = (90\alpha)^\circ$

5. Fractional Pole at Origin

It is seen that the TF of fractional pole at origin $T(s) = \frac{1}{s^\alpha}$ is inverse of the TF of fractional zero at origin. Therefore, one gets,

$$\begin{aligned}\angle T(j\omega) &= \angle \left[\frac{1}{(j\omega)^\alpha} \right] = -\angle [(j\omega)^\alpha] \\ &= -[\text{angle for fractional zero at origin}]\end{aligned}$$

6. Fractional [Zero]

Fractional [zero] has the TF $T(s) = (s + a)^\alpha$. Substituting $s = j\omega$ implies,

$$\begin{aligned} T(j\omega) &= (j\omega + a)^\alpha \\ &= (\omega^2 + a^2)^{\frac{\alpha}{2}} e^{j \tan^{-1}\left(\frac{\omega}{a}\right)\alpha} \end{aligned}$$

Therefore, phase angle $\angle T(j\omega)$ is obtained as:

$$\angle T(j\omega) = \tan^{-1}\left(\frac{\omega}{a}\right)\alpha$$

There are two cases (Refer APPENDIX E.2):

(i) $a > 0$

- For $\omega = 0$, $\angle T(j\omega) = 0 \text{ rad} = 0^\circ$
- For $\omega \rightarrow \infty$, $\angle T(j\omega) = \frac{\pi}{2}\alpha \text{ rad} = (90\alpha)^\circ$

(ii) $a < 0$

- For $\omega = 0$, $\angle T(j\omega) = \pi\alpha \text{ rad} = (180\alpha)^\circ$
- For $\omega \rightarrow \infty$, $\angle T(j\omega) = \frac{\pi\alpha}{2} \text{ rad} = (90\alpha)^\circ$

7. Fractional [Pole]

Fractional [pole] has TF $T(s) = \frac{1}{(s+a)^\alpha}$ which is the inverse of TF of fractional [zero]. Therefore, one gets,

$$\begin{aligned} \angle T(j\omega) &= \angle \left[\frac{1}{(j\omega + a)^\alpha} \right] = -\angle [(j\omega + a)^\alpha] \\ &= -[\text{angle for Fractional [Zero]}] \end{aligned}$$

8. Fractional Double-Term Zero

The TF of fractional double-term zero is given by,

$$T(s) = s^{\alpha+\beta} + a_1 s^\alpha + a_2$$

Therefore, substituting $s = j\omega$ leads to $T(j\omega) = (j\omega)^{\alpha+\beta} + a_1(j\omega)^\alpha + a_2$. On

simplification, one gets,

$$T(j\omega) = \left[\omega^{\alpha+\beta} \cos\left(\frac{\pi}{2}(\alpha + \beta)\right) + a_1 \omega^\alpha \cos\left(\frac{\pi}{2}(\alpha)\right) + a_2 \right] \\ + j \left[\omega^{\alpha+\beta} \sin\left(\frac{\pi}{2}(\alpha + \beta)\right) + a_1 \omega^\alpha \sin\left(\frac{\pi}{2}(\alpha)\right) \right]$$

Therefore, the phase angle $\angle T(j\omega)$ is obtained as:

$$\angle T(j\omega) = \tan^{-1} \left(\frac{\omega^{\alpha+\beta} \sin\left(\frac{\pi}{2}(\alpha + \beta)\right) + a_1 \omega^\alpha \sin\left(\frac{\pi}{2}(\alpha)\right)}{\omega^{\alpha+\beta} \cos\left(\frac{\pi}{2}(\alpha + \beta)\right) + a_1 \omega^\alpha \cos\left(\frac{\pi}{2}(\alpha)\right) + a_2} \right)$$

There are two cases (Refer APPENDIX E.3):

(i) $a_2 > 0$ (irrespective of sign of a_1)

- For $\omega = 0$, $\angle T(j\omega) = 0 \text{ rad} = 0^\circ$
- For $\omega \rightarrow \infty$, $\angle T(j\omega) = \frac{\pi(\alpha+\beta)}{2} \text{ rad} = (90(\alpha + \beta))^\circ$

(ii) $a_2 < 0$ (irrespective of sign of a_1)

- For $\omega = 0$, $\angle T(j\omega) = \pi \text{ rad} = 180^\circ$
- For $\omega \rightarrow \infty$, $\angle T(j\omega) \approx \frac{\pi(\alpha+\beta)}{2} \text{ rad} = (90(\alpha + \beta))^\circ$

9. Fractional Double-Term Pole:

The TF of fractional double-term pole $T(s) = \frac{1}{s^{\alpha+\beta} + a_1 s^\alpha + a_2}$ is the inverse of TF of fractional double-term zero. Therefore, one gets,

$$\angle T(j\omega) = \angle \left[\frac{1}{(j\omega)^{\alpha+\beta} + a_1 (j\omega)^\alpha + a_2} \right] = -\angle [(j\omega)^{\alpha+\beta} + a_1 (j\omega)^\alpha + a_2] \\ = -[\text{angle for Fractional Double-Term Zero}]$$

In the next subsection, the phase characteristics of the basic fractional-order terms are utilized to develop their asymptotic phase Bode plots.

6.3.2 Asymptotic Phase Bode Plots for Basic Fractional-Order Terms

It is commonly found that the parameters of FOCs are positive. Therefore, to develop the asymptotic phase Bode plots for the FOCS, we first obtain such plots for the basic

terms with *positive* parameters. For constructing asymptotic phase Bode plots based on the phase characteristics, one has to first estimate the critical frequency ω_c , i.e. the frequency around which phase transition occurs. The derivations for the selection of such ω_c for basic fractional-order terms with positive parameters have been given in APPENDIX F.

We now focus on the two terms, namely, fractional zero and fractional double-term pole and develop their asymptotic phase Bode plots. Later, similar results are provided for the remaining terms.

1. Fractional Zero

For positive parameter case, i.e. $a > 0$, the critical frequency (ω_c) is given by (Refer APPENDIX F.1),

$$\omega_c = \left(\frac{a}{\cos\left(\frac{\pi}{2}\alpha\right)} \right)^{\frac{1}{\alpha}}$$

Conventionally, for integer-order TFs, asymptotic phase Bode plots are drawn around ω_c based on decade approach [*Dorf and Bishop (2011)*], [*Benjamin (1995)*]. However, it is preferable to utilize the slope information of the exact phase Bode plot at the critical frequency ω_c for drawing reasonably accurate asymptotic phase Bode plots. We accomplish this as follows:

- The phase of $(45\alpha)^\circ$ (which is mid of 0° and $(90\alpha)^\circ$) is considered at ω_c and a line is drawn passing through it with slope m , where m is the slope of tangent to the phase curve of $T(s)$ at ω_c .
- The points ① and ② are obtained on such a line where it cuts 0° and $(90\alpha)^\circ$ lines respectively as shown in Figure 6.3.
- The equation of line passing through $(\omega_c, (45\alpha))$ and slope m is:

$$y = m \log_{10} \omega + c$$

Since it passes through $(\omega_c, (45\alpha))$, one gets $c = 45\alpha - m \log_{10} \omega_c$.

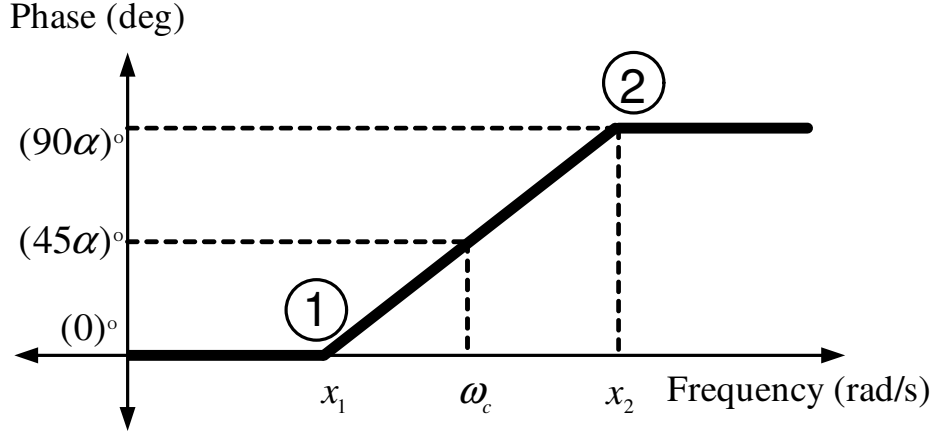


Figure 6.3: Asymptotic Phase Bode Plot for Fractional Zero

Therefore,

$$y = m \log_{10} \left(\frac{\omega}{\omega_c} \right) + 45\alpha$$

where, m in degree/decade is obtained as follows:

$$m = \left(\frac{d\angle T(j\omega)}{d \log_{10} \omega} \frac{180}{\pi} \right)_{\omega=\omega_c} = \left(\frac{d\angle T(j\omega)}{d\omega} \frac{d\omega}{d \log_{10} \omega} \frac{180}{\pi} \right)_{\omega=\omega_c}$$

Therefore,

$$m = \left(\frac{d\angle T(j\omega)}{d\omega} \omega \log_e 10 \frac{180}{\pi} \right)_{\omega=\omega_c}$$

Since,

$$\angle T(j\omega) = \tan^{-1} \left(\frac{\omega^\alpha \sin \left(\frac{\pi\alpha}{2} \right)}{a + \omega^\alpha \cos \left(\frac{\pi\alpha}{2} \right)} \right)$$

We get,

$$m = \frac{a\alpha\omega_c^\alpha \sin \left(\frac{\pi\alpha}{2} \right) \frac{180}{\pi} \log_e(10)}{a^2 + 2a\omega_c^\alpha \cos \left(\frac{\pi\alpha}{2} \right) + \omega_c^{2\alpha}} \quad (6.2)$$

At $\omega = x_1$, $y = 0$. Hence,

$$x_1 = 10^{\frac{-45\alpha}{m}} \omega_c \quad (6.3)$$

At $\omega = x_2$, $y = 90\alpha$. Therefore,

$$x_2 = 10^{\frac{45\alpha}{m}} \omega_c \quad (6.4)$$

Based on the above discussion, we suggest the following procedure for constructing the asymptotic phase Bode plot for fractional zero as shown in Figure 6.3.

Procedure

- (i) Compute m , x_1 , x_2 using (6.2), (6.3), (6.4) respectively.
- (ii) Locate points ① and ② corresponding to $(x_1, 0^\circ)$ and $(x_2, (90\alpha)^\circ)$ respectively.
- (iii) Draw the dark line as shown in Figure 6.3 to get the asymptotic phase Bode plot.

2. Fractional Double-Term Pole

For positive parameters case i.e. $a_1 > 0$, $a_2 > 0$, the critical frequency (ω_c) is given by (Refer APPENDIX F.3),

$$\omega_c = \left(\frac{a_2}{\cos\left(\frac{\pi}{2}(\alpha + \beta)\right)} \right)^{\frac{1}{\alpha + \beta}}$$

By adopting steps similar to the case of Fractional Zero, the asymptotic phase Bode plot for fractional double-term pole is obtained as shown in Figure 6.4.

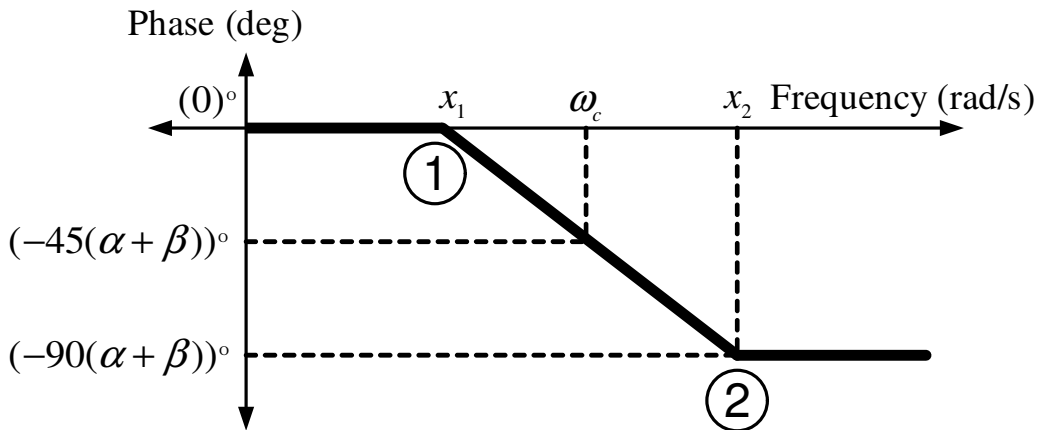


Figure 6.4: Asymptotic Phase Bode Plot for Fractional Double-Term Pole

In Figure 6.4, the expressions for x_1 and x_2 are as follows:

$$x_1 = 10^{\frac{45(\alpha+\beta)}{m}} \omega_c, x_2 = 10^{-\frac{45(\alpha+\beta)}{m}} \omega_c$$

where, $m = -\frac{A_1}{B_1} \frac{180}{\pi} \log_e(10)$ and,

$$A_1 = \beta a_1 \omega_c^{2\alpha+\beta} \sin\left(\frac{\pi\beta}{2}\right) + a_2 a_1 \alpha \omega_c^\alpha \sin\left(\frac{\pi\alpha}{2}\right) + a_2(\alpha + \beta) \omega_c^{\alpha+\beta} \sin\left(\frac{\pi(\alpha+\beta)}{2}\right)$$

$$B_1 = \omega_c^{2(\alpha+\beta)} + a_1^2 \omega_c^{2\alpha} + a_2^2 + 2a_1 \omega_c^{2\alpha+\beta} \cos\left(\frac{\pi\beta}{2}\right) + 2a_2 \omega_c^{\alpha+\beta} \cos\left(\frac{\pi(\alpha + \beta)}{2}\right) + 2a_1 a_2 \omega_c^\alpha \cos\left(\frac{\pi\alpha}{2}\right)$$

Similarly, one can obtain corresponding results for terms: $\frac{1}{s^{\alpha+a}}$, s^α , $\frac{1}{s^\alpha}$, $(s+a)^\alpha$, $\frac{1}{(s+a)^\alpha}$ and $s^{\alpha+\beta} + a_1 s^\alpha + a_2$. The results are summarized in Table 6.5.

Remark 6.2. *It can be observed that the TFs of fractional zero and fractional pole are reciprocal to each other. Due to this, their phase plots are mirror images of each other with respect to ω -axis as shown in Table 6.5. This is also true for pairs such as (fractional pole at origin, fractional zero at origin), (fractional [pole], fractional [zero]), (fractional double-term pole, fractional double-term zero).*

In the next section, the usefulness of these plots in constructing the asymptotic phase Bode plots for FOCs is illustrated.

6.3.3 Asymptotic Phase Bode Plots for Fractional-Order Controllers

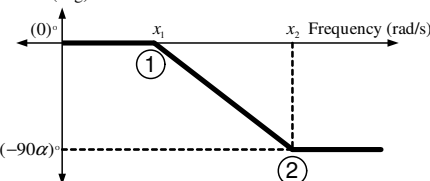
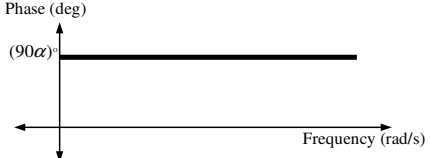
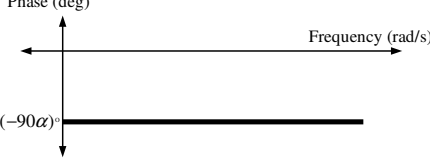
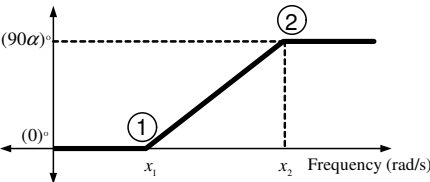
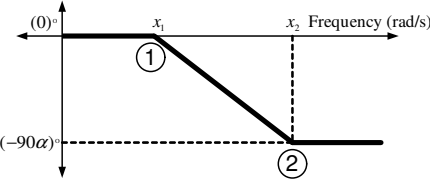
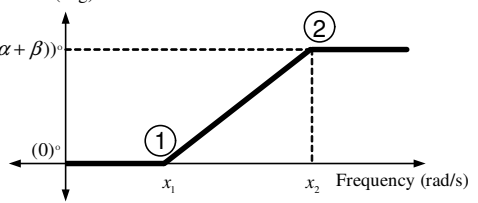
The asymptotic phase Bode plots of basic terms are utilized to obtain corresponding plots for FOCs such as PI^α , $[PI]^\alpha$, PD^β , $[PD]^\beta$, and $PI^\alpha D^\beta$ with positive parameters.

Let us consider PI^α controller which has the following TF:

$$\begin{aligned} C(s) &= K_p \left(1 + \frac{K_i}{s^\alpha}\right) \\ &= (K_p) (s^\alpha + K_i) \left(\frac{1}{s^\alpha}\right) \end{aligned} \quad (6.5)$$

As seen in (6.5), the PI^α controller TF can be expressed as the product of constant gain, fractional zero and fractional pole at origin. For drawing the asymptotic phase

Table 6.5: Asymptotic Phase Bode Plots for Remaining Basic Fractional-Order Terms

Term and Expressions	Asymptotic Phase Bode Plot
<p>Constant Gain, K</p>	
<p>Fractional Pole, $\frac{1}{s^\alpha + a}$</p> $m = -\frac{a\alpha\omega_c^\alpha \sin(\frac{\pi\alpha}{2}) \frac{180}{\pi} \log_e(10)}{a^2 + 2a\omega_c^\alpha \cos(\frac{\pi\alpha}{2}) + \omega_c^{2\alpha}}$ $x_1 = 10^{\frac{45\alpha}{m}} \omega_c, x_2 = 10^{\frac{-45\alpha}{m}} \omega_c$ $\omega_c = \left(\frac{a}{\cos(\frac{\pi\alpha}{2})} \right)^{\frac{1}{\alpha}}$	
<p>Fractional Zero at Origin, s^α</p>	
<p>Fractional Pole at Origin, $\frac{1}{s^\alpha}$</p>	
<p>Fractional [Zero], $(s + a)^\alpha$</p> $m = \frac{a\alpha\omega_c^\alpha \sin(\frac{\pi\alpha}{2}) \frac{180}{\pi} \log_e(10)}{a^2 + \omega_c^{2\alpha}}, \omega_c = a$ $x_1 = 10^{\frac{-45\alpha}{m}} \omega_c, x_2 = 10^{\frac{45\alpha}{m}} \omega_c$	
<p>Fractional [Pole], $\frac{1}{(s+a)^\alpha}$</p> $m = -\frac{a\alpha\omega_c^\alpha \sin(\frac{\pi\alpha}{2}) \frac{180}{\pi} \log_e(10)}{a^2 + \omega_c^{2\alpha}}, \omega_c = a$ $x_1 = 10^{\frac{45\alpha}{m}} \omega_c, x_2 = 10^{\frac{-45\alpha}{m}} \omega_c$	
<p>Fractional Double-Term Zero,</p> $s^{\alpha+\beta} + a_1 s^\alpha + a_2$ $m = \frac{A_1}{B_1} \frac{180}{\pi} \log_e(10)$ $x_1 = 10^{\frac{-45(\alpha+\beta)}{m}} \omega_c, x_2 = 10^{\frac{45(\alpha+\beta)}{m}} \omega_c$ $\omega_c = \left(\frac{a_2}{\cos(\frac{\pi}{2}(\alpha+\beta))} \right)^{\frac{1}{\alpha+\beta}}$	

Bode plot for PI^α controller, the plots of its constituent terms are added as shown in Table 6.6. Similarly, one can generate the asymptotic phase Bode plots for other FOCs such as $[PI]^\alpha$, PD^β , $[PD]^\beta$, and $PI^\alpha D^\beta$ which are presented in Table 6.7.

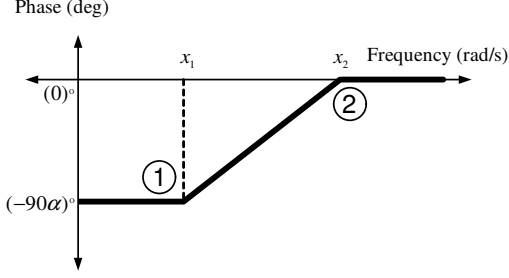
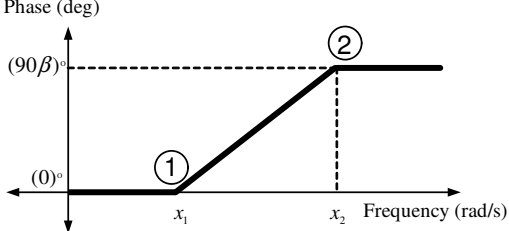
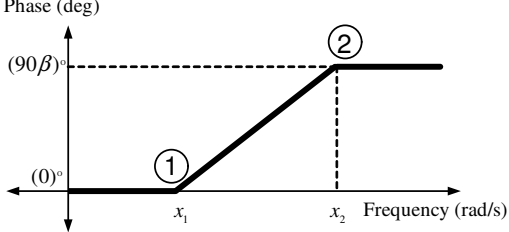
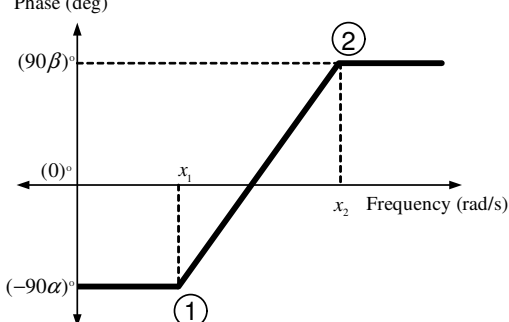
Table 6.6: Asymptotic Phase Bode Plot for PI^α Controller

Term and Expressions	Asymptotic Phase Bode Plot
K_p	
$m = \frac{s^\alpha + K_i}{K_i^2 + 2K_i\omega_c^\alpha \cos\left(\frac{\pi\alpha}{2}\right) + \omega_c^{2\alpha}}$ $x_1 = 10^{-\frac{45\alpha}{m}} \omega_c$ $x_2 = 10^{\frac{45\alpha}{m}} \omega_c$ $\omega_c = \left(\frac{K_i}{\cos\left(\frac{\pi}{2}\alpha\right)}\right)^{\frac{1}{\alpha}}$	
$\frac{1}{s^\alpha}$	

By combining the above plots, one gets:

PI^α	
-------------	--

Table 6.7: Asymptotic Phase Bode Plots for Other FOCs

Term and Expressions	Asymptotic Phase Bode Plot
$[PI]^\alpha = K_p \left(1 + \frac{K_i}{s}\right)^\alpha$ $= K_p (s + K_i)^\alpha \left(\frac{1}{s^\alpha}\right)$ $m = \frac{K_i \alpha \omega_c}{K_i^2 + \omega_c^2} \frac{180}{\pi} \log_e(10), \omega_c = K_i$ $x_1 = 10^{-\frac{45\alpha}{m}} \omega_c, x_2 = 10^{\frac{45\alpha}{m}} \omega_c$	
$PD^\beta = K_p (1 + K_d s^\beta)$ $= K_p K_d \left(s^\beta + \frac{1}{K_d}\right)$ $m = \frac{\left(\frac{1}{K_d}\right)^\beta \omega_c^\beta \sin\left(\frac{\pi\beta}{2}\right) \frac{180}{\pi} \log_e(10)}{\left(\frac{1}{K_d}\right)^2 + 2\left(\frac{1}{K_d}\right) \omega_c^\beta \cos\left(\frac{\pi\beta}{2}\right) + \omega_c^{2\beta}}$ $x_1 = 10^{-\frac{45\beta}{m}} \omega_c, x_2 = 10^{\frac{45\beta}{m}} \omega_c$ $\omega_c = \left(\frac{1/K_d}{\cos\left(\frac{\pi\beta}{2}\right)}\right)^{\frac{1}{\beta}}$	
$[PD]^\beta = K_p (1 + K_d s)^\beta$ $= K_p K_d^\beta \left(s + \frac{1}{K_d}\right)^\beta$ $m = \frac{\left(\frac{1}{K_d}\right)^\beta \omega_c \frac{180}{\pi} \log_e(10)}{\left(\frac{1}{K_d}\right)^2 + \omega_c^2}$ $x_1 = 10^{-\frac{45\beta}{m}} \omega_c, x_2 = 10^{\frac{45\beta}{m}} \omega_c$	
$PI^\alpha D^\beta = K_p \left(1 + \frac{K_i}{s^\alpha} + K_d s^\beta\right)$ $= K_p K_d \left(s^{\alpha+\beta} + \frac{s^\alpha}{K_d} + \frac{K_i}{K_d}\right) \frac{1}{s^\alpha}$ $m = \frac{A_2}{B_2} \frac{180}{\pi} \log_e(10)$ $x_1 = 10^{-\frac{45(\alpha+\beta)}{m}} \omega_c, x_2 = 10^{\frac{45(\alpha+\beta)}{m}} \omega_c$ $\omega_c = \left(\frac{\frac{K_i}{K_d}}{\cos\left(\frac{\pi}{2}(\alpha+\beta)\right)}\right)^{\frac{1}{\alpha+\beta}}$	

The terms A_2 and B_2 in Table 6.7 are given by,

$$A_2 = \beta \left(\frac{1}{K_d} \right) \omega_c^{2\alpha+\beta} \sin \left(\frac{\pi\beta}{2} \right) + \left(\frac{K_i}{K_d} \right) \left(\frac{1}{K_d} \right) \alpha \omega_c^\alpha \sin \left(\frac{\pi\alpha}{2} \right) + \left(\frac{K_i}{K_d} \right) (\alpha+\beta) \omega_c^{\alpha+\beta} \sin \left(\frac{\pi(\alpha+\beta)}{2} \right)$$

$$B_2 = \omega_c^{2(\alpha+\beta)} + \left(\frac{1}{K_d} \right)^2 \omega_c^{2\alpha} + \left(\frac{K_i}{K_d} \right)^2 + 2 \left(\frac{1}{K_d} \right) \omega_c^{2\alpha+\beta} \cos \left(\frac{\pi\beta}{2} \right) + 2 \left(\frac{K_i}{K_d} \right) \omega_c^{\alpha+\beta} \cos \left(\frac{\pi(\alpha+\beta)}{2} \right) + 2 \left(\frac{1}{K_d} \right) \left(\frac{K_i}{K_d} \right) \omega_c^\alpha \cos \left(\frac{\pi\alpha}{2} \right)$$

6.4 Asymptotic Magnitude and Phase Bode Plots for Fractional Commensurate Order TFs

Let us recall the discussion in Section 2.4 about the commensurate order of a general fractional-order TF,

$$\frac{Y(s)}{U(s)} = \frac{b_m s^{\beta_m} + b_{m-1} s^{\beta_{m-1}} + \dots + b_0 s^{\beta_0}}{a_n s^{\alpha_n} + a_{n-1} s^{\alpha_{n-1}} + \dots + a_0 s^{\alpha_0}} \quad (6.6)$$

The TF (6.6) represents a *commensurate* order system, if there exists a greatest common divisor $q \in \mathbb{R}$ such that $\alpha_i = qe_i (i = 0, 1, 2, \dots, n)$, $\beta_k = qf_k (k = 0, 1, 2, \dots, m)$; $e_i, f_k \in \mathbb{Z}$. Here, q is called the commensurate order, which can be rational or irrational. Therefore,

$$T(s) := \frac{Y(s)}{U(s)} = \frac{P(s^q)}{Q(s^q)}$$

where, $P(\cdot), Q(\cdot)$ are polynomial functions.

If we let $p = s^q$, then,

$$T(p) = \frac{P(p)}{Q(p)} \quad (6.7)$$

On factorization, (6.7) can be expressed as follows¹:

$$T(p) = \frac{\prod_{i=0}^{m_1} (p + c_i) \prod_{j=0}^{m_2} (d_j p^2 + e_j p + f_j)}{\prod_{k=0}^{m_3} (p + g_k) \prod_{l=0}^{m_4} (h_l p^2 + o_l p + z_l)}$$

where c_i ($i = 0, 1, \dots, m_1$), d_j, e_j, f_j ($j = 0, 1, \dots, m_2$), g_k ($k = 0, 1, \dots, m_3$), h_l, o_l, z_l ($l = 0, 1, \dots, m_4$) are real constants. m_1, m_2, m_3, m_4 are positive integers.

Now, by re-substituting $p = s^q$, one gets,

$$T(s) = \frac{\prod_{i=0}^{l_1} (s^q + c_i) \prod_{j=0}^{l_2} (d_j s^{2q} + e_j s^q + f_j)}{\prod_{k=0}^{l_3} (s^q + g_k) \prod_{l=0}^{l_4} (h_l s^{2q} + o_l s^q + z_l)} \quad (6.8)$$

It is seen that (6.8) is composed of fractional zeros, fractional poles, fractional double-term zeros and fractional double-term poles. Hence, one can construct asymptotic Bode plots of $T(s)$ by adding such plots of their constituent terms similar to the PI^α case explained in Tables 6.3 and 6.6.

6.5 Applications

In this section, we discuss the applications of asymptotic magnitude and phase Bode formulations. We first illustrate the identification of fractional-order TF from the given asymptotic magnitude Bode plot. Next, the usefulness of asymptotic magnitude and phase Bode plots for analysis of fractional control loop is explained in detail.

6.5.1 Identification of Fractional-Order Transfer Function

Let us consider the problem of identifying the TF from a given asymptotic magnitude Bode plot in which the straight-line approximations assume any arbitrary slope.² A

¹This is because any polynomial with real coefficients has either real roots or complex roots in pairs. The real roots lead to terms of the form $(p + c_i)$, $(p + g_k)$ and complex roots in pairs lead to terms such as $(d_j p^2 + e_j p + f_j)$, $(h_l p^2 + o_l p + z_l)$.

²In integer-order TF case, such slopes are always integer multiples of 20.

general case is shown in Figure 6.5 (Where $a_1, a_2, \dots, a_n \in \mathbb{R}_{>0}, b_1, b_2, \dots, b_{n+1} \in \mathbb{R}$). Prior to identification, it is essential to consider the asymptotic magnitude Bode plots of following composite terms:

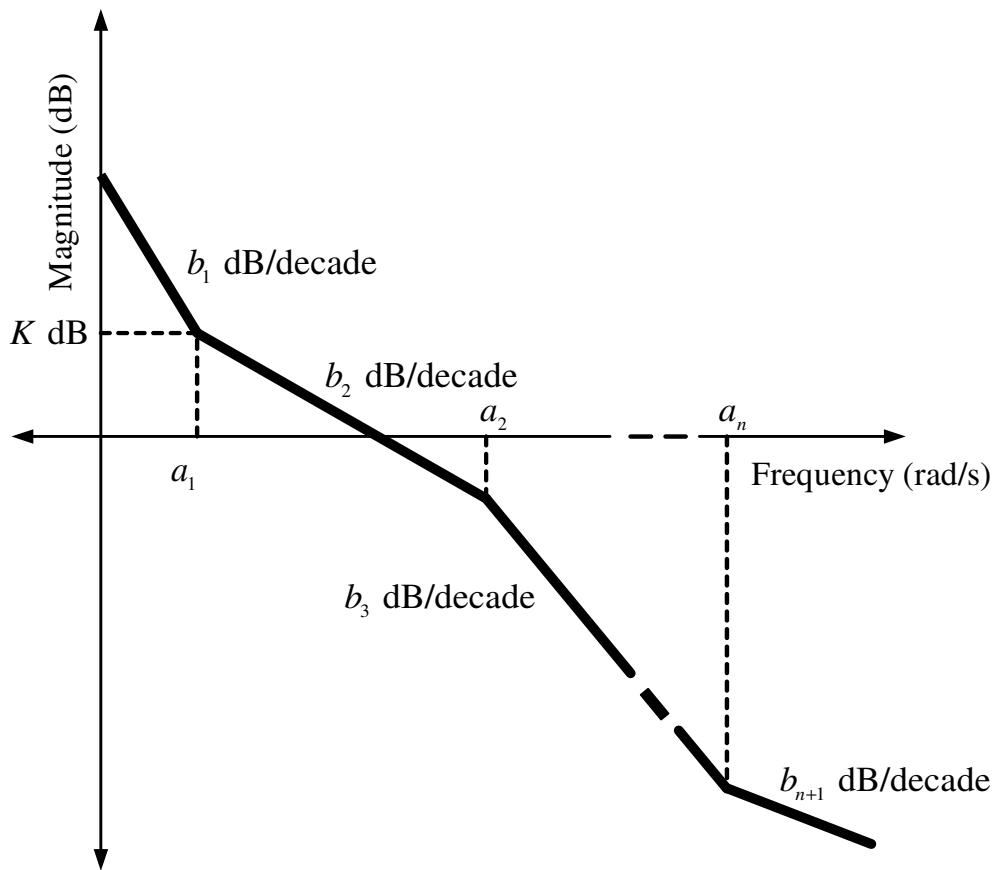


Figure 6.5: Identification of Fractional-Order TF from Asymptotic Magnitude Bode Plot

1. ks^α (where, $k, \alpha \in \mathbb{R}$)

ks^α is composed of constant gain k and the term s^α . Based on the value of α , there are following possible cases:

- (a) $\alpha > 0$: In such case, s^α is fractional zero at origin. Asymptotic magnitude Bode plot of ks^α obtained from its constituent terms is shown in Figure 6.6:³

³Figure is sketched for $|k| > 1$. One can also sketch the corresponding one for $|k| < 1$.

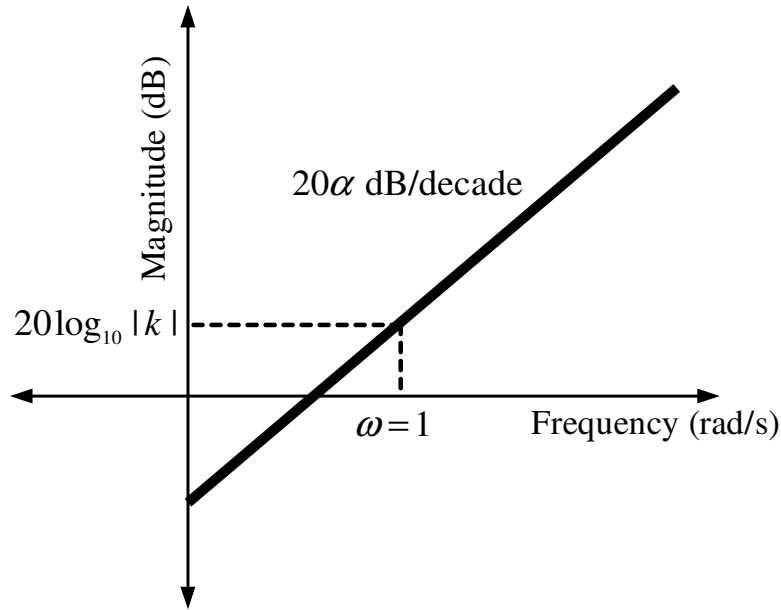


Figure 6.6: Asymptotic Magnitude Bode Plot for ks^α when $\alpha > 0$

(b) $\alpha < 0$: In this case, s^α represents fractional pole at origin. Figure 6.7 shows the asymptotic magnitude Bode plot for ks^α .

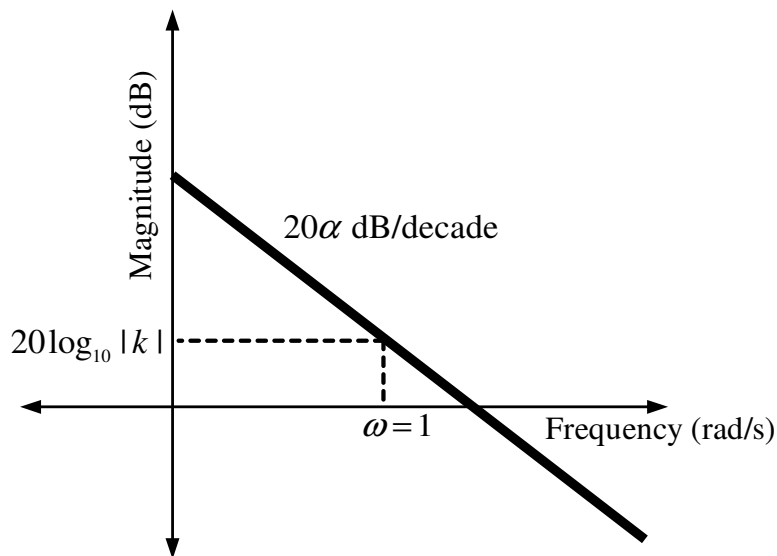


Figure 6.7: Asymptotic Magnitude Bode Plot for ks^α when $\alpha < 0$

(c) $\alpha = 0$: For this case, ks^α reduces to k . The discussion for asymptotic magnitude plot for such a term was made in Section 6.2.1.

Remark 6.3. *It can be inferred from the above asymptotic plots that the term ks^α is identified when a line of given slope offset by a known magnitude is observed.*

2. $\frac{(s+a)^\alpha}{a^\alpha}$ (where, $a \in \mathbb{R}$, $\alpha \in \mathbb{R}_{\neq 0}$)

$\frac{(s+a)^\alpha}{a^\alpha}$ is composed of constant gain $\frac{1}{a^\alpha}$ and the term $(s+a)^\alpha$. When $\alpha > 0$, $(s+a)^\alpha$ represents fractional [zero]. For such case, the asymptotic magnitude plot of $\frac{(s+a)^\alpha}{a^\alpha}$ obtained from its constituent elements is as shown in Figure 6.8.

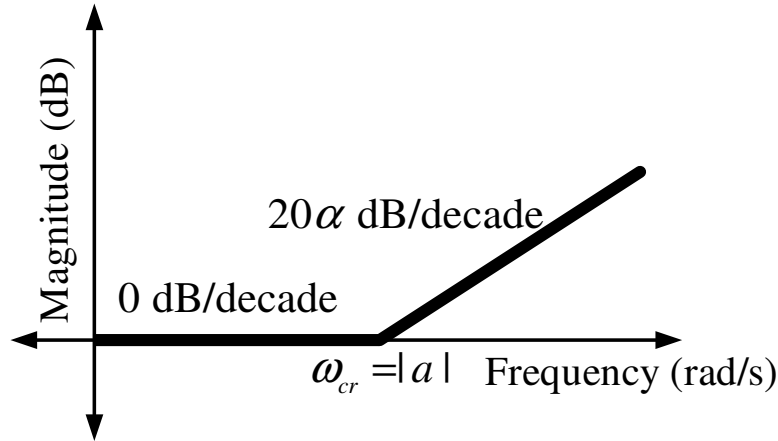


Figure 6.8: Asymptotic Magnitude Bode Plot for $\frac{(s+a)^\alpha}{a^\alpha}$ when $\alpha > 0$

On the other hand, for $\alpha < 0$, $(s+a)^\alpha$ represents fractional [pole]. Therefore, the asymptotic magnitude plot of $\frac{(s+a)^\alpha}{a^\alpha}$ in this case takes the shape as shown in Figure 6.9.

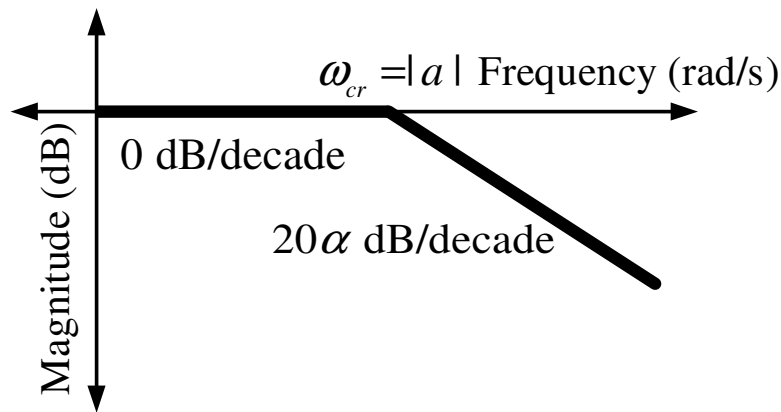


Figure 6.9: Asymptotic Magnitude Bode Plot for $\frac{(s+a)^\alpha}{a^\alpha}$ when $\alpha < 0$

Remark 6.4. It can be observed from Figures 6.8 and 6.9 that,

- $\frac{(s+a)^\alpha}{a^\alpha}$ with $\alpha > 0$ is identified when there is an increase in slope at given corner frequency.
- $\frac{(s+a)^\alpha}{a^\alpha}$ with $\alpha < 0$ is identified when there is a decrease in slope at given corner frequency.

Based on above discussion, we identify the fractional-order TF from the asymptotic magnitude Bode plot given in Figure 6.5 as follows:

- (i) From Figure 6.5, it is seen that for the frequency range from 0 to a_1 , the plot is a line with slope b_1 dB/decade. Recalling Remark 6.3, we identify the corresponding term as ks^α with $\alpha = \frac{b_1}{20}$ (Since, $20\alpha = b_1$). The constant k is obtained as follows:

From Figure 6.5,

$$20\log_{10}|ks^\alpha|_{s=ja_1} = K$$

Therefore,

$$|k| = \frac{10^{\frac{K}{20}}}{a_1^\alpha}$$

So we get,

$$k = \pm \frac{10^{\frac{K}{20}}}{a_1^{\frac{b_1}{20}}}$$

- (ii) At corner frequency a_1 , there is an observed increase of slope from b_1 to b_2 . From Remark 6.4, this corresponds to the term $\frac{(s+a)^\alpha}{a^\alpha}$ with $\alpha = \frac{b_2-b_1}{20}$, $a = a_1$. (Since, $b_2 > b_1$, $\alpha > 0$). Similarly, at corner frequency a_2 , there is an observed decrease of slope from b_2 to b_3 . From Remark 6.4, we get the corresponding term as $\frac{(s+a)^\alpha}{a^\alpha}$ with $\alpha = \frac{b_3-b_2}{20}$, $a = a_2$. (Since, $b_3 < b_2$, $\alpha < 0$). One can similarly obtain the terms for observed change in slopes at a_3, a_4, \dots, a_n .
- (iii) The individual identified terms are multiplied to get the complete TF $T(s)$ for the asymptotic magnitude plot given in Figure 6.5 as follows:

$$T(s) = \pm \left(\frac{10^{\frac{K}{20}} s^{\frac{b_1}{20}}}{a_1^{\frac{b_1}{20}}} \right) \left(\frac{(s+a_1)^{\frac{b_2-b_1}{20}}}{a_1^{\frac{b_2-b_1}{20}}} \right) \left(\frac{(s+a_2)^{\frac{b_3-b_2}{20}}}{a_2^{\frac{b_3-b_2}{20}}} \right) \cdots \left(\frac{(s+a_n)^{\frac{b_{n+1}-b_n}{20}}}{a_n^{\frac{b_{n+1}-b_n}{20}}} \right)$$

It is important to note that the above general case considers asymptotic magnitude Bode plots containing lines with arbitrary slopes. Therefore, it also includes the integer-order TF cases when slopes are integer multiples of 20.

6.5.2 Analysis of Fractional Control Loop

In present subsection, we illustrate the application of asymptotic magnitude and phase Bode plot formulation for analyzing the performance of given fractional control loop. For this purpose, let us consider a typical control example in which a $[PD]^\beta$ controller is tuned for a type-1 motion plant $\frac{K}{s(Ts+1)}$ so as to meet Wang-et-al specifications.

Suppose the numerical values are: $K = 1, T = 0.4, \omega_{gc} = 10 \text{ rad/s}, \phi_m = 70^\circ$. The controller is obtained by utilizing the unified expressions derived in Chapter 3. Plant $G(s)$, designed controller $C(s)$, and loop TF $L(s)$ are as follows:

- Plant, $G(s) = \frac{1}{s(0.4s+1)}$
- Controller, $C(s) = 16.7780(1 + 0.2992s)^{0.7826}$
- Loop TF:

$$\begin{aligned}
 L(s) &= C(s)G(s) \\
 &= 16.7780(1 + 0.2992s)^{0.7826} \frac{1}{s(0.4s + 1)} \\
 &= (16.3143) \left(s + \frac{1}{0.2992} \right)^{0.7826} \left(\frac{1}{s^1} \right) \frac{1}{(s^1 + 2.5)} \quad (6.9)
 \end{aligned}$$

The asymptotic Bode plots of $L(s)$ can be used to verify its Wang-et-al performance (i.e. $\omega_{gc} = 10 \text{ rad/s}, \phi_m = 70^\circ$). It is seen in (6.9) that $L(s)$ is composed of basic terms such as constant gain, fractional [zero], fractional pole at origin, and fractional pole. Therefore, one can draw the asymptotic Bode plot for $L(s)$ by adding such plots of its constituent terms. Figure 6.10 presents exact as well as asymptotic magnitude and phase Bode plots for $L(s)$.

It is seen in Figure 6.10 that the exact and asymptotic magnitude Bode plots are very close and lead to $\omega_{gc} = 10 \text{ rad/s}$. Corresponding to $\omega_{gc} = 10 \text{ rad/s}$, the ϕ_m values obtained from exact and asymptotic phase Bode plots are 70° and 65° respectively. Thus, in conclusion, asymptotic magnitude and phase plots give a fair enough estimate of performance of $L(s)$.

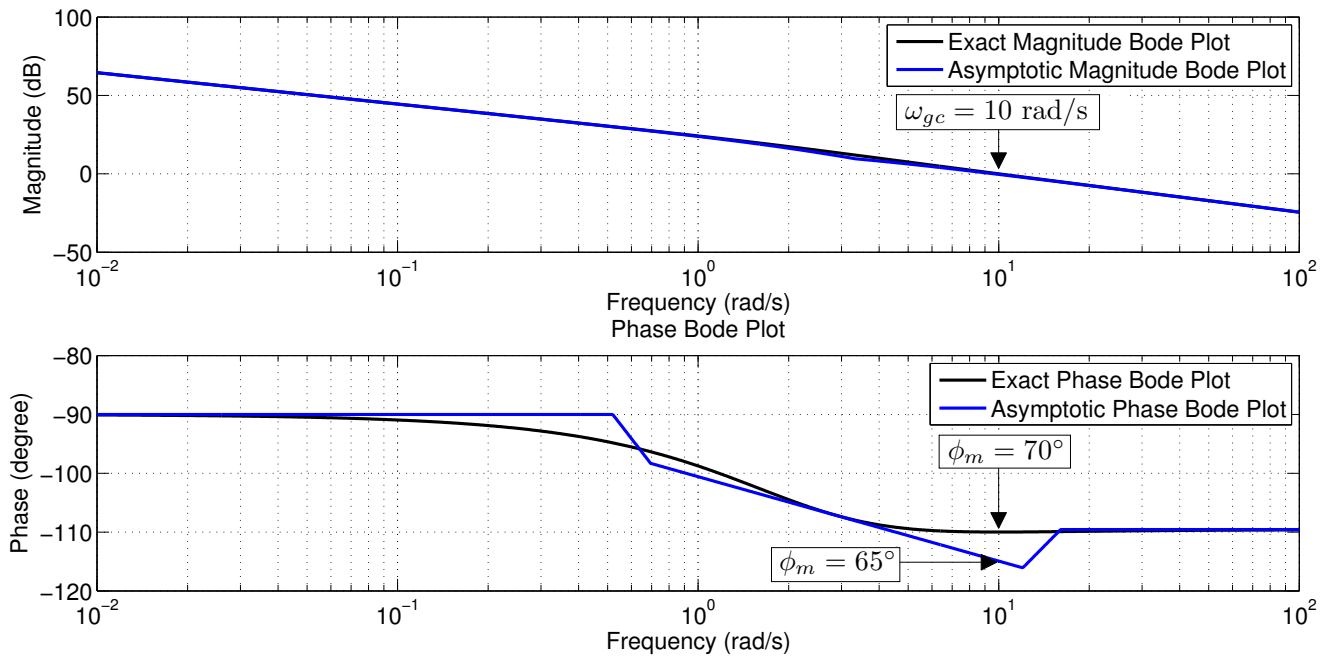


Figure 6.10: Loop Analysis using Asymptotic Magnitude and Phase Bode Plots

6.6 Summary

This chapter developed the formulations for asymptotic magnitude and phase Bode plots of FOCs such as PI^α , $[PI]^\alpha$, PD^β , $[PD]^\beta$, and $PI^\alpha D^\beta$. For this purpose, a few basic terms were introduced. It was shown that the asymptotic magnitude and phase Bode plots of FOCs can be constructed by combining such plots of these basic terms. Furthermore, the similar construction was explained for fractional commensurate order TFs in general.

An application of asymptotic magnitude Bode plot formulation for identification of fractional-order TF was illustrated. Additionally, the application of asymptotic magnitude and phase Bode plots for analyzing the designed fractional control loop was also demonstrated using a numerical example.

CHAPTER 7

Conclusions and Future Scope

The concept of conventional integer-order calculus is generalized in the form of Fractional Calculus (FC) which handles derivatives and integrals of arbitrary orders. The inception of FC in the control theory enables the design of Fractional-Order Controllers (FOCs) such as PI^α , $[PI]^\alpha$, PD^β , $[PD]^\beta$, and $PI^\alpha D^\beta$, whose dynamics are governed by fractional-order differential equations. The main focus in our thesis was to investigate the limit cycle performance and asymptotic Bode characteristics of such FOCs.

- The thesis began with the development of unified tuning expressions for three-parameter FOCs such as PI^α , $[PI]^\alpha$, PD^β , and $[PD]^\beta$ to meet Wang-et-al specifications. This was accomplished by introducing a universal plant structure which accommodates any integer or fractional-order Transfer Function (TF).
- After such unification, we focused on the plants containing a separable nonlinearity. First, we designed three-parameter fractional and integer-order controllers for the plant TFs using earlier derived unified tuning expressions, after which, the limit cycle performances of the designed controllers were examined in the presence of separable nonlinearity. The observations hinted towards the potential of FOCs in achieving better limit cycle performance over the integer-order controllers. Mounting on this observation, more detailed controller design problems were considered for plants, one containing backlash and another having relay nonlinearity. Limit cycle performance was specifically targeted for such plants for the suppression of sustained oscillation amplitudes while proposing the controller design frameworks. The controllers were also constrained to satisfy certain loop performance specifications. Under these formulations, design of FOCs was illustrated and their superiority over integer-order counterparts was claimed. The investigation made an efficient use of Describing Function (DF) of the nonlinearity for design and analysis of control systems.
- The thesis further contributed for the development of asymptotic magnitude and Phase Bode plots for FOCs. Such construction was also developed for fractional

commensurate order TFs in general. Later, we illustrated the identification of fractional-order TF from the given asymptotic magnitude Bode plot. Furthermore, the application of asymptotic magnitude and Phase Bode plots for manually analyzing the designed fractional control loop is demonstrated in detail.

The future scope for the research work in this thesis is as follows:

- Although the Wang-et-al specifications were considered in this thesis for obtaining unified tuning expressions, one may also consider any other set of three specifications. Furthermore, the term e^{-Ls^γ} introduced in Remark 3.1 needs to be examined for its possible physical meaning so that the universal plant structure can be subsequently improved.
- For plants containing separable nonlinearity, the design frameworks were developed for cases where Nyquist plot of the designed loop intersects $-\frac{1}{N(X)}$ curve only once in the complex plane. One needs to explore further in this direction to come up with the class of nonlinear loops which satisfy such requirement. One can also consider the loop cases for which there occur multiple crossing points. A future work is needed to handle even more general cases when multiple nonlinearities are present in the control loop. The limit cycle performances of FOCs for plants with other kind of nonlinearities such as saturation, dead-zone etc. is also an interesting future direction to this work.
- The asymptotic Bode plots developed in our thesis gives the knowledge about role of each parameter of FOCs in determining the shapes of their Bode responses. This knowledge can be very useful to a practical engineer to develop a systematic manual design procedure for FOCs in future. Additionally, referring to the discussion in APPENDIX E.3, the monotonicity of $\angle T(j\omega)$ with respect to ω is not guaranteed *in general* when $T(s)$ represents fractional double-term zero or pole. Therefore, one can explore in future the conditions to be met by the parameters of such $T(s)$ so that $\angle T(j\omega)$ is monotonic.

REFERENCES

1. Ahmad, W., Ei-Khazali, R., and Elwakil, A. (2001). Fractional-order wien-bridge oscillator. *Electronics Letters*, 37, 1110–1112.
2. Atherton, D. (2011). *An introduction to nonlinearity in control systems*. Bookboon.
3. Atherton, D. P. (1975). *Nonlinear control engineering*, .
4. Atherton, D. P., Tan, N., Yeroglu, C., Kavuran, G., and Yüce, A. (2014). Limit cycles in nonlinear systems with fractional order plants. *Machines*, 2, 176–201.
5. Axtell, M., and Bise, M. E. (1990). Fractional calculus application in control systems. In *Aerospace and Electronics Conference, 1990. NAECON 1990., Proceedings of the IEEE 1990 National* (pp. 563–566). IEEE.
6. Azenha, A., and Machado, J. T. (1998). On the describing function method and the prediction of limit cycles in nonlinear dynamical systems. *Systems Analysis Modelling Simulation*, 33, 307–320.
7. Bagley, R. L., and Torvik, P. (1983). A theoretical basis for the application of fractional calculus to viscoelasticity. *Journal of Rheology (1978-present)*, 27, 201–210.
8. Baleanu, D. (2012). *Fractional Calculus: Models and Numerical Methods* volume 3. World Scientific.
9. Baleanu, D., Güvenç, Z. B., and Machado, J. T. (2010). *New trends in nanotechnology and fractional calculus applications*. Springer.
10. Barbosa, R. S., and Machado, J. T. (2002). Describing function analysis of systems with impacts and backlash. *Nonlinear Dynamics*, 29, 235–250.
11. Barbosa, R. S., Machado, J. T., and Ferreira, I. M. (2004). PID controller tuning using fractional calculus concepts. *Fractional Calculus and Applied Analysis*, 7, 119–134.

12. Barbosa, R. S., Machado, J. T., and Galhano, A. M. (2007). Performance of fractional PID algorithms controlling nonlinear systems with saturation and backlash phenomena. *Journal of Vibration and Control*, *13*, 1407–1418.
13. Bateman, H., and Erdelyi, A. (1955). Higher transcendental functions, vol. 3: Elliptic and automorphic functions, lamé and mathieu functions.
14. Benjamin, C. (1995). Kuo, automatic control systems.
15. Bode, H. W. (1940). Relations between attenuation and phase in feedback amplifier design. *Bell System Technical Journal*, *19*, 421–454.
16. Bode, H. W. (1945). *Network analysis and feedback amplifier design* volume 11. van Nostrand New York.
17. Butzer, P., and Westphal, U. (2000). An introduction to fractional calculus.
18. Cafagna, D. (2007). Fractional calculus: A mathematical tool from the past for present engineers [past and present]. *Industrial Electronics Magazine, IEEE*, *1*, 35–40.
19. Caponetto, R. (2010). *Fractional order systems: modeling and control applications* volume 72. World Scientific.
20. Caputo, M., and Mainardi, F. (1971). A new dissipation model based on memory mechanism. *Pure and Applied Geophysics*, *91*, 134–147.
21. Carlson, G., and Halijak, C. (1964). Approximation of fractional capacitors by a regular newton process. *Circuit Theory, IEEE Transactions on*, *11*, 210–213.
22. Chang, C.-H., and Chang, M.-K. (1994). Analysis of gain margins and phase margins of a nonlinear reactor control system. *Nuclear Science, IEEE Transactions on*, *41*, 1686–1691.
23. Charef, A. (2006). Analogue realisation of fractional-order integrator, differentiator and fractional $PI^\lambda D^\mu$ controller. *IEE Proceedings-Control Theory and Applications*, *153*, 714–720.
24. Cheever, E., and Li, Y. (1998). A tool for construction of bode diagrams from piecewise linear asymptotic approximations. *International Journal of Engineering Education*, .

25. Chen, Y. (2006). Ubiquitous fractional order controls. In *Proceedings of the 2nd IFAC Workshop on Fractional Differentiation and Its Applications*. volume 2.
26. Chen, Y., Dou, H., Vinagre, B. M., and Monje, C. A. (2006). A robust tuning method for fractional order PI controllers. In *The Second IFAC Symposium on Fractional Derivatives and Applications, Porto, Portugal*.
27. Chen, Y., Hu, C., and Moore, K. L. (2003). Relay feedback tuning of robust PID controllers with iso-damping property. In *Decision and Control, 2003. Proceedings. 42nd IEEE Conference on* (pp. 2180–2185). IEEE volume 3.
28. Chen, Y., and Vinagre, B. M. (2010). *Fractional-order systems and controls: fundamentals and applications*. Springer.
29. Chen, Y. Q., and Moore, K. L. (2002). Discretization schemes for fractional-order differentiators and integrators. *Circuits and Systems I: Fundamental Theory and Applications, IEEE Transactions on*, 49, 363–367.
30. Chen, Y. Q., Petras, I., and Xue, D. (2009). Fractional order control-a tutorial. In *American Control Conference, 2009. ACC'09*. (pp. 1397–1411). IEEE.
31. Das, S. (2011). *Functional fractional calculus*. Springer.
32. Diethelm, K. (1997). An algorithm for the numerical solution of differential equations of fractional order. *Electronic transactions on numerical analysis*, 5, 1–6.
33. DiStefano, J. J., Stubberud, A. R., and Williams, I. J. (1967). *Theory and problems of feedback and control systems*. McGraw-Hill New York, St. Louis, San Francisco, Toronto, Sydney.
34. Dorf, R. C., and Bishop, R. H. (2011). *Modern control systems*. Pearson.
35. Duarte, F. B., and Machado, J. T. (2009a). Describing function of two masses with backlash. *Nonlinear Dynamics*, 56, 409–413.
36. Duarte, F. B., and Machado, J. T. (2009b). Fractional describing function of systems with coulomb friction. *Nonlinear dynamics*, 56, 381–387.
37. Duarte, F. B., and Machado, J. T. (2009c). Fractional describing function of systems with nonlinear friction. In *Intelligent Engineering Systems and Computational Cybernetics* (pp. 257–266). Springer.

38. Engheia, N. (1997). On the role of fractional calculus in electromagnetic theory. *Antennas and Propagation Magazine, IEEE*, 39, 35–46.
39. Engheta, N. (1996). On fractional calculus and fractional multipoles in electromagnetism. *Antennas and Propagation, IEEE Transactions on*, 44, 554–566.
40. Gajdošík, D., and Žáková, K. (2011). Bode plots in maxima computer algebra system. In *Proceedings of the 18th International Conference on Process Control* (pp. 352–355).
41. Gopal, M. (2012). *Digital Cont & State Var Met*. Tata McGraw-Hill Education.
42. Gorenflo, R., and Mainardi, F. (1997). *Fractional calculus*. Springer.
43. Heleschewitz, D., and Matignon, D. (1998). Diffusive realisations of fractional integrodifferential operators: structural analysis under approximation, .
44. Herrmann, R. (2011). *Fractional calculus: An introduction for physicists*. World Scientific.
45. Hilfer, R., Butzer, P., Westphal, U., Douglas, J., Schneider, W., Zaslavsky, G., Nonnemacher, T., Blumen, A., and West, B. (2000). *Applications of fractional calculus in physics* volume 5. World Scientific.
46. Jesus, I. S., and Machado, J. T. (2009). Development of fractional order capacitors based on electrolyte processes. *Nonlinear Dynamics*, 56, 45–55.
47. Kesarkar, A. A., and Narayanasamy, S. (2014). Investigation on superior performance by fractional controller for cart-servo laboratory set-up. *Advances in Electrical and Electronic Engineering*, 12, 201–209.
48. Khalil, H. K., and Grizzle, J. (2002). *Nonlinear systems* volume 3. Prentice hall Upper Saddle River.
49. Kilbas, A. A. A., Srivastava, H. M., and Trujillo, J. J. (2006). *Theory and applications of fractional differential equations* volume 204. Elsevier Science Limited.
50. Kiryakova, V. S. (1993). *Generalized fractional calculus and applications*. CRC Press.
51. Koeller, R. (1984). Applications of fractional calculus to the theory of viscoelasticity. *Journal of Applied Mechanics*, 51, 299–307.

52. Kuo, B. C. (1981). *Automatic control systems*. Prentice Hall PTR.
53. Li, H., and Chen, Y. Q. (2008). A fractional order proportional and derivative (FOPD) controller tuning algorithm. In *Control and Decision Conference, 2008. CCDC 2008. Chinese* (pp. 4059–4063). IEEE.
54. Li, H., Luo, Y., and Chen, Y. Q. (2010). A fractional order proportional and derivative (FOPD) motion controller: tuning rule and experiments. *Control Systems Technology, IEEE Transactions on*, 18, 516–520.
55. Loverro, A. (2004). Fractional calculus: history, definitions and applications for the engineer. *Report, Department of Aerospace and Mechanical Engineering, Notre Dame, IN*, 46556.
56. Luo, Y., and Chen, Y. (2009a). Fractional order [proportional derivative] controller for a class of fractional order systems. *Automatica*, 45, 2446–2450.
57. Luo, Y., Chen, Y., and Pi, Y. (2011a). Experimental study of fractional order proportional derivative controller synthesis for fractional order systems. *Mechatronics*, 21, 204–214.
58. Luo, Y., Chen, Y., and Pi, Y. (2011b). Fractional order ultra low-speed position servo: Improved performance via describing function analysis. *ISA transactions*, 50, 53–60.
59. Luo, Y., and Chen, Y. Q. (2009b). Fractional-order [proportional derivative] controller for robust motion control: Tuning procedure and validation. In *American Control Conference, 2009. ACC'09*. (pp. 1412–1417). IEEE.
60. Luo, Y., Chen, Y. Q., Wang, C. Y., and Pi, Y. G. (2010). Tuning fractional order proportional integral controllers for fractional order systems. *Journal of Process Control*, 20, 823–831.
61. Ma, C., and Hori, Y. (2003). Backlash vibration suppression control of torsional system by novel fractional order PID^k controller. *IEEJ Trans.* XX, 123.
62. Ma, C., and Hori, Y. (2004a). The application backlash of fractional order control to vibration suppression. In *American Control Conference, 2004. Proceedings of the 2004* (pp. 2901–2906). IEEE volume 3.

63. Ma, C., and Hori, Y. (2004b). Backlash vibration suppression in torsional system based on the fractional order Q-filter of disturbance observer. In *Advanced Motion Control, 2004. AMC'04. The 8th IEEE International Workshop on* (pp. 577–582). IEEE.
64. Machado, J. T., Kiryakova, V., and Mainardi, F. (2011). Recent history of fractional calculus. *Communications in Nonlinear Science and Numerical Simulation*, 16, 1140–1153.
65. Magin, R. L. (2006). *Fractional calculus in bioengineering*. Begell House Redding.
66. Magin, R. L. (2010). Fractional calculus models of complex dynamics in biological tissues. *Computers & Mathematics with Applications*, 59, 1586–1593.
67. Mainardi, F. (1997). *Fractals and fractional calculus in continuum mechanics*. 378. Springer Verlag.
68. Mainardi, F. (2010). *Fractional calculus and waves in linear viscoelasticity: an introduction to mathematical models*. World Scientific.
69. Manabe, S. (1963). The system design by the use of a model consisting of a saturation and non-integer integrals. *ETJ of Japan*, 8, 147–150.
70. Manabe, S. (2003). Early development of fractional order control. In *ASME 2003 International Design Engineering Technical Conferences and Computers and Information in Engineering Conference* (pp. 609–616). American Society of Mechanical Engineers.
71. Manabe, S. (2004). Design of fractional order control system under strong influence of saturation. In *First IFAC Workshop on Fractional Differentiation and its Applications (FDA'04)(Bordeaux, France)* (pp. 676–681).
72. Manual (33-927S). *Precision Modular Servo Control Experiments*. Feedback Instruments Ltd., UK.
73. Matignon, D. (1998). Generalized fractional differential and difference equations: stability properties and modelling issues. In *Proceedings of the Mathematical Theory of Networks and Systems symposium (MTNS'98), Padova, Italy* (pp. 503–506).
74. MATLAB (2010). *version 7.10.0 (R2010a)*. Natick, Massachusetts: The MathWorks Inc.

75. Matsuda, K., and Fujii, H. (1993). H (infinity) optimized wave-absorbing control-analytical and experimental results. *Journal of Guidance, Control, and Dynamics*, 16, 1146–1153.
76. Micharet, C. A. M. (2006). *Design methods of fractional order controllers for industrial applications*.
77. Miller, K. S., and Ross, B. (1993). *An introduction to the fractional calculus and fractional differential equations*. John Wiley & Sons.
78. Monje, C., Vinagre, B., Chen, Y., Feliu, V., Lanusse, P., and Sabatier, J. (2004a). Proposals for fractional $PI^\lambda D^\mu$ tuning. In *Proceedings of The First IFAC Symposium on Fractional Differentiation and its Applications (FDA04)* (pp. 115–120).
79. Monje, C. A., Calderón, A. J., Vinagre, B. M., and Feliu, V. (2004b). The fractional order lead compensator. In *Computational Cybernetics, 2004. ICC 2004. Second IEEE International Conference on* (pp. 347–352). IEEE.
80. Monje, C. A., Chen, Y., Vinagre, B. M., Xue, D., and Feliu-Batlle, V. (2010). *Fractional-order systems and controls: fundamentals and applications*. Springer.
81. Monje, C. A., Vinagre, B. M., Chen, Y., Feliu, V., Lanusse, P., and Sabatier, J. (2005). Optimal tunings for fractional $PI^\lambda D^\mu$. *Fractional Derivatives and Their Applications*, Le Mehauté, A., Tenreiro Machado, JA, Trigeassou, JC, Sabatier, J.(eds.) UBooks, Augsburg, 3, 675–686.
82. Monje, C. A., Vinagre, B. M., Feliu, V., and Chen, Y. (2008). Tuning and auto-tuning of fractional order controllers for industry applications. *Control Engineering Practice*, 16, 798–812.
83. Nagrath, I., and Gopal, M. (1982). *Control systems engineering*.
84. Nataraj, P., and Kalla, R. (2009). Computation of limit cycles for uncertain nonlinear fractional-order systems. *Physica Scripta*, 2009, 014021.
85. Ogata, K., and Yang, Y. (1970). *Modern control engineering*, .
86. Oldham, K. B. (2010). Fractional differential equations in electrochemistry. *Advances in Engineering Software*, 41, 9–12.

87. Oldham, K. B., and Spanier, J. (1974). *The fractional calculus: theory and applications of differentiation and integration to arbitrary order* volume 111. Academic press New York.
88. Oliveira, N., Kienitz, K., and Misawa, E. (2003). An algebraic approach to the design of robust limit cycle controllers. In *American Control Conference, 2003. Proceedings of the 2003* (pp. 2419–2423). IEEE volume 3.
89. Oliveira, N., Kienitz, K., and Misawa, E. (2006). A describing function approach to limit cycle controller design. In *American Control Conference, 2006* (pp. 1511–1516). IEEE.
90. Oliveira, N., Kienitz, K., and Misawa, E. (2012). A describing function approach to the design of robust limit-cycle controllers. *Nonlinear Dynamics*, 67, 357–363.
91. de Oliveira Valério, D. P. M. (2005). *Fractional Robust System Control*. Ph.D. thesis Universidade Técnica de Lisboa.
92. Olsson, H. (1995). Describing function analysis of a system with friction. In *Control Applications, 1995., Proceedings of the 4th IEEE Conference on* (pp. 310–315). IEEE.
93. Ortigueira, M. D. (2011). *Fractional calculus for scientists and engineers* volume 84. Springer.
94. Ortigueira, M. D., and Machado, J. (2006). Fractional calculus applications in signals and systems. *Signal Processing*, 86, 2503–2504.
95. Oustaloup, A., Levron, F., Mathieu, B., and Nanot, F. M. (2000). Frequency-band complex noninteger differentiator: characterization and synthesis. *Circuits and Systems I: Fundamental Theory and Applications, IEEE Transactions on*, 47, 25–39.
96. Padula, F., and Visioli, A. (2011). Tuning rules for optimal PID and fractional-order PID controllers. *Journal of Process Control*, 21, 69–81.
97. Petráš, I. (2008). A note on the fractional-order chua's system. *Chaos, Solitons & Fractals*, 38, 140–147.
98. Petras, I. (2011). *Fractional-order nonlinear systems: modeling, analysis and simulation*. Springer.

99. Petráš, I., Chen, Y., and Vinagre, B. M. (2002a). A robust stability test procedure for a class of uncertain LTI fractional order systems. In *Proc. of ICC2002, May* (pp. 27–30).
100. Petráš, I., Vinagre, B. M., Dorčák, L., and Feliu, V. (2002b). Fractional digital control of a heat solid: Experimental results. In *International Carpathian Control Conference, Malenovice* (pp. 365–370).
101. Podlubny, I. (1999a). *Fractional Differential Equations. An Introduction to Fractional Derivatives, Fractional Differential Equations, Some Methods of Their Solution and Some of Their Applications*. Academic Press, San Diego - New York - London.
102. Podlubny, I. (1999b). Fractional-order systems and $PI^\lambda D^\mu$ -controllers. *Automatic Control, IEEE Transactions on*, 44, 208–214.
103. Podlubny, I., Petráš, I., Vinagre, B. M., O’leary, P., and Dorčák, L. (2002). Analogue realizations of fractional-order controllers. *Nonlinear dynamics*, 29, 281–296.
104. Ross, B. (1975). A brief history and exposition of the fundamental theory of fractional calculus. In *Fractional calculus and its applications* (pp. 1–36). Springer.
105. Ross, B. (1977). Fractional calculus: An historical apologia for the development of a calculus using differentiation and antidifferentiation of noninteger orders. *Mathematics Magazine*, 50, 115–122.
106. Roy, S. (1967). On the realization of a constant-argument immittance or fractional operator. *Circuit Theory, IEEE Transactions on*, 14, 264–274.
107. Sabatier, J., Agrawal, O. P., and Machado, J. T. (2007). *Advances in fractional calculus*. Springer.
108. Samko, S. G., Kilbas, A. A., and Marichev, O. I. (1993). Fractional integrals and derivatives. *Theory and Applications, Gordon and Breach, Yverdon, 1993*.
109. Schiessel, H., Friedrich, C., and Blumen, A. (2000). Applications to problems in polymer physics and rheology. *Applications of fractional calculus in physics*, 376.
110. Slotine, J.-J. E., Li, W. et al. (1991). *Applied nonlinear control* volume 199. Prentice-Hall Englewood Cliffs, NJ.

111. Sridhar, R. (1960). A general method for deriving the describing functions for a certain class of nonlinearities. *Automatic Control, IRE Transactions on*, 5, 135–141.
112. Tarasov, V. E. (2011). *Fractional Dynamics: Applications of Fractional Calculus to Dynamics of Particles, Fields and Media*. Springer.
113. TATOM, F. B. (1995). The relationship between fractional calculus and fractals. *Fractals*, 3, 217–229.
114. Tavazoei, M. S. (2012). From traditional to fractional PI control: a key for generalization. *Industrial Electronics Magazine, IEEE*, 6, 41–51.
115. Tenreiro Machado, J. (2013). Fractional order modelling of dynamic backlash. *Mechanics*, 23, 741–745.
116. Tenreiro Machado, J. (2014). Fractional order describing functions. *Signal Processing, Elsevier (article in press)*, .
117. Torvik, P. J., and Bagley, R. L. (1984). On the appearance of the fractional derivative in the behavior of real materials. *Journal of Applied Mechanics*, 51, 294–298.
118. TSypkin, I. Z. (1984). *Relay control systems*. CUP Archive.
119. Tsytkin, Y. (1955). *Teoriya relejnykh sistem avtomaticheskovo regulirovaniya*,. Gostekhizdat, Moscow.
120. Valério, D., and da Costa, J. S. (2004). Ninteger: a non-integer control toolbox for matlab. In *Proceedings of the First IFAC Workshop on Fractional Differentiation and Applications, Bordeaux, France* (pp. 208–213).
121. Valério, D., and Da Costa, J. S. (2006). Tuning-rules for fractional PID controllers. In *Proceedings of the Second IFAC Symposium on Fractional Differentiation and Its Applications (FDA06)*.
122. Valerio, D., and Da Costa, J. S. (2013). *An introduction to fractional control* volume 91. IET.
123. Vander Velde, W. E. (1968). *Multiple-input describing functions and nonlinear system design*. New York: McGraw-Hill.

124. Vinagre, B., Podlubny, I., Hernandez, A., and Feliu, V. (2000). Some approximations of fractional order operators used in control theory and applications. *Fractional calculus and applied analysis*, 3, 231–248.
125. Vinagre, B. M., and Chen, Y. (2002). Fractional calculus applications in automatic control and robotics. In *IEEE Proc. on Conference on Decision and Control*.
126. Vinagre, B. M., Monje, C., and Calderon, A. (2002). Fractional order systems and fractional order control actions. In *IEEE Conference on Decision and Control* (pp. 2550–2554).
127. Vinagre, B. M., Monje, C. A., Calderón, A. J., and Suárez, J. I. (2007). Fractional PID controllers for industry application. a brief introduction. *Journal of Vibration and Control*, 13, 1419–1429.
128. Wallén, A., ÅRström, K., and Hägglun, T. (2002). Loop-shaping design of PID controllers with constant T_i/T_d ratio. *Asian Journal of Control*, 4, 403–409.
129. Wang, C., Luo, Y., and Chen, Y. Q. (2009a). An analytical design of fractional order proportional integral and [proportional integral] controllers for robust velocity servo. In *Industrial Electronics and Applications, 2009. ICIEA 2009. 4th IEEE Conference on* (pp. 3448–3453). IEEE.
130. Wang, C., Luo, Y., and Chen, Y. Q. (2009b). Fractional order proportional integral (FOPI) and [proportional integral] (FO[PI]) controller designs for first order plus time delay (FOPTD) systems. In *Control and Decision Conference, 2009. CCDC'09. Chinese* (pp. 329–334). IEEE.
131. Xue, D., Chen, Y., and Atherton, D. P. (2007). *Linear feedback control: analysis and design with MATLAB* volume 14. Siam.
132. Xue, D., Zhao, C., and Chen, Y. (2006a). Fractional order PID control of a DC-motor with elastic shaft: a case study. In *Proceedings of American control conference* (pp. 3182–3187). volume 7.
133. Xue, D., Zhao, C., and Chen, Y. Q. (2006b). A modified approximation method of fractional order system. In *Mechatronics and Automation, Proceedings of the 2006 IEEE International Conference on* (pp. 1043–1048). IEEE.

134. Yeroglu, C., and Tan, N. (2010). Limit cycle prediction for fractional order systems with static nonlinearities. In *Periodic Control Systems* (pp. 144–149). volume 4.
135. Yeroglu, C., and Tan, N. (2011). Note on fractional-order proportional–integral–differential controller design. *IET control theory & applications*, 5, 1978–1989.
136. Zhao, C., Xue, D., and Chen, Y. Q. (2005). A fractional order PID tuning algorithm for a class of fractional order plants. In *Mechatronics and Automation, 2005 IEEE International Conference* (pp. 216–221). IEEE volume 1.

APPENDIX A

Some Important Properties in Fractional Calculus

A.1 Stability of Fractional-Order Linear Time-Invariant Systems

For the stability of class of fractional-order LTI systems having commensurate order $q \in (0, 1]$, the following theorem must be satisfied:

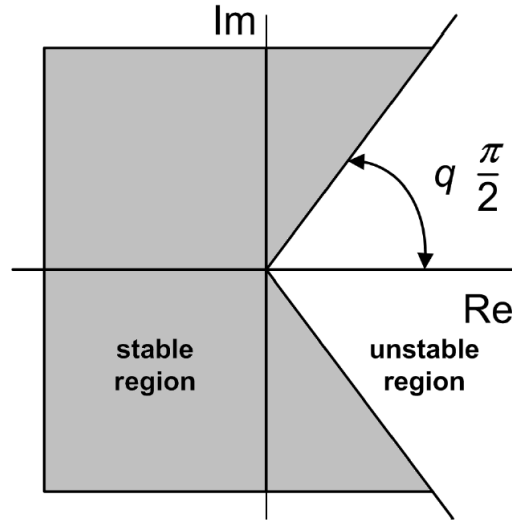


Figure A.1: Pictorial Representation of Matignon's Stability

Matignon's stability theorem [Matignon (1998)]: *The fractional-order TF $G(s) = \frac{Z(s)}{P(s)}$ is stable if and only if the following condition is satisfied in s -plane (Pictorial representation has been shown in Figure A.1):*

$$|\angle(\sigma_i)| > q \frac{\pi}{2}, \forall \sigma_i \in \mathbb{C}, P(\sigma_i) = 0 \quad (\text{A.1})$$

Where, $\sigma := s^q$

For integer-order LTI systems, $q = 1$. Therefore, (A.1) becomes $|\angle(\sigma_i)| > \frac{\pi}{2}$, which means that all the roots of the characteristic polynomial must be located on the left half of the complex plane.

A.2 Analytical Solution of Fractional-Order Differential Equations

In the solution of integer-order calculus equations, the exponential function e^z plays an important role. In case of fractional-order calculus equations, exponential function is replaced by the Mittag-Leffler function. The two-parameter Mittag-Leffler function is defined as follows [Bateman and Erdelyi (1955)]:

$$E_{\alpha,\beta}(z) = \sum_{k=0}^{\infty} \frac{z^k}{\Gamma(\alpha k + \beta)}; \quad (\alpha > 0, \beta > 0) \quad (\text{A.2})$$

For $\beta = 1$, (A.2) results into the following one-parameter Mittag-Leffler function:

$$E_{\alpha}(z) := E_{\alpha,1}(z) = \sum_{k=0}^{\infty} \frac{z^k}{\Gamma(\alpha k + 1)} \quad (\text{A.3})$$

It can be followed from (A.2) that:

$$E_{1,1}(z) = e^z, E_{2,1}(z) = \cosh(\sqrt{z}), E_{1,2}(z) = \frac{e^z - 1}{z}, E_{2,2}(z) = \frac{\sinh(\sqrt{z})}{\sqrt{z}}, \text{ etc.} \quad (\text{A.4})$$

The following Laplace transform identity holds true [Das (2011)]:

$$\mathcal{L}\{t^{\alpha k + \beta - 1} E_{\alpha,\beta}^{(k)}(at^{\alpha})\} = \frac{s^{\alpha - \beta} k!}{(s^{\alpha} - a)^{k+1}} \quad (\text{A.5})$$

where,

$$E_{\alpha,\beta}^{(k)} = \frac{d^{(k)}}{dt^{(k)}} E_{\alpha,\beta}$$

The property (A.5) is useful while obtaining the analytical solution of fractional-order differential equation using Laplace transform method. The following example is considered for demonstration:

Example 2 Find solution of:

$$D_{RL}^{\frac{1}{2}} f(t) + a_1 f(t) = 0 \quad (\text{A.6})$$

given that, $D_{RL}^{-\frac{1}{2}}f(0) = C$.

Solution: On taking the Laplace transform of (A.6) using (2.27), we get,

$$s^{\frac{1}{2}}F(s) - D_{RL}^{-\frac{1}{2}}f(0) + a_1F(s) = 0$$

Therefore,

$$F(s) = \frac{C}{s^{\frac{1}{2}} + a_1} \quad (\text{A.7})$$

On taking inverse Laplace transform of (A.7) using (A.5), we get,

$$f(t) = Ct^{-\frac{1}{2}}E_{\frac{1}{2}, \frac{1}{2}}(-a_1\sqrt{t})$$

APPENDIX B

Derivations of Unified Tuning Expressions for $[PI]^\alpha$ and $[PD]^\beta$ Controllers

B.1 $[PI]^\alpha$ Controller

The universal plant structure as given in (3.4) is:

$$G(s) = K \frac{\sum_{i=0}^m (a_i s^{\alpha_i})}{\sum_{k=0}^n (b_k s^{\beta_k})} e^{-Ls}$$

The $[PI]^\alpha$ controller has following structure as given in (2.43):

$$C(s) = K_p \left(1 + \frac{K_i}{s} \right)^\alpha$$

Therefore,

$$\begin{aligned} [G(s)C(s)]_{s=j\omega} &= K \frac{\sum_{i=0}^m (a_i (j\omega)^{\alpha_i})}{\sum_{k=0}^n (b_k (j\omega)^{\beta_k})} e^{-L(j\omega)} K_p \left(1 + \frac{K_i}{j\omega} \right)^\alpha \\ &= K \frac{\sum_{i=0}^m (a_i \omega^{\alpha_i} j^{\alpha_i})}{\sum_{k=0}^n (b_k \omega^{\beta_k} j^{\beta_k})} e^{-L(j\omega)} K_p \left(1 - j \frac{K_i}{\omega} \right)^\alpha \\ &= K \frac{\sum_{i=0}^m (a_i \omega^{\alpha_i} e^{j\frac{\pi}{2}\alpha_i})}{\sum_{k=0}^n (b_k \omega^{\beta_k} e^{j\frac{\pi}{2}\beta_k})} e^{-L(j\omega)} K_p \left(1 - j \frac{K_i}{\omega} \right)^\alpha \\ &= K \frac{\sum_{i=0}^m (a_i \omega^{\alpha_i} (\cos(\frac{\pi}{2}\alpha_i) + j \sin(\frac{\pi}{2}\alpha_i)))}{\sum_{k=0}^n (b_k \omega^{\beta_k} (\cos(\frac{\pi}{2}\beta_k) + j \sin(\frac{\pi}{2}\beta_k)))} e^{-L(j\omega)} K_p \left(\sqrt{1 + \left(\frac{K_i}{\omega} \right)^2} e^{j \tan^{-1} \left(-\frac{K_i}{\omega} \right)} \right)^\alpha \end{aligned}$$

Therefore,

$$[G(s)C(s)]_{s=j\omega_{gc}} = K \frac{p_1 + jq_1}{p_2 + jq_2} e^{-L(j\omega_{gc})} K_p \left(\sqrt{1 + \left(\frac{K_i}{\omega_{gc}}\right)^2} e^{j \tan^{-1}\left(-\frac{K_i}{\omega_{gc}}\right)} \right)^\alpha$$

where,

$$p_1 = \sum_{i=0}^m \left(a_i \omega_{gc}^{\alpha_i} \cos\left(\frac{\pi}{2} \alpha_i\right) \right), q_1 = \sum_{i=0}^m \left(a_i \omega_{gc}^{\alpha_i} \sin\left(\frac{\pi}{2} \alpha_i\right) \right)$$

$$p_2 = \sum_{k=0}^n \left(b_k \omega_{gc}^{\beta_k} \cos\left(\frac{\pi}{2} \beta_k\right) \right), q_2 = \sum_{k=0}^n \left(b_k \omega_{gc}^{\beta_k} \sin\left(\frac{\pi}{2} \beta_k\right) \right)$$

Recalling gain crossover frequency specification (3.1):

$$|C(j\omega_{gc})G(j\omega_{gc})| = 1$$

$$\therefore K \frac{\sqrt{p_1^2 + q_1^2}}{\sqrt{p_2^2 + q_2^2}} K_p \left(\sqrt{1 + \left(\frac{K_i}{\omega_{gc}}\right)^2} \right)^\alpha = 1$$

$$\therefore K_p = \frac{1}{K} \sqrt{\frac{(p_2^2 + q_2^2)}{(p_1^2 + q_1^2) \left(1 + \left(\frac{K_i}{\omega_{gc}}\right)^2\right)^\alpha}} \quad (\text{B.1})$$

Recalling phase margin specification (3.2):

$$\angle[C(j\omega_{gc})G(j\omega_{gc})] = -\pi + \phi_m$$

Therefore,

$$\tan^{-1}\left(\frac{q_1}{p_1}\right) - \tan^{-1}\left(\frac{q_2}{p_2}\right) - L\omega_{gc} + \alpha \tan^{-1}\left(-\frac{K_i}{\omega_{gc}}\right) = -\pi + \phi_m$$

Hence,

$$K_i = -\omega_{gc} \tan \left(\frac{-\tan^{-1} \left(\frac{q_1}{p_1} \right) + \tan^{-1} \left(\frac{q_2}{p_2} \right) + L\omega_{gc} - \pi + \phi_m}{\alpha} \right) \quad (\text{B.2})$$

Recalling the isodamping condition (3.3):

$$\left(\frac{d(\angle[C(j\omega)G(j\omega)])}{d\omega} \right)_{\omega=\omega_{gc}} = 0$$

Therefore,

$$\begin{aligned} & \frac{p_1 \left(\sum_{i=0}^m (a_i \alpha_i \omega_{gc}^{\alpha_i-1} \sin \left(\frac{\pi}{2} \alpha_i \right)) \right) - q_1 \left(\sum_{i=0}^m (a_i \alpha_i \omega_{gc}^{\alpha_i-1} \cos \left(\frac{\pi}{2} \alpha_i \right)) \right)}{p_1^2 + q_1^2} \\ & - \frac{p_2 \left(\sum_{k=0}^n (b_k \beta_k \omega_{gc}^{\beta_k-1} \sin \left(\frac{\pi}{2} \beta_k \right)) \right) - q_2 \left(\sum_{k=0}^n (b_k \beta_k \omega_{gc}^{\beta_k-1} \cos \left(\frac{\pi}{2} \beta_k \right)) \right)}{p_2^2 + q_2^2} \\ & - L + \alpha \frac{\frac{K_i}{\omega_{gc}^2}}{1 + \left(-\frac{K_i}{\omega_{gc}} \right)^2} = 0 \end{aligned}$$

Let,

$$\begin{aligned} N = & \frac{-p_1 \left(\sum_{i=0}^m (a_i \alpha_i \omega_{gc}^{\alpha_i-1} \sin \left(\frac{\pi}{2} \alpha_i \right)) \right) + q_1 \left(\sum_{i=0}^m (a_i \alpha_i \omega_{gc}^{\alpha_i-1} \cos \left(\frac{\pi}{2} \alpha_i \right)) \right)}{p_1^2 + q_1^2} \\ & + L + \frac{p_2 \left(\sum_{k=0}^n (b_k \beta_k \omega_{gc}^{\beta_k-1} \sin \left(\frac{\pi}{2} \beta_k \right)) \right) - q_2 \left(\sum_{k=0}^n (b_k \beta_k \omega_{gc}^{\beta_k-1} \cos \left(\frac{\pi}{2} \beta_k \right)) \right)}{p_2^2 + q_2^2} \end{aligned}$$

Therefore,

$$-N + \frac{\alpha K_i}{\omega_{gc}^2 + K_i^2} = 0$$

Therefore,

$$K_i = \frac{\alpha \pm \sqrt{\alpha^2 - 4N^2\omega_{gc}^2}}{2N} \quad (\text{B.3})$$

On solving (B.1), (B.2), and (B.3) simultaneously, one can obtain the parameters of (2.43).

B.2 $[PD]^\beta$ Controller

The universal plant structure as given in (3.4) is:

$$G(s) = K \frac{\sum_{i=0}^m (a_i s^{\alpha_i})}{\sum_{k=0}^n (b_k s^{\beta_k})} e^{-Ls}$$

The $[PD]^\beta$ controller has following structure as given in (2.45):

$$C(s) = K_p (1 + K_d s)^\beta$$

Therefore,

$$\begin{aligned} [G(s)C(s)]_{s=j\omega} &= K \frac{\sum_{i=0}^m (a_i (j\omega)^{\alpha_i})}{\sum_{k=0}^n (b_k (j\omega)^{\beta_k})} e^{-L(j\omega)} K_p (1 + K_d (j\omega))^\beta \\ &= K \frac{\sum_{i=0}^m (a_i \omega^{\alpha_i} j^{\alpha_i})}{\sum_{k=0}^n (b_k \omega^{\beta_k} j^{\beta_k})} e^{-L(j\omega)} K_p (1 + K_d (j\omega))^\beta \\ &= K \frac{\sum_{i=0}^m (a_i \omega^{\alpha_i} e^{j\frac{\pi}{2}\alpha_i})}{\sum_{k=0}^n (b_k \omega^{\beta_k} e^{j\frac{\pi}{2}\beta_k})} e^{-L(j\omega)} K_p (1 + K_d (j\omega))^\beta \\ &= K \frac{\sum_{i=0}^m (a_i \omega^{\alpha_i} (\cos(\frac{\pi}{2}\alpha_i) + j\sin(\frac{\pi}{2}\alpha_i)))}{\sum_{k=0}^n (b_k \omega^{\beta_k} (\cos(\frac{\pi}{2}\beta_k) + j\sin(\frac{\pi}{2}\beta_k)))} e^{-L(j\omega)} K_p (1 + K_d (j\omega))^\beta \end{aligned}$$

Therefore,

$$[G(s)C(s)]_{s=j\omega_{gc}} = K \frac{p_1 + jq_1}{p_2 + jq_2} e^{-L(j\omega_{gc})} K_p (1 + K_d(j\omega_{gc}))^\beta$$

where,

$$p_1 = \sum_{i=0}^m \left(a_i \omega_{gc}^{\alpha_i} \cos \left(\frac{\pi}{2} \alpha_i \right) \right), \quad q_1 = \sum_{i=0}^m \left(a_i \omega_{gc}^{\alpha_i} \sin \left(\frac{\pi}{2} \alpha_i \right) \right)$$

$$p_2 = \sum_{k=0}^n \left(b_k \omega_{gc}^{\beta_k} \cos \left(\frac{\pi}{2} \beta_k \right) \right), \quad q_2 = \sum_{k=0}^n \left(b_k \omega_{gc}^{\beta_k} \sin \left(\frac{\pi}{2} \beta_k \right) \right)$$

Therefore,

$$G(j\omega_{gc})C(j\omega_{gc}) = K \frac{p_1 + jq_1}{p_2 + jq_2} e^{-L(j\omega_{gc})} K_p \left(\sqrt{1 + (K_d \omega_{gc})^2} e^{j \tan^{-1}(K_d \omega_{gc})} \right)^\beta$$

Recalling gain crossover frequency specification (3.1):

$$|C(j\omega_{gc})G(j\omega_{gc})| = 1$$

Therefore,

$$K \frac{\sqrt{p_1^2 + q_1^2}}{\sqrt{p_2^2 + q_2^2}} K_p \left(\sqrt{1 + (K_d \omega_{gc})^2} \right)^\beta = 1$$

Therefore,

$$K_p = \frac{1}{K} \sqrt{\frac{(p_2^2 + q_2^2)}{(p_1^2 + q_1^2) (1 + (K_d \omega_{gc})^2)^\beta}} \quad (\text{B.4})$$

Recalling phase margin specification (3.2):

$$\angle [C(j\omega_{gc})G(j\omega_{gc})] = -\pi + \phi_m$$

Therefore,

$$\tan^{-1}\left(\frac{q_1}{p_1}\right) - \tan^{-1}\left(\frac{q_2}{p_2}\right) - L\omega_{gc} + \beta \tan^{-1}(K_d\omega_{gc}) = -\pi + \phi_m$$

Therefore,

$$K_d = \frac{\tan\left(\frac{-\tan^{-1}\left(\frac{q_1}{p_1}\right) + \tan^{-1}\left(\frac{q_2}{p_2}\right) + L\omega_{gc} - \pi + \phi_m}{\beta}\right)}{\omega_{gc}} \quad (\text{B.5})$$

Recalling the isodamping condition (3.3):

$$\left(\frac{d(\angle[C(j\omega)G(j\omega)])}{d\omega}\right)_{\omega=\omega_{gc}} = 0$$

Therefore,

$$\begin{aligned} & \frac{p_1 \left(\sum_{i=0}^m (a_i \alpha_i \omega_{gc}^{\alpha_i-1} \sin(\frac{\pi}{2} \alpha_i)) \right) - q_1 \left(\sum_{i=0}^m (a_i \alpha_i \omega_{gc}^{\alpha_i-1} \cos(\frac{\pi}{2} \alpha_i)) \right)}{p_1^2 + q_1^2} \\ & - \frac{p_2 \left(\sum_{k=0}^n (b_k \beta_k \omega_{gc}^{\beta_k-1} \sin(\frac{\pi}{2} \beta_k)) \right) - q_2 \left(\sum_{k=0}^n (b_k \beta_k \omega_{gc}^{\beta_k-1} \cos(\frac{\pi}{2} \beta_k)) \right)}{p_2^2 + q_2^2} \\ & -L + \frac{\beta K_d}{1 + (\omega_{gc} K_d)^2} = 0 \end{aligned}$$

Let,

$$\begin{aligned} N = & \frac{-p_1 \left(\sum_{i=0}^m (a_i \alpha_i \omega_{gc}^{\alpha_i-1} \sin(\frac{\pi}{2} \alpha_i)) \right) + q_1 \left(\sum_{i=0}^m (a_i \alpha_i \omega_{gc}^{\alpha_i-1} \cos(\frac{\pi}{2} \alpha_i)) \right)}{p_1^2 + q_1^2} \\ & +L + \frac{p_2 \left(\sum_{k=0}^n (b_k \beta_k \omega_{gc}^{\beta_k-1} \sin(\frac{\pi}{2} \beta_k)) \right) - q_2 \left(\sum_{k=0}^n (b_k \beta_k \omega_{gc}^{\beta_k-1} \cos(\frac{\pi}{2} \beta_k)) \right)}{p_2^2 + q_2^2} \end{aligned}$$

Therefore,

$$-N + \frac{\beta K_d}{1 + (\omega_{gc} K_d)^2} = 0$$

Therefore,

$$K_d = \frac{\beta \pm \sqrt{\beta^2 - 4N^2\omega_{gc}^2}}{2N\omega_{gc}^2} \quad (\text{B.6})$$

On solving (B.4), (B.5), and (B.6) simultaneously, one can obtain the parameters of (2.45).

APPENDIX C

Unified Tuning Expressions for *PID* Controller

The integer *PID* controller has following Transfer Function (TF):

$$C(s) = K_p \left(1 + \frac{K_i}{s} + K_d s \right) \quad (\text{C.1})$$

The substitution of $G(s)$ (3.4) and $C(s)$ (C.1) expressions in the Wang-et-al specifications (3.1), (3.2), and (3.3) yields following expressions for K_p , K_i and K_d :

$$K_d = \frac{M + N\omega_{gc}(1 + M^2)}{2\omega_{gc}} \quad (\text{C.2})$$

$$K_i = K_d\omega_{gc}^2 - M\omega_{gc} \quad (\text{C.3})$$

$$K_p = \frac{1}{K} \sqrt{\frac{(p_2^2 + q_2^2)}{(p_1^2 + q_1^2) \left(1 + \left(K_d\omega_{gc} - \frac{K_i}{\omega_{gc}} \right)^2 \right)}} \quad (\text{C.4})$$

Where, $M = \tan \left(-\tan^{-1} \left(\frac{q_1}{p_1} \right) + \tan^{-1} \left(\frac{q_2}{p_2} \right) + L\omega_{gc} - \pi + \phi_m \right)$.

$$N = \frac{-p_1 \left(\sum_{i=0}^m (a_i \alpha_i \omega_{gc}^{\alpha_i - 1} \sin \left(\frac{\pi}{2} \alpha_i \right)) \right) + q_1 \left(\sum_{i=0}^m (a_i \alpha_i \omega_{gc}^{\alpha_i - 1} \cos \left(\frac{\pi}{2} \alpha_i \right)) \right)}{p_1^2 + q_1^2} + L$$

$$+ \frac{p_2 \left(\sum_{k=0}^n (b_k \beta_k \omega_{gc}^{\beta_k - 1} \sin \left(\frac{\pi}{2} \beta_k \right)) \right) - q_2 \left(\sum_{k=0}^n (b_k \beta_k \omega_{gc}^{\beta_k - 1} \cos \left(\frac{\pi}{2} \beta_k \right)) \right)}{p_2^2 + q_2^2}$$

and,

$$p_1 = \sum_{i=0}^m \left(a_i \omega_{gc}^{\alpha_i} \cos \left(\frac{\pi}{2} \alpha_i \right) \right), \quad q_1 = \sum_{i=0}^m \left(a_i \omega_{gc}^{\alpha_i} \sin \left(\frac{\pi}{2} \alpha_i \right) \right)$$

$$p_2 = \sum_{k=0}^n \left(b_k \omega_{gc}^{\beta_k} \cos \left(\frac{\pi}{2} \beta_k \right) \right), \quad q_2 = \sum_{k=0}^n \left(b_k \omega_{gc}^{\beta_k} \sin \left(\frac{\pi}{2} \beta_k \right) \right)$$

On solving (C.2), (C.3), and (C.4) simultaneously, one gets the parameters of controller (C.1).

APPENDIX D

Limit Cycle Stability Condition for PI^α and

$$G(s) = \frac{K}{s(s+b)}$$

We have the following Loop Transfer Function (TF):

$$L(s) = G(s)C(s) = \frac{K}{s(s+b)} K_p \left(1 + \frac{K_i}{s^\alpha} \right)$$

On substituting $s = j\omega$,

$$L(j\omega) = \frac{K}{j\omega(j\omega+b)} K_p \left(1 + \frac{K_i}{(j\omega)^\alpha} \right)$$

Imaginary portion of $L(j\omega)$ is obtained as:

$$Im(L(j\omega)) = \frac{KK_p}{\omega^3 + b^2\omega} \left[\frac{K_i}{\omega^{\alpha-1}} \sin\left(\frac{\pi}{2}\alpha\right) - b \left(1 + \frac{K_i}{\omega^\alpha} \cos\left(\frac{\pi}{2}\alpha\right) \right) \right] \quad (D.1)$$

Recalling the Tsytkin's Condition (5.10) for Stability of Limit Cycle:

$$\left[\frac{d}{d\omega} (Im(L(j\omega))) \right]_{\omega=\omega_0} > 0 \quad (D.2)$$

Therefore, from (D.1) and (D.2) we get the following condition for limit cycle stability for PI^α and $G(s) = \frac{K}{s(s+b)}$,

$$\begin{aligned} & [(\omega^3 + b^2\omega) \left(K_i(1-\alpha)\omega^{-\alpha} \sin\left(\frac{\pi}{2}\alpha\right) + bK_i\alpha\omega^{-\alpha} \cos\left(\frac{\pi}{2}\alpha\right) \right) - \\ & \left(\frac{K_i}{\omega^{\alpha-1}} \sin\left(\frac{\pi}{2}\alpha\right) - b \left(1 + \frac{K_i}{\omega^\alpha} \cos\left(\frac{\pi}{2}\alpha\right) \right) \right) (3\omega^2 + b^2)]_{\omega=\omega_0} > 0 \end{aligned}$$

APPENDIX E

Monotonicity Property of Phase Angles

The monotonicity property of phase arguments with respect to ω is discussed here for the basic terms, namely Fractional Zero, Fractional [Zero] and Fractional Double-Term Zero. Since the argument of Fractional-Pole is negative of the argument of Fractional Zero, the results for the monotonicity of Fractional Zero and Fractional Pole are identical. The similar is true for the pairs, (Fractional [Zero], Fractional [Pole]) and (Fractional Double-Term Zero, Fractional Double-Term Pole).

E.1 Fractional Zero

The Transfer Function (TF) of fractional zero is:

$$T(s) = s^\alpha + a$$

where, $0 < \alpha < 1$.

The argument of $T(s)$ for any ω is given by:

$$\angle T(j\omega) = \tan^{-1} \left(\frac{\omega^\alpha \sin \left(\frac{\pi}{2} \alpha \right)}{\omega^\alpha \cos \left(\frac{\pi}{2} \alpha \right) + a} \right)$$

Therefore, for $0 < \omega < \infty$,

$$\angle T(j\omega) = \tan^{-1} \left(\frac{\sin \left(\frac{\pi}{2} \alpha \right)}{\cos \left(\frac{\pi}{2} \alpha \right) + \frac{a}{\omega^\alpha}} \right)$$

Let us assume $Y = \sin \left(\frac{\pi}{2} \alpha \right)$ and $X = \cos \left(\frac{\pi}{2} \alpha \right) + \frac{a}{\omega^\alpha}$. Therefore,

$$\angle T(j\omega) = \tan^{-1} \left(\frac{Y}{X} \right)$$

For $0 < \alpha < 1$, we have $Y = \sin\left(\frac{\pi}{2}\alpha\right) > 0$. Also, $\cos\left(\frac{\pi}{2}\alpha\right) > 0$.

There are following two cases:

1. $a > 0$

- When $\omega = 0$, it is easy to verify that $\angle T(j\omega) = 0$.
- $X = \cos\left(\frac{\pi}{2}\alpha\right) + \frac{a}{\omega^\alpha} > 0$. Therefore, $\angle T(j\omega)$ remains in first quadrant. As ω increases from 0^+ to ∞ , X decreases smoothly for given Y and the argument increases monotonically from 0^+ to $\left(\frac{\pi}{2}\alpha\right)$.

2. $a < 0$

- It can be seen that at $\omega = 0$, $\angle T(j\omega)$ is π .
- For very small values of ω , $X = \cos\left(\frac{\pi}{2}\alpha\right) + \frac{a}{\omega^\alpha} < 0$. Therefore, $\angle T(j\omega)$ remains in second quadrant.
- For $\omega < \omega_1$, where ω_1 is such that $\cos\left(\frac{\pi}{2}\alpha\right) + \frac{a}{\omega_1^\alpha} = 0$, $X < 0$ and increases smoothly as ω increases. Therefore, $\angle T(j\omega)$ decreases monotonically from π to $\frac{\pi}{2}$.
- For $\omega_1 < \omega < \infty$, $X > 0$. So, $\angle T(j\omega)$ is in first quadrant which decreases smoothly from $\frac{\pi}{2}$ to $\left(\frac{\pi}{2}\alpha\right)$ as ω increases further.

Hence, from the above two cases we conclude that $\angle T(j\omega)$ is monotonic with respect to ω when $T(s)$ represents fractional-zero.

E.2 Fractional [Zero]

The TF of fractional [zero] is:

$$T(s) = (s + a)^\alpha$$

where, $0 < \alpha < 1$.

The argument of $T(s)$ for any ω is given by:

$$\angle T(j\omega) = \tan^{-1}\left(\frac{\omega}{a}\right) \alpha$$

We have following two cases to investigate the monotonicity of $\angle T(j\omega)$:

1. $a > 0$

Since $X = a > 0$, the argument $\tan^{-1} \left(\frac{\omega}{a} \right) \alpha$ remains in first quadrant. As ω increases from 0 to ∞ , $\angle T(j\omega)$ also increases smoothly from 0 to $\left(\frac{\pi}{2} \alpha \right)$.

2. $a < 0$

Since $X = a < 0$, the argument $\tan^{-1} \left(\frac{\omega}{a} \right) \alpha$ remains in second quadrant. As ω increases from 0 to ∞ , $\tan^{-1} \left(\frac{\omega}{a} \right) \alpha$ decreases monotonically from $\pi\alpha$ to $\frac{\pi}{2}\alpha$.

Therefore, it is concluded that $\angle T(j\omega)$ is monotonic with respect to ω when $T(s)$ represents fractional [zero].

E.3 Fractional Double-Term Zero

The TF of fractional double-term zero is:

$$T(s) = s^{\alpha+\beta} + a_1 s^\alpha + a_2$$

where, $0 < \alpha < 1, 0 < \beta < 1$.

We get,

$$\angle T(j\omega) = \tan^{-1} \left(\frac{\omega^{\alpha+\beta} \sin \left(\frac{\pi}{2} (\alpha + \beta) \right) + a_1 \omega^\alpha \sin \left(\frac{\pi}{2} \alpha \right)}{\omega^{\alpha+\beta} \cos \left(\frac{\pi}{2} (\alpha + \beta) \right) + a_1 \omega^\alpha \cos \left(\frac{\pi}{2} \alpha \right) + a_2} \right)$$

It is easy to verify that:

- For $a_2 > 0$ (irrespective of sign of a_1):
 - $\angle T(j\omega) = 0$ at $\omega = 0$
 - $\angle T(j\omega) = \frac{\pi}{2} (\alpha + \beta)$ at $\omega \rightarrow \infty$
- For $a_2 < 0$ (irrespective of sign of a_1):

- $\angle T(j\omega) = \pi$ at $\omega = 0$
- $\angle T(j\omega) = \frac{\pi}{2}(\alpha + \beta)$ at $\omega \rightarrow \infty$

Let us assume $Y = \omega^{\alpha+\beta} \sin\left(\frac{\pi}{2}(\alpha + \beta)\right) + a_1 \omega^\alpha \sin\left(\frac{\pi}{2}\alpha\right)$ and $X = \omega^{\alpha+\beta} \cos\left(\frac{\pi}{2}(\alpha + \beta)\right) + a_1 \omega^\alpha \cos\left(\frac{\pi}{2}\alpha\right) + a_2$. Therefore,

$$\angle T(j\omega) = \tan^{-1} \left(\frac{Y}{X} \right)$$

In $\angle T(j\omega)$, both Y and X vary as ω changes. Therefore, a general conclusion about the monotonicity of their ratio $\left(\frac{Y}{X}\right)$ with respect to ω cannot be drawn. Due to this, one cannot guarantee the monotonicity of $\angle T(j\omega)$ with respect to ω .¹ However, when the non-monotonic local variations are small enough for the given numerical case of fractional double-term zero, its asymptotic phase plot turns out to be a sufficiently good approximation.

¹Since, the function $\tan^{-1}(x)$ is monotonic with respect to x .

APPENDIX F

Selection of Critical Frequency

The critical frequency (ω_c) expressions are derived here for Fractional-Zero, Fractional-[Zero], and Fractional Double-Term Zero. Since the argument for Fractional-Pole is negative of Fractional-Zero-argument, both have the same ω_c . The similar is true for the pairs such as, (Fractional-[Zero], Fractional-[Pole]) and (Fractional Double-Term Zero, Fractional Double-Term Pole).

F.1 Fractional-Zero

$$\angle T(j\omega) = \tan^{-1} \left(\frac{\omega^\alpha \sin \left(\frac{\pi}{2} \alpha \right)}{\omega^\alpha \cos \left(\frac{\pi}{2} \alpha \right) + a} \right)$$

In above term, a dominates at lower frequencies, i.e. $(\omega^\alpha \cos \left(\frac{\pi}{2} \alpha \right) + a) \approx a$. Therefore,

$$\angle T(j\omega)_{lower} = \tan^{-1} \left(\frac{\omega^\alpha \sin \left(\frac{\pi}{2} \alpha \right)}{a} \right)$$

Similarly, one can notice that at higher frequencies, the term $\omega^\alpha \cos \left(\frac{\pi}{2} \alpha \right)$ dominates. Therefore, $(\omega^\alpha \cos \left(\frac{\pi}{2} \alpha \right) + a) \approx \omega^\alpha \cos \left(\frac{\pi}{2} \alpha \right)$.

$$\angle T(j\omega)_{higher} = \tan^{-1} \left(\frac{\omega^\alpha \sin \left(\frac{\pi}{2} \alpha \right)}{\omega^\alpha \cos \left(\frac{\pi}{2} \alpha \right)} \right)$$

We select the critical frequency ω_c at which these terms are equal as follows:

$$\begin{aligned} \angle T(j\omega_c)_{lower} &= \angle T(j\omega_c)_{higher} \\ \therefore \tan^{-1} \left(\frac{\omega_c^\alpha \sin \left(\frac{\pi}{2} \alpha \right)}{a} \right) &= \tan^{-1} \left(\frac{\omega_c^\alpha \sin \left(\frac{\pi}{2} \alpha \right)}{\omega_c^\alpha \cos \left(\frac{\pi}{2} \alpha \right)} \right) \end{aligned}$$

Therefore,

$$\omega_c = \left(\frac{a}{\cos\left(\frac{\pi}{2}\alpha\right)} \right)^{\frac{1}{\alpha}}$$

F.2 Fractional-[Zero]

$$\angle T(j\omega) = \tan^{-1}\left(\frac{\omega}{a}\right) \alpha$$

For simplicity, we can write the above expression as follows:

$$\begin{aligned} \angle T(j\omega) &= \tan^{-1}\left(\frac{\omega + a - a}{a}\right) \alpha \\ &= \tan^{-1}\left(\frac{\omega + a}{a} - 1\right) \alpha \end{aligned}$$

In the above term, one can see that the term a dominates at lower frequencies.

Therefore, $\left(\frac{\omega+a}{a} - 1\right) \approx \left(\frac{a}{a} - 1\right)$.

$$\angle T(j\omega)_{lower} = \tan^{-1}(0) \alpha = 0$$

Similarly, at higher frequencies the term ω dominates. Therefore, $\left(\frac{\omega+a}{a} - 1\right) \approx \left(\frac{\omega}{a} - 1\right)$.

$$\angle T(j\omega)_{higher} = \tan^{-1}\left(\frac{\omega}{a} - 1\right) \alpha$$

We select the critical frequency (or break frequency) ω_c at which these terms are equal as follows:

$$\begin{aligned} \angle T(j\omega_c)_{lower} &= \angle T(j\omega_c)_{higher} \\ \therefore \tan^{-1}(0) \alpha &= \tan^{-1}\left(\frac{\omega_c}{a} - 1\right) \alpha \end{aligned}$$

Therefore,

$$\omega_c = a$$

F.3 Fractional Double-Term Zero

$$\angle T(j\omega) = \tan^{-1} \left(\frac{\omega^{\alpha+\beta} \sin \left(\frac{\pi}{2}(\alpha + \beta) \right) + a_1 \omega^\alpha \sin \left(\frac{\pi}{2}(\alpha) \right)}{\omega^{\alpha+\beta} \cos \left(\frac{\pi}{2}(\alpha + \beta) \right) + a_1 \omega^\alpha \cos \left(\frac{\pi}{2}(\alpha) \right) + a_2} \right)$$

In the above term, one can see that the term a_2 dominates at lower frequencies. Therefore, $\omega^{\alpha+\beta} \cos \left(\frac{\pi}{2}(\alpha + \beta) \right) + a_1 \omega^\alpha \cos \left(\frac{\pi}{2}(\alpha) \right) + a_2 \approx a_2$.

$$\angle T(j\omega)_{lower} = \tan^{-1} \left(\frac{\omega^{\alpha+\beta} \sin \left(\frac{\pi}{2}(\alpha + \beta) \right) + a_1 \omega^\alpha \sin \left(\frac{\pi}{2}(\alpha) \right)}{a_2} \right)$$

Similarly, one can notice that at higher frequencies, the term $\omega^{\alpha+\beta} \cos \left(\frac{\pi}{2}(\alpha + \beta) \right)$ dominates.

$$\angle T(j\omega)_{higher} = \tan^{-1} \left(\frac{\omega^{\alpha+\beta} \sin \left(\frac{\pi}{2}(\alpha + \beta) \right) + a_1 \omega^\alpha \sin \left(\frac{\pi}{2}(\alpha) \right)}{\omega^{\alpha+\beta} \cos \left(\frac{\pi}{2}(\alpha + \beta) \right)} \right)$$

We select the critical frequency (or break frequency) ω_c at which these terms are equal as follows:

$$\angle T(j\omega_c)_{lower} = \angle T(j\omega_c)_{higher}$$

$$\begin{aligned} \therefore \tan^{-1} \left(\frac{\omega_c^{\alpha+\beta} \sin \left(\frac{\pi}{2}(\alpha + \beta) \right) + a_1 \omega_c^\alpha \sin \left(\frac{\pi}{2}(\alpha) \right)}{a_2} \right) \\ = \tan^{-1} \left(\frac{\omega_c^{\alpha+\beta} \sin \left(\frac{\pi}{2}(\alpha + \beta) \right) + a_1 \omega_c^\alpha \sin \left(\frac{\pi}{2}(\alpha) \right)}{\omega_c^{\alpha+\beta} \cos \left(\frac{\pi}{2}(\alpha + \beta) \right)} \right) \end{aligned}$$

Therefore,

$$\omega_c = \left(\frac{a_2}{\cos\left(\frac{\pi}{2}(\alpha + \beta)\right)} \right)^{\frac{1}{\alpha + \beta}}$$

LIST OF PUBLICATIONS BASED ON THESIS

Papers in Refereed International Journals

1. **Ameya Anil Kesarkar**, N. Selvaganesan, and H. Priyadarshan. *A Novel Framework to Design and Compare Limit Cycle Minimizing Controllers: Demonstration with Integer and Fractional-Order Controllers*, *Nonlinear Dynamics*, Springer, 78(4): 2871-2882, 2014.
2. **Ameya Anil Kesarkar**, N. Selvaganesan, and H. Priyadarshan. *Novel Controller Design for Plants with Relay Nonlinearity to Reduce Amplitude of Sustained Oscillations: Illustration with a Fractional Controller*, *ISA Transactions*, Elsevier. (Accepted)
3. **Ameya Anil Kesarkar** and N. Selvaganesan. Novel Tuning Expressions for Fractional Order ($[PD]^\beta$ and $[PI]^\alpha$) Controllers Using a Generalized Plant Structure. *Journal of Control Engineering and Applied Informatics*, Romanian Society of Control Engineering and Technical Informatics, 17(1): 70-80, 2015.
4. **Ameya Anil Kesarkar** and N. Selvaganesan. Superiority of Fractional Order Controllers in Limit Cycle Suppression. *International Journal of Automation and Control*, Inderscience, 7(3): 166-182, 2013.

Papers in Proceedings of International Conferences

1. **Ameya Anil Kesarkar** and N. Selvaganesan. Fractional Control of Precision Modular Servo Setup for Better Limit Cycle Suppression, *In Proceedings of IEEE Multi-Conference on Systems and Control (MSC)*, Hyderabad, India, pp. 467-471 (2013)
2. **Ameya Anil Kesarkar** and N. Selvaganesan. Design of Fractional Order Robust Controller for Universal Plant Structure, *In Proceedings of IEEE International*

Conference on Current Trends in Technology (NUiCONE), Gujrat, India, pp. 1-4, (2011)

3. **Ameya Anil Kesarkar** and N. Selvaganesan. Tuning of robust PI^α/PD^β controller for generalized plant structure, *In Proceedings of IEEE International Conference on Recent Advancements in Electrical, Electronics and Control Engineering (ICONRAEeCE)*, Tamilnadu, India, pp. 104-108, (2011)

Journal Papers (Under Review/ Submitted)

1. **Ameya Anil Kesarkar**, N. Selvaganesan, and H. Priyadarshan. *Development of Asymptotic Phase Bode Plots for Fractional Order Controllers*, ISA Transactions, Elsevier. (Under Review)
2. **Ameya Anil Kesarkar**, N. Selvaganesan, and H. Priyadarshan. *Development of Asymptotic Magnitude Bode Plots for Fractional Order Transfer Functions*, IEEE Transactions on Circuits and Systems, IEEE. (Submitted)